Fluid Structure Interaction in Piping Systems

Bjørnar Svingen

The Norwegian University of Science and Technology
Faculty of Mechanical Engineering

September 1996

This Thesis has been submitted to
the Faculty of Mechanical Engineering
at The Norwegian University of Science and Technology

in partial fulfilment of the
requirements for the Norwegian academic degree

Doktor Ingeniør

September 1996

Abstract

Fluid structure interaction in piping systems with internal liquid is analyzed in the frequency domain. The governing equations are the waterhammer equations for the liquid, and the beam-equations for the structure. The fluid and structural equations are coupled through axial stresses and fluid continuity relations controlled by the contraction factor (Poisson coupling), and continuity and force relations at the boundaries (junction coupling).

A computer program has been developed using the Finite Element Method as a discretization technique both for the fluid and for the structure. The discretization is made to permit analyses of large systems including branches and loops, as well as including hydraulic piping components. The discretization and the computer program are verified with experiments, and excellent agreements are found. Comparisons of coupled and uncoupled calculations with experiments justify the need to include fluid structure interaction.

The experiments are made with a piping system designed for investigations of fluid structure interaction. Excitations are made with a special hydraulic "disc-valve" capable of maintaining perfect sine function and constant amplitude in a frequency range from zero Hz, and up to at least one thousand Hz.

Frequency dependent friction is modelled as stiffness proportional Rayleigh damping both for the fluid and for the structure. With respect to the waterhammer equations, stiffness proportional damping is seen as an artificial (bulk) viscosity term. A physical interpretation of this term in relation to transient/oscillating hydraulic pipe-friction is given.

Acknowledgments

This work has been performed at The Norwegian University of Science and Technology (NTNU), Faculty of Mechanical Engineering / SINTEF Energy. It is a part of the research program: EFFEN-PRODUKSJON, (Effektiv Energisystem) by Norwegian Electricity Federation (EnFO) and The Research Council of Norway (NFR). The scholarship given by EnFO and NFR through this research program is greatly appreciated.

My supervisor Professor Hermod Brekke has been very supportive and helpful throughout this study and has always shown me confidence. I wish to express my deepest gratitude towards him.

I wish to thank Dr. Arris S. Tijsseling at the University of Dundee for being very helpful with literature and for valuable discussions concerning the mathematical and physical basis on which this thesis is built.

The staff at the Water Power Laboratory has been helpful and friendly throughout this study. In particular I want to thank Viggo B. Pedersen for his interest in the experimental rig and for all the help with the construction and the modifications.

I am very grateful to all my fellow students and colleagues at the Water Power Laboratory for their friendship and valuable discussions. A special thank is given to Morten Kjeldsen and Jo Jernsletten as long-time companions. The linguistic remarks from Terje Sivertsen, Roar Vennatrø, Conny Larsson and Marcus Oledal are greatly appreciated.

Finally I want to thank my fiancée Anne Karin Veisetaune and our son Ørjan for their moral support during this study, and their patience and understanding in the last months.

Outline and Publications

Chapter 1: Review and conclusions of the work in this thesis.

Chapter 2: General introduction and a short historical review of Fluid Structure Interaction in piping systems. Objectives and achievements are also included.

Chapter 3: The mathematical derivation and the physical fundamentals for the equations governing the interaction between fluid and structure in piping systems. The derivation leads to the so-called extended water-hammer equations.

Chapter 4: The special Finite Element discretization of the governing equations used in the computer program, as well as extensions of using the Finite Element Method (FEM) in pure hydraulic piping analysis.

Chapter 5: A mathematical derivation and a physical explanation of the frequency-dependent damping model presented in this thesis. Included is an analytical time-domain solution to the linearized water-hammer equations.

Chapter 6: Various piping components found in literature are briefly described in relation to the Finite Element discretization.

Chapter 7: The layout and design of the experiments, and a description of the computer program written in C++.

Chapter 8: Experimental and numerical results.

Chapter 9: A general discussion of the results, and suggestions for further work.

Several papers, as part of this thesis, have been published during the study. They reflect the work in a rather evolutionary manner. (They are numbered in accordance with the bibliography at the end of this thesis):

[3] H. Brekke and B. Svingen. Self excited and hydromechanical vibrations in piping systems. In *Work Group on The Behavior of Hydraulic Machinery under Steady Oscillatory Conditions*, Lausanne, Switzerland, 1993, IAHR.

[45] B. Svingen. A frequency domain solution of the coupled hydromechanical vibrations in piping systems by the finite element method. In *XVII IAHR Symposium*, pages 1259-1269. IAHR, 1994.

[48] B. Svingen. Frequency dependent friction and modal solutions of pipe flow by the finite element method. In *Work Group on The Behavior of Hydraulic Machinery under Steady Oscillatory Conditions*, Ljubljana, Slovenia, 1995. IAHR.

[49] B. Svingen. Fluid structure interaction in slender pipes. In *Pressure Surges and Fluid Transients in Pipelines and Open Channels*, pages 385-396, Bury st Edmunds and London, UK, 1996. bHr Group, Mechanical Engineering Publications Limited.

[50] B. Svingen and M. Kjeldsen. Fluid structure interaction in piping systems. In *Proceedings of the Ninth International Conference on Finite Elements in Fluids New Trends and Applications*, pages 955-963. IACM, 1995.

Contents

Nomenclature

Roman letters

a	wave velocity	m/s
A	pipe cross-sectional area	m^2
$\mathbf{C}$	general coupling matrix	
d	pipe diameter (inner)	m
D	pipe diameter (outer)	m
$\mathbf{D}$	damping matrix	
e	pipe wall thickness	m
E	Young's modulus	Pa
f	stationary friction factor	
f	force	N
F	force	N
$\mathbf{F}$	force vector	
g	gravity constant	m/s^2
G	shear modulus	N
h	pressure head	m
$\mathbf{h}$	pressure head vector	m
h_w	Allievi's pipe constant	
H	pressure head	m
$\mathbf{H}$	pressure head vector	m
I	moment of inertia	m^4
$\mathbf{I}$	identity matrix	
K	fluid bulk modulus	Pa
$\mathbf{K}$	general mathematical potensial energy matrix. (stiffness matrix)	
l	length	m
L	pipe length (general)	m
M	Mach number	
$\mathbf{M}$	general mathematical kinetic energy matrix (mass matrix)	
n	shape function	
$\mathbf{N}$	shape function vector	
p	pressure	Pa
P	pressure	Pa
$\mathbf{P}$	pressure vector	Pa
q	flow	m^3/s
$\mathbf{q}$	flow vector	m^3/s
Q	flow	m^3/s
$\mathbf{Q}$	flow vector	m^3/s
r	radial coordinate	m
R	pipe radius	m
$\mathbf{R}$	transformation matrix	
s	Laplace operator	$j\omega$
t	time	s
u	displacement in x direction	m
$\mathbf{U}$	global vector of variables	
v	fluid velocity	m/s
V	fluid velocity	m/s
$\mathbf{V}$	fluid velocity vector	m^3/s
w	displacement in y and z dir.	m
x	coordinate	m
y	valve opening	m or mm
Y	valve opening	m or mm

Greek letters

α	stationary damping constant (mass proportional factor)	$1/s$
β	general frequency-dependent damping factor (stiffness proportional)	s
γ	damping ratio	
δ	arbitrary weight function	
δ_{ij}	Kronecker delta	
ϵ	strain	
η	generalized pressure	
$\boldsymbol{\eta}$	generalized pressure vector	
θ	angular displacement	rad
κ	bulk viscosity	Ns/m^2
λ	second viscosity coefficient	Ns/m^2
λ_f	frequency-dependent fluid friction factor	Ns/m^2
$\mathbf{\Lambda}$	modal eigenfrequency matrix	
μ	viscosity	Ns/m^2
ν	Poisson's ratio	
ρ	density	kg/m^3
σ	stress	Pa
τ	shear stress	Pa
$\mathbf{\Phi}$	modal eigenvector matrix	
ψ	wave velocity constant	
ω	frequency	rad/s
∂	partial derivative operator	

Sub- and superscript

0	steady state
1	node/element number one
2	node/element number two
a	node a
b	node b
e	over/in element
ex	excitation
f	fluid (in pipe)
g	global
ij	element number i
	node number j
p	pipe
r	radial direction
	or mode number
T	transposed
x,y,z	x, y and z direction
x	for matrices and vectors: the derivative in x direction
xp	x dir. due to pressure
xu	x dir. due to displacement
$*$	non-dimensional
$\bullet$	time derivative

Other

Bold fonts represent vectors and matrices.

The mass and stiffness matrices have retained their names from the original FEM structural analysis. In this thesis the mass and stiffness matrices are defined as:

$$\mathbf{M} = A_1 \int_e \mathbf{N}\mathbf{N}^T dx$$

$$\mathbf{K} = A_2 \int_e \mathbf{N}_x \mathbf{N}_x^T dx$$

where A_1 and A_2 are arbitrary constants with arbitrary units.

Variables not corresponding to this nomenclature are stated explicit in the text.

Chapter 1

Review and conclusion

A theoretical and experimental study of Fluid Structure Interaction (FSI) in piping systems is presented. The work is performed in the frequency-domain, and the interaction is between the pipes and internal liquid.

Three objectives have been achieved in addition to a new hydraulic damping model:

- A general computer program for frequency-domain FSI calculations of hydraulic piping systems has been produced.
- An experimental rig to verify and improve the computer program and for future FSI research has been built.
- A new frequency-dependent damping model for use in hydraulic calculations both in frequency and time-domain is proposed, as well as an analytical solution to the waterhammer equations.
- Continuation of the research on non-stationary flow phenomenon at the Water Power Laboratory at NTNU.

The computer program uses the Finite Element Method (FEM) as a discretization method both for the fluid and the structure. Because of the choice of variables and their positions in the matrix system, it is capable of analyzing systems with loops and branches. Other hydraulic piping components such as pumps and valves are included, and inclusion of different structural boundary conditions is straightforward because of the FEM discretization. The program is based on the extended waterhammer equations. This means that the Poisson FSI coupling is included within the governing equations. Coupling at junctions is included in the discretization and consists of pressure forces acting on the pipe and changes in the continuity because of moving boundaries. The program is verified with experiments made on the experimental rig.

The experimental apparatus consists of an L-shaped piping system (one horizontal and one vertical reach) supported only at the upstream and downstream end. The pipes are long, slender and thin walled, which ensure that FSI effects are large. Oscillations are made with a specially designed valve which is capable of opening and closing in a *perfect sine shape* in a wide frequency range. (The range is 0 to 300 Hz in the current version, but the can be extended up to at least 1000 Hz by changing a disc responsible for the sine functions). Excellent agreement between calculations and experiments are found.

For the particular experimental system presented, calculations without FSI give maximum acceleration amplitudes 10 times larger than those measured and correctly predicted by calculations performed with FSI. This demonstrates the importance of including FSI in the calculations. At other frequencies, pressure-amplitude peaks calculated without FSI are in fact nonexistent in both measurements and calculations with FSI and vice versa.

A new frequency-dependent damping model for hydraulic flow is proposed. The model is essentially stiffness proportional damping, which is found to be an artificial bulk viscosity term in the Navier-Stoke's equations. Because the model is integrated directly into the governing equations, it can be used in both time and frequency-domain. The use of it requires no iteration because the frequency and amplitude dependence are included implicitly, thus the speed of the calculations will be almost identical to undamped calculations. The model is compared with experiments presented in this thesis and experiments found in literature, and it is clear that excellent agreements can be achieved. In relation to FSI the model simplifies the calculations considerably because the same damping model is used both for fluid and structure. However, the model is in its early stages of development and further work is needed before it can be used in practical calculations.

As a concluding remark it can be stated that the program is capable of calculating FSI in piping systems in the frequency-domain. Both fluid pressures and structural accelerations can be calculated with a high degree of accuracy. Currently the program can calculate general two-dimensional (planar) piping systems with loops, branches and hydraulic components. Since all the fluid structure interaction mechanisms are included, an extension to three dimensions is straight forward.

Chapter 2

Introduction

Fluid Structure Interaction (FSI) in piping systems is the study of both the hydraulic and the structural behaviour of a piping system where the interactive forces between the two elements are taken into account. In general FSI is considered a *dynamic phenomenon*, (transient or oscillatory motion), as opposed to hydrostatic phenomena.

Traditionally, and still today, the dynamic structural behaviour of a piping system caused by waterhammer is calculated using the results of a waterhammer analysis as input to the structural analysis (this is called an *uncoupled* analysis). In many cases the results obtained from this analysis are adequate, but in other cases the results may equally well be erroneous. It is also important to note that uncoupled *hydraulic pressure and flow calculations* in many circumstances will produce wrong results. Research and development of calculation and design methods aiming at safer and more reliable piping systems is therefore of interest for scientific, engineering and commercial reasons.

Equations describing the hydraulic and structural behaviour with interaction, have been available for some time in scientific literature, and several scientists and researchers have made contributions with experiments and analytical work. Still, development of general purpose piping software that include FSI is in its infancy, although commercial time-domain software, based on iteration procedures, have existed for a few years (FLUSTRIN [53]). Programs for frequency-domain calculations are not commercially available, but several proposals can be found in the literature. None of these programs are capable of analyzing systems with loops and/or branches (as far as the author knows). Thus, a lot of work has to be done before the knowledge, both mathematical/numerical and practical/experimental, is made available for use in general engineering purposes.

FSI is by its very nature the marriage of two different disciplines. The problems this raises are just as much of a human nature as of a physical/mathematical nature. In structural engineering the Finite Element Method (FEM) is by far the method

of choice and has been so for a long time. Many very sophisticated commercial programs exist both for time- and frequency-domain calculations. In the hydraulic communities FEM is apparently obsolete, and the method of choice is the Transfer Matrix Method (TMM) for frequency-domain calculations, and the Method Of Characteristics (MOC) for time-domain calculations. This adds some extra difficulties both in the process of defending the choice of method and in explaining the details.

Since FSI in piping systems is a relatively new line of research the work that has to be done and is being done with respect to FSI in piping systems can be summarized in four points:

1. Experimental research to give a broader basis for development of good computer programs and to increase the general understanding and knowledge.

2. Development of numerical schemes and computer programs, both as a research tool and for use in engineering work.

3. Make guides based on experiments, on site measurements and computer programs as to show when FSI is of importance for more thoroughly calculations of a piping system including FSI.

4. Find design criteria for piping systems that can be used for everyday engineering purposes to prevent unwanted FSI to occur.

The work presented in this thesis addresses the first two points and partly the third. New contributions in the form of experiments and the prototype of a general purpose computer program for FSI calculations in frequency-domain are presented (eigenvalue- and frequency response analysis). The program is based on the Finite Element Method (FEM).

The last two points which may have the largest practical interest and value in everyday engineering practice, must be based on points one and two. It is the authors hope that the developed FEM software along with the experiments will contribute to the making of these guides and criteria to be used in the design of safer, more reliable and less noisy piping systems.

2.1 Definitions

The following definitions are used different in various literature. In this thesis the definitions relating to FSI are:

- A calculation is said to be *coupled* when two or more different variables[1] (typically fluid flow and structural displacement), affect each other *mutually* through one or more *couplings*.
- In an *uncoupled* calculation there are *no linkage* between two types of variables, *or* the linkage acts only one way.
- A *coupling* is a mechanism that links one type of variable to the other, but not *necessarily* back again. (A typical traditional calculation of structural displacements due to waterhammer, has coupling from fluid to structure, but not from structure to fluid. Thus, the calculation is *uncoupled*).
- In an FSI (Fluid Structure Interaction) calculation, there are couplings both ways. That is, *FSI calculations are always coupled*. In this thesis all *FSI calculations* have Poisson coupling and two-way junction coupling.
- The *extended waterhammer equations* are the two one-dimensional coupled wave equations describing the longitudinal equation of motion for the pipe, and the momentum and continuity for the fluid. (In literature this name is often used for the more general two-dimensional equations describing the equations of motion for the pipe and the momentum and continuity relations for the fluid, with different levels of simplification.)
- The name *four-equation model* is used in the literature as the name for the four coupled first order one-dimensional equations describing the longitudinal equation of motion for the pipe and the momentum and continuity for the fluid. They are essentially the same as the extended waterhammer equation defined above, since two one-dimensional wave equations can be described by four first order equations. For use in MOC they must be described as first order equations, but when using FEM it is often more practical to use wave equations. In this thesis the name four-equation model is a pseudonym for the name extended waterhammer equations.

[1] In modal analysis the word *coupled* and *uncoupled* are used to describe the matrices.

2.2 Waterhammer

The equations describing the dynamic behaviour of fluid flow in pipes are often called the waterhammer equations or Allievi's equations after L. Allievi who pioneered research in this area in the beginning of this century. The equations are two coupled one-dimensional linear partial differential equations (continuity and momentum) relating fluid pressure and fluid velocity.

Mathematically, the equations are standard one-dimensional wave equations, often with a nonlinear damping term. The convective term can be neglected for liquid flows because of low Mach numbers. This wave behaviour of the equations is used to its full extent in the most popular solution method, the method of characteristics. Because of the linearity the equations are easily transformed to the frequency-domain where they can be solved analytically.

These equations can be derived in several ways. Later in this thesis (Chapter 3.1) they are derived from the Navier-Stokes equations.

2.3 Structural dynamics

The pipe structure is described using beam equations. In other words, the pipe can bend in two directions, stretch in one direction and obtain torsional moment. All these equations are wave and quasi-wave equations that are independent of one another, second order effects are neglected. The simplifications made are actually quite large when one considers the pipe as a thin-shelled structure. However, for the majority of piping structures these simplifications have literally no measurable effect. The reason for this is that the length to diameter ratio is so large that all frequencies of interest are either axial or transversal (bending). Only for very high frequencies will radial shell modes be excited. Therefore, modelling the pipe with three-dimensional shell elements complicates the calculations in many orders of magnitude, and the accuracy gained is in no comparison to the extra cost of modelling and solving.

Today the beam equations are solved almost exclusively with the finite element method, both in frequency and time-domain, and many commercial piping programs for structural calculations exist.

2.4 The Finite Element Method, FEM

The Finite Element Method, (FEM), was first developed by aircraft engineers in the late forties to calculate stresses in complex geometries. The idea was to divide a complex unsolvable geometry into simple pieces for which solutions could be

found. An approximation to the complex structure was then built with these simple *elements*. Later on, mathematical development combined with the increase in computer power has developed the method, and *today FEM is considered a general discretization procedure for solving partial differential equations.*

In structural mechanics some sort of finite element methods are the only methods used in calculations today (with only a few specific exceptions). FEM is used for all types of calculations, (ordinary stress/strain calculations, transient, oscillatory and nonlinear plasticity calculations).

Calculation of transient and dynamic hydraulics in piping using FEM is rare and not well known in the hydraulic communities. However, a substantial amount of work has been done in developing general two- and three-dimensional fluid codes using FEM as the discretization technique, and several commercial programs exist.

All in all, the main characteristic of the Finite Element Method is that it is a general discretization technique. It can be derived from a pure mathematical point of view through variational approximation. It is intuitively understandable (at least for mechanical analysis). From a practical point of view its best characteristics is that it is extremely consistent in all its aspects and that it seems "as made for" object oriented programming, which truly makes it a strong analysis tool made for the future.

2.5 Fluid Structure Interaction, FSI

As stated on page 3, fluid structure interaction is the study of the dynamic interactive behaviour of fluid and structure. This may be in a ship-sea, airplane-air connection, or as in this case, pipe and internal fluid. In many cases this interaction can be disregarded because it is small compared to other parameters. However the trend with thinner materials, higher velocities and pressures, seems to continue due to the economical benefits this has. A problem this trend causes is of course that fluid structure interaction which could be disregarded before, suddenly has large consequences. This, together with the increase in computer power making the interactive equations solvable, make FSI an important branch of research.

In piping systems at least three different forms of FSI can be found:

1. FSI due to external fluid, (oil risers, sea pipes etc.).
2. FSI due to internal liquids, (*Poisson* and *junction* coupling, oil hydraulics and most piping conveying liquids).
3. FSI due to unsteady internal shear layers, (acoustics, gases and liquids).
4. Any combination of the former three.

The work in this thesis deals with FSI due to internal liquids.

2.6 Frequency-domain

To assert the general dynamic behaviour of a system one has to do a frequency-domain analysis. With this analysis one will find the eigenvalues of the system (resonant-frequencies with corresponding eigenvectors), and one can do a frequency response analysis.

With the eigenvalues one will find which frequencies excite the system and where in the system the maximum amplitudes will occur. Relating to piping systems, this information is of significant value when the position of the supports are decided.

Frequency response is used to find the amplitudes at various frequencies when the system is disturbed by a steady oscillatory disturbance (vibrations generated from pumps, motors etc.). This information is very valuable in the design phase of a piping system, and in finding the cause of - and a solution to - vibration and noise problems. Frequency response can also be used in a fatigue analysis to find where the system is most likely to break. Other important uses for frequency response is for control applications in oil hydraulics or hydro power, and in general acoustic analysis.

2.7 Previous work

FSI in piping systems is the marriage of two very distinct disciplines. This distinction is clearly reflected in most of the available literature where hydraulics and mechanics approaches the problem from different angles and with different solution strategies.

Two review papers have been written in the last ten years, [66, Wiggert] and [53, Tijsseling]. Both papers are excellent starting points for further research. The latter, being fully up-to-date at the time of writing, has a very comprehensive list of references as well as an excellent introduction to FSI in piping systems given in a historical perspective. The emphasis of the latter review is on time-domain analysis. An excellent introduction can also be found in [67, Wiggert].

This thesis deals mainly with FSI in the frequency-domain. The emphasis of the following review is therefore on work done in the frequency-domain, and the general history of FSI in piping is only briefly presented. This review is therefore by no means complete with respect to including all the work previously done, but is aimed at giving a historical look at the development seen in relation to the work in this thesis.

2.7.1 Poisson coupling

When the pressure in a pipe rises, the pipe walls obtain tangential stress. Through the Poisson ratio, ν, these tangential stresses causes axial stresses trying to shorten the pipe. Axial stresses also causes the pipe to contract in radial direction, thus

decreasing the internal volume. For a stationary case the forces will rest at a point of equilibrium. In a transient or oscillatory case, these effects will cause changes to both the fluid variables and the structural variables because stress waves and pressure waves travel with different speeds. A pressure wave traveling at the speed of sound in fluid, causes tangential stress in the pipe wall. This tangential stress is the cause of an axial stress wave traveling at the speed of sound of the pipe material, thus, much faster than the pressure wave. Following this axial stress wave is another pressure wave (precursor wave). This pressure wave is caused by the radial contraction. The Poisson number is a key factor to this dynamic behaviour, and the name of this coupling is therefore the *Poisson coupling*.

The development of the four-equation model which incorporate the Poisson coupling used in calculations today can be traced as far back as to the 19th century. In 1878 Korteweg presented equations for the velocity of sound of fluid in an elastic pipe:

$$a_f = \sqrt{\frac{K}{\rho_f}\left(1 + \frac{DK}{eE}\right)^{-1}}$$

where K is bulk modulus of the fluid, ρ_f is fluid density, D is pipe diameter, e is pipe wall thickness and E is Young's modulus of the pipe. He also pointed out that the Poisson ratio is of importance when including axial pipe stresses.

In 1956 Skalak [41] presented the equations (four-equation model) that, with minor modifications, are used today. These equations permit precursor waves without the dispersion effects found in earlier models, and are valid when the fluid wave length is long compared to the diameter. The equations are longitudinal structural equation of motion for the pipe coupled with the waterhammer equations through the Poisson effect. In this thesis the Skalak model is used.

2.7.2 Junction coupling

Any discontinuities in a piping system (bends, T-connections etc.) that have some degree of freedom, will produce mutually dependent forces on the structure and the liquid when the pressure changes, or the pipe moves. This kind of coupling is called junction coupling.

The coupling consists of two parts:

1. Pressure forces acting on the structure, (pressure-based junction coupling).

2. Structural movement causing changes to the fluid continuity, (continuity-based junction coupling).

Both effects must be included to obtain *interaction* between fluid and structure.

2.7.3 General research

During the last 10 to 15 years the main subject of research has been the development of reliable and practical software for calculation of FSI. Along with these developments, some experimental research has also been done. In FSI in piping systems, as in all other branches of research, experimental work is much more expensive, both in labour and actual cost than software development. Literature containing experiments is therefore somewhat sparse compared to literature containing analytical and numerical research. In frequency-domain research, the experiments done in 1969 by Davidson and Smith [7], are still used to validate software.

Different approaches are used in making FSI software. Commercial structural and fluid programs have existed for some time, so one approach is to try to combine this software in some kind of iteration procedure by making interface programs or by modifying existing code. Although this looks like a fast and easy approach, the result is an inconsistent program that is slow, hard to use and often manual user intervention is needed (see for instance [53, Tijsseling]). Modifying existing FEM piping software has been a popular approach, and although the junction coupling can be modelled correctly, the inclusion of Poisson coupling is very difficult (often skipped). More important, the inclusion of hydraulic components (pumps, turbines) is literally impossible.

Gibert et al. [15] used an existing FEM software to compute acoustics and vibrations in piping systems. In the computations, the one-dimensional beam model was used. The interaction was modelled as locally acoustical source term acting from fluid to structure. Emphasis was put on transfer function modelling of these source terms coming from fluid turbulence because of discontinuities (bends, etc.). Poisson coupling was not included and the only FSI coupling was junction coupling. Calculations were compared with experiments showing accelerations. Later Axisa and Gibert [1] presents a more thorough description of their method along with some calculations including nonlinear effects (time-domain). To obtain symmetric matrices a variable π is used. The definition of π is given by the relation: $\ddot{\pi} = p$, where p is the plane acoustic pressure. The physical representation of π is the *velocity potential*.

Schwirian and Karabin [40] modelled the fluid as spar elements to be able to use existing FEM structural programs, no Poisson coupling was modelled, only coupling from pressure to structural displacement at junctions (one way junction coupling). Later Schwirian [38] developed this approach and also proposed a multi-dimensional fluid element with a quasi-Poisson coupling incorporated, as well as cavitation. Cavitation was modelled as spring/mass[2] elements with a GAP which

[2]The use of spring/mass elements is the same as "lumping" the matrices (concentrating the mass and stiffness at node points), thus greatly reducing the accuracy. A GAP is component that opens (looses contact) when the tensile stress reaches a pre-defined value.

opens when the pressure drops below the cavitation pressure.

Everstine [12] used a similar model as Schwirian and Karabin, and he also pointed out and included the important flexibility factors at bends. In his paper he included a three-dimensional acoustic FSI calculation (shell - brick) for comparison with the beam solution. In the beam solution the unknown nodal values were fluid displacement, not fluid pressure, and no Poisson coupling was included. The calculations were compared with the experiments of Davidson and Smith [7]. Everstine found that a beam solution with the appropriate flexibility factors was adequate for frequencies up to 63% of the first radial fluid-filled pipe mode, thus far beyond the frequencies of interest in general piping systems. Everstine concluded that the very time consuming and expensive three-dimensional approach could be used for verification of simpler models and for calculations of small details where accuracy was of importance. Commercial three-dimensional acoustic FSI programs are now available (i.e. ANSYS).

An interesting (time-domain) approach was proposed by Xianglin et al. [72]. The four-equation model was solved with FEM, both for the fluid and for the structure, and numerical examples for one straight pipe were given. The fluid elements were discretized with first order polynomials for the pressure and third order Hermite polynomials for the velocity, hence producing a total of six degrees of freedom for each fluid element. The structure was discretized in standard FEM manner. Iteration was done at each time step to couple the fluid and structure similar to the MOC-FEM method used in FLUSTRIN [29].

During the 1980's the work at Michigan State University (for instance [17] [68] [69] [30]) has been of great importance in the development and understanding of FSI in piping systems. Through numerous publications in journals and conferences this field of research has been introduced to a broad audience. The research has been both in the time- and the frequency-domain. In the frequency-domain, Hatfield et al. [17] presented a component synthesis method. In this method the structure was represented with a limited number of eigenvalues computed with available FEM software. Only junction coupling was included. In 1987 and 1990 Lesmez et al. [30] presented a transfer matrix solution (TMM) to the four-equation model [41, Skalak]. In this solution both Poisson and junction coupling was incorporated. Solving of the same equations has been investigated in time-domain with the method of characteristics by Wiggert et al. [69]. Both the time and frequency-domain computations were validated with data from experiments.

The transfer matrix approach has later been adopted by many investigators. Charley and Caignaert [6] used the TMM with the flow, q, as the parameter, not the fluid displacement originally presented in Lesmez et al. [30]. Gajić et al. [14] included steady state friction. de Jong [8] presented a considerable amount of valuable experimental data along with his calculations.

Although the research at the university of Dundee in the UK and at Delft

Hydraulics in The Netherlands mainly concerns time-domain analysis, the large amounts of publications from these institutes have been very important to this field of research. Among developments of software, FLUSTRIN [29], and numerical schemes, the most important contribution in a historical scientific context has been the validation of the four-equation model through large scale and precisely executed experiments (see for example [52, Tijsseling]). It is safe to say that the acceptance of the four-equation model as the appropriate model describing the fluid structure interaction in piping systems, is largely due to the work done at these institutes [55] [19] [57] together with the work at Michigan State University.

An approach somewhere in between TMM and FEM was presented by Xinxin and Nielsen [74]. This method is based on the Structure Matrix Method (SMM) adopted for use in hydro power simulations by Brekke [2]. It is similar to TMM because the wave equations are solved analytically in frequency-domain for a pipe element. Instead of making a transfer matrix connecting all the variables from one point on the pipe to another point, the pressure and all the displacements are set on the left hand side while the flow and forces are set on the right hand side ($\mathbf{Au} = \mathbf{f}$), where $\mathbf{u}$ is the vector of pressures and displacement while $\mathbf{f}$ is the vector of flow and forces. The method is similar to FEM [77, Zienkiewicz] in the way the global matrices are built, and in the way the variables are grouped. In fact, some elements can be interchanged between the two methods (FEM and SMM). The method was used with the four-equation model on a numerical example[74, Xinxin], however no junction coupling was included. Originally the idea was to develop this method further. The reason for choosing FEM is mainly its flexibility concerning discretization compared with a quasi-analytical method. This flexibility is seen when including different mathematical beam models (Euler-Bernoulli/Timoshenko etc.), and especially when including piping support and surrounding structure.

Svingen [3] [45] presented a FEM solution similar to Schwirian and Karabin [40], but with the inclusion of Poisson coupling (four-equation model). The use of velocity potential or fluid displacement as the unknown to obtain symmetric matrices was discarded, and instead the fluid pressure was used as the unknown and the fluid flow as the known variables, similar to the SMM. The computations were validated with the experiments by Davidson and Smith [7]. An experimental piping system for FSI experiments is given in Svingen [49].

2.8 Objective

The research presented in this thesis is aimed at the development of frequency-domain calculation of piping systems including the effect of fluid structure interaction. Objectives can be categorized as follows:

- Develope a computer program (prototype) for FSI in piping systems, capable of:
  - Computing frequency response and eigenvalues.
  - Analyzing complete systems including branches and loops without any complications.
  - Including components such as turbines, valves, pumps etc. as described in Brekke [2].
  - Including supports and surrounding structure easily and effectively.
- Construct an experimental rig for frequency-domain FSI analysis of piping systems:
  - To verify and improve numerical schemes.
  - Assure that the FSI couplings involved are dominating the structural and fluid responses.
  - Oscillating valve to make sinusoidal disturbances.
- A part of the research program: EFFEN-PRODUKSJON, (Effektiv Energisystem) by Norwegian Electricity Federation (EnFO) and The Research Council of Norway.
- A part of the continuing research on non-stationary flow phenomena at the Water Power Laboratory at NTNU.

2.9 Achievements

Having the objectives, and the more general points given on page 4 in mind, the main achievement is the development of a general purpose computer program (prototype) for frequency-domain FSI analysis of piping systems. The program was built from scratch using object oriented C++ as the main programming language and using existing FORTRAN subroutines for matrix solving. Currently the program can analyze plane piping systems, but the extension to three dimensions is straight

forward because *all the fluid structure interaction modelling* which complicates the solution process is taken care of for two dimensions.

The main difference between the approach presented here and approaches found in earlier literature is the choice of fluid variables and their position in the matrix system.

The use of an existing structural FEM program for general piping analysis produces some major problems. When using structural programs for fluid equations it is necessary to convert the fluid variables from an Eulerian to a Lagrangian frame of reference, Schwirian [39]. This can be done by using the fluid displacement, or the velocity potential and pressure. Both of these approaches leads to symmetric matrices resulting in computational advantages especially for three-dimensional calculations. Using fluid displacement has two disadvantages. The number of unknowns increases (especially for three-dimensional calculations) and nonphysical rotational modes of fluid vibrations are made. Using the velocity potential and pressure produces no such rotational modes, but leads to a fictitious damped system.

Sandberg [36] presented a method using the pressure and the *fluid displacement potential* as variables, where the displacement potential ψ is defined as: $\mathbf{u}_f = \nabla\psi$ where $\mathbf{u}_f$ is the fluid displacement vector. This approach produces symmetric matrices without the fictitious damping found in the method using velocity potential and pressure. From a pure fluid-structure point of view this is all fine. However, when one also wants to include hydraulic piping components such as valves, pumps and orifices, problems arises. For one-dimensional calculations, fluid displacement *could* be used with some modifications to the equations describing other hydraulic components, but additional problems would arise when loops and branches are included, as described in the next paragraph. Using either velocity potential/pressure or displacement potential/pressure causes the inclusion of hydraulic components to be literally impossible. Since the objective is in the making of a general-purpose computer program, the choice of the fluid variables in this thesis is the flow, Q, and pressure, P.

When modelling piping systems with branches and loops, the position the variables have in the matrix equations are of importance. Using the Transfer Matrix Method [71, Wylie and Streeter] all variables (Q, P, U, F) in one place are connected to another place using a "transfer matrix". For straight pipes this works fine, but problems arise in systems with loops and branches where special considerations have to be made to assure continuity [8, de Jong]. Also when using existing FEM software where nodal displacement or velocity potential are the dependent variables, special considerations have to be made to assure continuity at branches. In the structure matrix method developed by Brekke [2], this problem is solved in an elegant manner. By using the pressure as the dependent variable and the flow as the free variable with positive direction of flow out of the pipe at each end, the continuity at branches is assured by setting the flow equal to zero at all places except

where flow leaves or enters the system. The matrix equations (hydraulic) will have the form:

$$\mathbf{A}(\omega)\mathbf{P} = \mathbf{Q}$$

where $\mathbf{A}$ is the system matrix, $\mathbf{P}$ is the pressure vector and $\mathbf{Q}$ is the flow vector. This approach is adopted here with the extra advantage of being able to use literally all the hydraulic piping components developed for the structure matrix method [2, Brekke] [73, Xinxin]. The use of finite elements as the method of discretization also assures that including piping supports and surrounding structure is an easy task [33, Petyt].

Computations made with the program are compared with results from the experiments done with a piping system designed for FSI experiments. Large fluid structure effects are both measured and correctly predicted by the program. The experimental rig is made with long, thin walled, pipes to assure that FSI effects (Poisson and junction) are dominating the dynamic responses. A special valve that opens and closes with a sine function is designed to excite the system.

When using FEM for structural calculations, a common way of modelling the frequency-dependent damping is the use of proportional damping, often called Rayleigh damping [33, Petyt]. The frequency-dependent damping matrix is proportional to the stiffness matrix by a specified constant. In structural mechanics this damping constant can be found in text books for different structures and materials[3]. While using this kind of damping model for the pipe structure, it is obviously attractive to also use it for the fluid because it would simplify the calculations. This is done in this thesis, and it is shown that the frequency dependence is good compared with experiments and that it is extremely efficient. A physical and mathematical interpretation is also proposed. The mass proportional part of the Rayleigh damping matrix is shown to be the linearized stationary damping term given in the Allievi equations. This term evolves automatically through the discretization.

An analytical time-domain solution to the linearized waterhammer equations with frequency-dependent friction is found. The solution is found by separation of variables, and can be used to show the properties of the specific damping model, and for verification of computer codes.

Time-domain calculations of the waterhammer equations with nonlinear steady-state friction are usually done with the *method of characteristics*. A special discretization technique, making it possible also to include the proposed frequency-dependent/transient friction model, is presented along with some calculations.

Extensions to modal analysis and stationary analysis are also sub-parts of this thesis.

[3]Often the constant is not given directly, but rather as modal damping ratios.

Chapter 3

The extended waterhammer equations

In this chapter the extended waterhammer equations are derived. They are the equations that include the coupling between hydraulics and structural pipe movement in axial direction because of the Poisson effect, hence they are one-dimensional [41, Skalak]. The goal is to reach the so called four-equation model used in the numerical program. Assumptions and simplifications are stated through the process, and the less obvious ones are treated in appendices. Bending and torsion causes no direct fluid structure interaction and are therefore not derived herein (they can be found in text books, i.e. [35, Rao]).

Deriving these equations can be done in many different ways [41, Skalak] [52, Tijsseling]. The derivation herein is done to obtain equations suitable for the Finite Element Method in particular and oscillation-calculations in general.

3.1 Fluid

The starting point for the fluid equations is two-dimensional Navier-Stoke's equations in cylindrical coordinates. (Note- axial coordinate is x, see Figure 3.1).

- Continuity

$$\frac{\partial \rho_f}{\partial t} + v_x \frac{\partial \rho_f}{\partial x} + v_r \frac{\partial \rho_f}{\partial r} + \rho_f \frac{\partial v_x}{\partial x} + \frac{\rho_f}{r} \frac{\partial}{\partial r} (r v_r) = 0 \tag{3.1}$$

- Axial momentum

$$\begin{gathered} \rho_f \frac{\partial v_x}{\partial t} + \rho_f v_x \frac{\partial v_x}{\partial x} + \rho_f v_r \frac{\partial v_x}{\partial r} + \frac{\partial p}{\partial x} = \\ F_x + \left(\kappa + \frac{1}{3}\mu\right) \frac{\partial}{\partial x} \left(\frac{\partial v_x}{\partial x} + \frac{1}{r} \frac{\partial (r v_r)}{\partial r}\right) + \mu \left(\frac{1}{r} \frac{\partial}{\partial r} \left(r \frac{\partial v_x}{\partial r}\right) + \frac{\partial^2 v_x}{\partial x^2}\right) \end{gathered} \tag{3.2}$$

- Radial momentum

$$\begin{gathered} \rho_f \frac{\partial v_r}{\partial t} + \rho_f v_x \frac{\partial v_r}{\partial x} + \rho_f v_r \frac{\partial v_r}{\partial r} + \frac{\partial p}{\partial r} = \\ F_r + \left(\kappa + \frac{1}{3}\mu\right) \frac{\partial}{\partial r} \left(\frac{\partial v_x}{\partial x} + \frac{1}{r} \frac{\partial (r v_r)}{\partial r}\right) + \mu \left(\frac{1}{r} \frac{\partial}{\partial r} \left(r \frac{\partial v_r}{\partial r}\right) + \frac{\partial^2 v_r}{\partial x^2}\right) \end{gathered} \tag{3.3}$$

These equations are general in the sense that the only simplification is the assumption of symmetry and isothermal flow. κ and μ are the bulk viscosity and the dynamic viscosity.

> Gases are highly compressible as well as having negligible density compared with the pipe material. This makes internal gas flow somewhat uninteresting in FSI analysis, thus shortening the analysis in this thesis to liquids only. However, in recent years several cases of FSI in natural gas pipes have been reported where severe structural vibrations due to resonance have occurred[16, Graf and Ziada][10, Durgin and Graf]. The FSI in these cases are caused mainly by flow-instabilities in shear layers and due to geometrical changes inside the pipe, thus Poisson and junction coupling is not important.

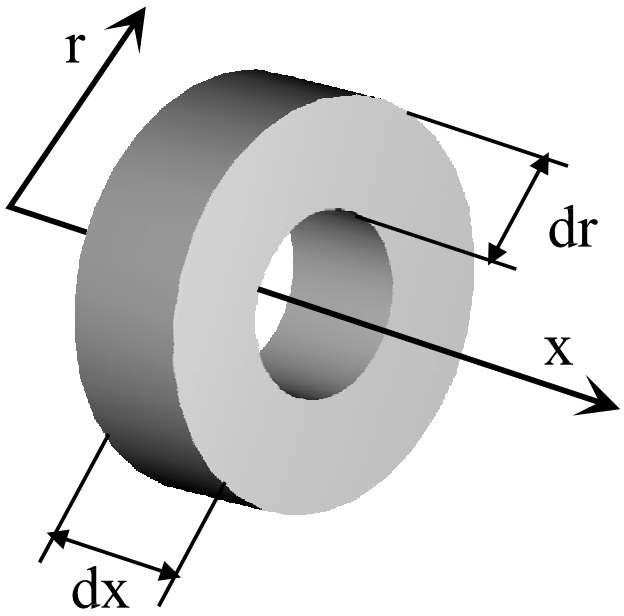

Figure 3.1: Fluid element in axis-symetric cylindrical coordinates.

By assuming very low compressibility the variation of density with respect to pressure is approximated by a constant value.

$$\frac{\partial \rho_f}{\partial p} = \frac{\rho_f}{K} = \frac{1}{c_f^2} \tag{3.4}$$

In this chapter all the viscosity terms are neglected for the sake of clarity (see Chapter 5 for a discussion). By assuming very low Mach numbers ($M^2 \ll 1$) all the convective terms are neglected, see Appendix A. Actually this can be defended *only* for the continuity equation, (Equation 3.1) and not for the momentum equations (Equation 3.2 and Equation 3.3) at this stage since the equations still are two-dimensional. In two and three dimensions the convective terms in the momentum equations usually play a major part of the flow picture [65, White]. However, one-dimensionality will soon be assumed. Since the interest is taken in oscillations about a stationary value all the external body forces are neglected. This reduces Equation 3.1, Equation 3.2 and Equation 3.3 to:

$$\frac{1}{K}\frac{\partial p}{\partial t} + \frac{\partial v_x}{\partial x} + \frac{1}{r}\frac{\partial}{\partial r}\left(r v_r\right) = 0 \tag{3.5}$$

$$\rho_f \frac{\partial v_x}{\partial t} + \frac{\partial p}{\partial x} = 0 \tag{3.6}$$

$$\rho_f \frac{\partial v_r}{\partial t} + \frac{\partial p}{\partial r} = 0 \tag{3.7}$$

Equation 3.5 and Equation 3.6 are made one-dimensional by averaging the pressure and flow across the cross section. This is done by multiplying with $2\pi r$, integrating with respect to r from 0 to R, and dividing by πR^2.

$$\frac{1}{K}\frac{\partial P}{\partial t} + \frac{\partial V}{\partial x} + \frac{2}{R} v_r|_{r=R} = 0 \tag{3.8}$$

$$\rho_f \frac{\partial V}{\partial t} + \frac{\partial P}{\partial x} = 0 \tag{3.9}$$

Where the average pressure and velocity are

$$V = \frac{1}{\pi R^2} \int_0^R 2\pi r v_x dr \tag{3.10}$$

$$P = \frac{1}{\pi R^2} \int_0^R 2\pi r p dr \tag{3.11}$$

The next assumption is based on the fact that the characteristic fluid length scale, L_0, compared with the diameter, D_0, in piping systems is large ($L_0/D_0 \gg 1$). With this assumption the radial inertia is very small compared to the axial inertia and can therefore be neglected with the constraint that the wavelength is long (long wavelength approximation). Proof and dimensional analysis is found in Appendix B. Everstine [12] found by comparing a beam model and a three-dimensional acoustic (brick-shell) model that this approximation is valid for frequencies up to 63% of the first radial fluid-filled pipe frequency. (Equation 3.7 will then become $\frac{\partial p}{\partial r} = 0$ when the radial inertia is neglected, which only states that the pressure is constant in a cross section).

On the pipe wall the radial fluid velocity must be equal to the radial pipe velocity:

$$v_r|_{r=R} = \dot{u}_r|_{r=R} \tag{3.12}$$

Using Equation 3.12 in Equation 3.8, together with Equation 3.9 gives one-dimensional equations, except for the radial pipe velocity term.

$$\frac{1}{K}\frac{\partial P}{\partial t} + \frac{\partial V}{\partial x} + \frac{2}{R} \dot{u}_r|_{r=R} = 0 \tag{3.13}$$

$$\rho_f \frac{\partial V}{\partial t} + \frac{\partial P}{\partial x} = 0 \tag{3.14}$$

Hooke's law in cylindrical coordinates is expressed as:

$$\epsilon_\phi = \frac{u_r}{r} \tag{3.15}$$

$$\epsilon_\phi = \frac{1}{E}\left(\sigma_\phi - \nu\left(\sigma_x + \sigma_r\right)\right) \tag{3.16}$$

Combining Equation 3.13, Equation 3.15 and Equation 3.16:

$$\frac{\partial V}{\partial x} + \frac{1}{K}\frac{\partial P}{\partial t} + \frac{2}{E}\frac{\partial}{\partial t}\left(\sigma_\phi|_{r=R} - \nu\sigma_x|_{r=R} - \nu\sigma_r|_{r=R}\right) = 0 \tag{3.17}$$

It is already assumed and argued that radial inertia is unimportant (see Appendix B), therefore the radial and tangential stress terms in Equation 3.17 can be approximated by the quasi-stationary relations for a thin-walled cylinder found in text books [21, Irgens] assuming $e \ll R$.

$$\sigma_\phi \approx \frac{R}{e}P \quad \sigma_r \approx 0$$

Equation 3.17 now becomes

$$\frac{\partial V}{\partial x} + \left(\frac{1}{K} + \frac{2}{E}\frac{R}{e}\right)\frac{\partial P}{\partial t} - \frac{2\nu}{E}\frac{\partial \sigma_x}{\partial t} = 0 \tag{3.18}$$

Equation 3.18 is now one-dimensional, hence the stress term σ_x can be substituted by $E\frac{\partial u}{\partial x}$. The fluid equations as used in the discretization are:

$$\frac{1}{A_f}\frac{\partial Q}{\partial x} + \left(\frac{1}{K} + \frac{2}{E}\frac{R}{e}\right)\frac{\partial P}{\partial t} - 2\nu\frac{\partial}{\partial t}\left[\frac{\partial u}{\partial x}\right] = 0 \tag{3.19}$$

$$\frac{\rho_f}{A_f}\frac{\partial Q}{\partial t} + \frac{\partial P}{\partial x} = 0 \tag{3.20}$$

The term $\left(\frac{1}{K} + \frac{2}{E}\frac{R}{e}\right)$ is used to approximate the wave propagation velocity (when multiplied by ρ_f), $c_f^2 = \frac{K}{\rho_f}\left(1 + \psi\frac{DK}{eE}\right)^{-1}$. When the pipe is free to move axially the constant ψ is set to 1, and if the pipe cannot move axially, $\psi = (1 - \nu^2)$, [71, Wylie and Streeter]. Anyhow, the difference in calculated wave speed for the experimental rig using the two alternatives is 1.5%.

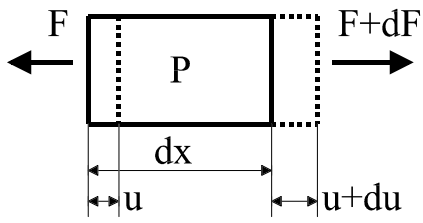

Figure 3.2: Thin walled pipe element of length dx

3.2 Pipe

The pipe equations are derived in a much simpler way by making the assumptions of one-dimensionality and thin walls. Considering a pipe element of length dx and an internal pressure, P, as given in Figure 3.2, the following force-stress relation is valid [35, Rao], [21, Irgens].

$$F = \sigma_{xu} A_p + \sigma_{xp} A_p = E A_p \frac{\partial u}{\partial x} + A_p \nu \frac{R}{e} P \tag{3.21}$$

The pressure term in this equation acting in the x direction is due to the axial tensile stress in the pipe wall because of the Poisson effect. The equation of motion for this element when $f(x,t)$ is an external force per unit length:

$$(F + dF) + f dx - F = \rho_p A_p dx \frac{\partial^2 u}{\partial t^2} \tag{3.22}$$

By using the relation $dF = (\partial F/\partial x)dx$ and Equation 3.21, the equation of motion becomes:

$$-E A_p \frac{\partial^2 u}{\partial x^2} + \rho_p A_p \frac{\partial^2 u}{\partial t^2} - A_p \nu \frac{R}{e} \frac{\partial P}{\partial x} = f(x,t) \tag{3.23}$$

3.3 Torsion and bending

For the sake of completeness the equations describing torsion and bending are included. These equations can be found in most text books (i.e. [33, Petyt] [35, Rao]), thus no derivation is presented here.

Torsional vibrations for a uniform pipe:

$$-G \frac{\partial^2 \theta}{\partial x^2} + \rho_p \frac{\partial^2 \theta}{\partial t^2} = f_T(x,t) \tag{3.24}$$

where $f_T(x,t)$ is the external torque per unit length.

Equations for bending vibrations of pipes can be expressed in many different forms depending on the nature of the pipe and the forces acting on them. In piping

analysis where the pipes can be described by long thin beams, the Euler-Bernoulli theory is usually used. The weight of the fluid inside must also be included.

$$EI_p \frac{\partial^4 w}{\partial x^4} + (\rho_p A_p + \rho_f A_f) \frac{\partial^2 w}{\partial t^2} = f(x,t) \tag{3.25}$$

In Wiggert [69] and Tijsseling [52] the Timoshenko beam theory is used. The reason for this is that when solving with MOC (time-domain), one needs to have hyperbolic equations (the Euler-Bernoulli equations is not). The Timoshenko beam theory incorporates shear deformation and rotary inertia effects and is valid for slender beams also at high frequencies:

$$\begin{aligned} EI_p \frac{\partial^4 w}{\partial x^4} + (\rho_p A_p + \rho_f A_f) \frac{\partial^2 w}{\partial t^2} - \rho_p I_p (1 - \frac{E}{kG}) \frac{\partial^4 w}{\partial x^2 \partial t^2} \\ + \frac{\rho_p I_p}{kG} \frac{\partial^4 w}{\partial t^4} + \frac{EI_p}{kA_p G} \frac{\partial^2 f}{\partial x^2} - \frac{\rho_p I_p}{kA_p G} \frac{\partial^2 f}{\partial t^2} - f(x,t) = 0 \end{aligned} \tag{3.26}$$

where the shear modulus $G = E/2(1+\nu)$, and k is the Timoshenko shear coefficient. (For thin walled cylinders $k \approx 2(1+\nu)/(4+3\nu)$ [52, Tijsseling]). It should also be noted that using Timoshenko theory for bending while neglecting radial inertia in the axial equations is somewhat dubious. However, the frequencies excited in a piping system are so low compared to the radial frequencies that literally no differences are seen between the two models. From a practical point of view when using FEM, the only difference between Timoshenko and Euler Bernoulli is some extra constants in the mass and stiffness matrix, [33, Petyt].

3.4 Poisson coupling

The Poisson coupling is incorporated in Equation 3.23 and Equation 3.19. Looking at these equations one can see that the continuity equation, (Equation 3.19) is modified with a contraction factor. Physically this is the same effect one gets when stretching a hose and the cross section shrinks. (Pumps exist that use this principle). The pressure term in Equation 3.23 works as a distributed force trying to shrink the pipe in the axial direction when the pressure increases. The name *Poisson coupling* is rather obvious, thus setting the Poisson number to zero uncouples the equations. The Poisson coupling is a two-way (mutual working) coupling.

In Figure 3.3 the propagating pressure wave and the axial stress wave can be seen. The pressure widens the pipe in radial direction, causing an axial stress wave due to the contraction factor. This stress wave causes the pipe to shrink in radial direction, and this shrinking is the cause of the so-called precursor wave (pressure wave following the axial stress wave). The existence of these precursor waves have been known for almost a century, but was seen for the first time in 1969 by Thorley [51]

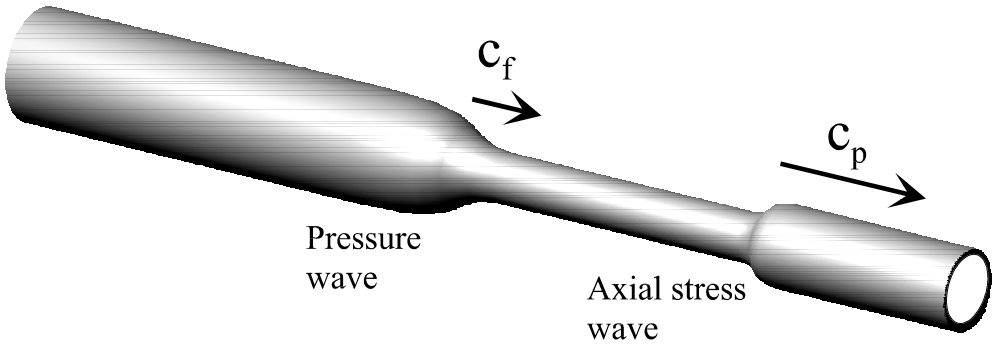

Figure 3.3: A view of the Poisson coupling, exaggerated.

3.5 Junction coupling

The junction coupling is modelled in the boundary conditions, where a junction is a place in the piping system where the flow changes direction or the cross sectional area changes(bend, T-connections etc.). The junction coupling works in two different ways:

1. Hydraulic pressure causes a force acting on the pipe (see Figure 3.4).
2. Structural displacement at junctions causes a change of volume in the pipe (see Figure 3.5).

Bending, axial and torsional movements are also coupled at junctions. These couplings exist whether or not the pipe is filled with fluid, and is taken care of in the FEM assembly through the transformation matrix. It is therefore not a coupling from a FSI point of view.

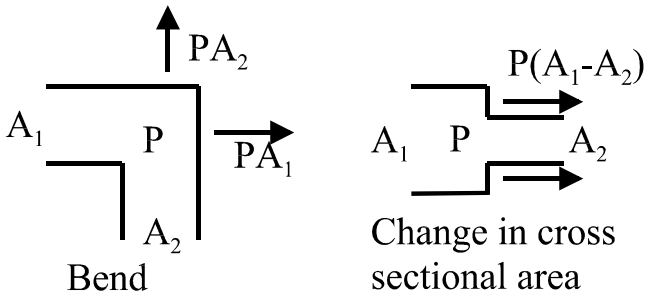

Figure 3.4: Junction coupling (pressure force)

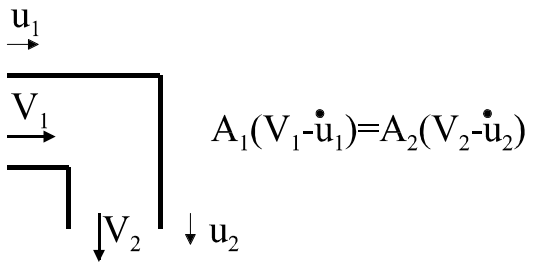

Figure 3.5: Junction coupling (continuity)

3.6 Summary

The extended waterhammer equations (four-equation model) for FSI in piping systems have been derived. An easy to grasp and correct picture is that the piping structure is described by (hollow) beams which can obtain bending, torsion and axial stress. The fluid is described by one-dimensional wave equations (Allievi's equations) tied to the pipes in lateral direction, but free to move in the axial direction. The coupling between fluid and structure is twofold:

- Pressure causing axial stress, and axial stress causing changes to the continuity relation (Poisson coupling).
- Pressure-forces and continuity at junctions (junction coupling).

The equations are valid for frequencies up to about 63% of the first radial fluid filled resonance frequency, hence they can be used for most practical piping layout applications.

In deriving the equations all friction forces were neglected. A discussion of friction models can be found in Chapter 5.

Chapter 4

FEM discretization

4.1 Basics

When using the finite element method a complicated continuum is divided into several manageable pieces called *elements*. These elements are connected to each other only at specified *nodes* at the boundary of each element. Within the elements several additional nodes may be specified. The functional value within the element is approximated as polynomial functions over the nodes. A first order one-dimensional element has two linear polynomials while a second order element has three square polynomials. Each of these polynomials are linearly independent, thus the polynomials for an $n'th$ order one-dimensional element spans out an $(n+1)$-dimensional space.

Looking at the pressure along a pipe the functional value in one element can be approximated as:

$$p(x) \approx \sum_{i=1}^{m} p_i n_i(x) \tag{4.1}$$

where m is the number of nodes. Setting $m = 2$ gives the polynomial approximation for a first order element:

$$p(x) \approx p_1 n_1(x) + p_2 n_2(x) = (1 - \frac{x}{l})p_1 + (\frac{x}{l})p_2 \tag{4.2}$$

where p_1 and p_2 are the values at the nodes and $n_1(x)$ and $n_2(x)$ are the polynomials. In matrix (vector) form Equation 4.2 becomes:

$$p(x) \approx \begin{bmatrix} (1 - \frac{x}{l}) & (\frac{x}{l}) \end{bmatrix} \begin{bmatrix} p_1 \\ p_2 \end{bmatrix} = \mathbf{N}^T \mathbf{p} \tag{4.3}$$

Taking the derivative of this equation with respect to x gives:

$$\frac{\partial p}{\partial x} \approx \begin{bmatrix} -\frac{1}{l} & \frac{1}{l} \end{bmatrix} \begin{bmatrix} p_1 \\ p_2 \end{bmatrix} = \frac{\partial \mathbf{N}^T}{\partial x}\mathbf{p} = \mathbf{N}_x^T \mathbf{p} \tag{4.4}$$

In addition the following constraints must be applied to achieve linear independence:

$$n_i^e(x) = 0 \quad \text{if } x \text{ not in element } e$$

$$n_i(x_j) = \delta ij$$

$$\sum_i n_i^e(x) = 1 \quad \text{for all } x \in e$$

This is the basis for all finite element methods. Since the functional value is approximated with polynomials it is obvious that the accuracy is increased with increasing degree of the polynomial. It is also obvious that increased accuracy is obtained by increasing the number of elements.

4.2 Fluid Structure Interaction

The particular discretization of the extended waterhammer equations (four-equation model) as presented in this thesis has not been found elsewhere in available literature. The FEM discretization is performed in the time-domain to obtain generality. Later, in Chapter 4.2.2, they are Laplace transformed to the frequency-domain as used in the computer program. Some extensions of this discretization for time-domain and stationary analysis of piping systems is given in Chapter 4.6.

4.2.1 Element equation

The starting point is Equation 3.19, Equation 3.20 and Equation 3.23. Taking the derivative of Equation 3.19 with respect to t and using Equation 3.20 after the derivative is taken with respect to x, together with Equation 3.23:

$$-EA_p\frac{\partial^2 u_x}{\partial x^2} + \rho_p A_p\frac{\partial^2 u_x}{\partial t^2} - A_p\rho_f g\frac{\nu R}{e}\frac{\partial H}{\partial x} = f_x(x,t) \tag{4.5}$$

$$-g\frac{\partial^2 H}{\partial x^2} + \frac{g}{c_f^2}\frac{\partial^2 H}{\partial t^2} - 2\nu\frac{\partial^3 u_x}{\partial x \partial t^2} = 0 \tag{4.6}$$

where

$$c_f^2 = \rho_f\left(\frac{1}{K} + \psi\frac{2R}{eE}\right) \tag{4.7}$$

The pressure P, is substituted with the pressure head H. These equations are equivalent with the so called *four-equation model* used for MOC, considering that stationary friction is neglected (actually, neglecting the stationary friction term make them valid only for dynamic calculations).

The equations are multiplied with an arbitrary weighting function, δ, and integrated in x direction from point a to point b:

$$-EA_p \int_a^b \delta \frac{\partial^2 u_x}{\partial x^2} dx + \rho_p A_p \int_a^b \delta \ddot{u}_x dx - A_p \rho_f g \frac{\nu R}{e} \int_a^b \delta \frac{\partial H}{\partial x} dx = \int_a^b \delta f_x(x,t) dx \tag{4.8}$$

$$-g \int_a^b \delta \frac{\partial^2 H}{\partial x^2} dx + \frac{g}{c_f^2} \int_a^b \delta \ddot{H} dx - 2\nu \int_a^b \delta \frac{\partial \ddot{u}_x}{\partial x} dx = 0 \tag{4.9}$$

Applying integration by parts:

$$EA_p \int_a^b \frac{\partial \delta}{\partial x} \frac{\partial u_x}{\partial x} dx + \rho_p A_p \int_a^b \delta \ddot{u}_x dx - A_p \rho_f g \frac{\nu R}{e} \int_a^b \delta \frac{\partial H}{\partial x} dx = \int_a^b \delta f_x(x,t) dx + EA_p \left[\delta \frac{\partial u}{\partial x} \right]_a^b \tag{4.10}$$

$$g \int_a^b \frac{\partial \delta}{\partial x} \frac{\partial H}{\partial x} dx + \frac{g}{c_f^2} \int_a^b \delta \ddot{H} dx - 2\nu \int_a^b \delta \frac{\partial \ddot{u}_x}{\partial x} dx = g \left[\delta \frac{\partial H}{\partial x} \right]_a^b \tag{4.11}$$

The last terms in Equation 4.10 and Equation 4.11 are the boundary conditions. The boundary condition $EA_p \left[\delta \frac{\partial u}{\partial x} \right]_a^b$ in Equation 4.10 can be included in the external force $\int_a^b \delta f_x(x,t) dx$, so this term is disregarded [13, Fiskvatn][1].

The directions of the variables are set as shown in Figure 4.1. Note, the positive direction of flow is out of the element and rising pressure is positive. The weighting function is substituted with the polynomial vector, $\mathbf{N}$, and the variables (pressure and displacement) are discretized as described in the previous chapter (Chapter 4.1).

$$H(x) \approx \mathbf{N}^T \mathbf{H} \quad u(x) \approx \mathbf{N}^T \mathbf{u}$$

This particular form of finite element formulation is called Galerkin formulation [77, Zienkiewicz]. Equation 4.12 and Equation 4.13 are therefore the Galerkin discretized equations:

$$gA_f \int_a^b \mathbf{N}_x \mathbf{N}_x^T dx \mathbf{H} + \frac{gA_f}{c_f^2} \int_a^b \mathbf{N}\mathbf{N}^T dx \ddot{\mathbf{H}} - 2\nu A_f \int_a^b \mathbf{N}\mathbf{N}_x^T dx \ddot{\mathbf{u}}_x = \begin{bmatrix} -\dot{Q}_a \\ -\dot{Q}_b \end{bmatrix} = -\dot{\mathbf{Q}} \tag{4.12}$$

[1] Both of these relations are sufficient boundary conditions in a mathematical sense. The difference between them is that the last term (integral relation), is *consistent*. This means that only node forces can be applied with the first relation, while *distributed* forces can be applied with the last. (i e. the pressure forces in equation 4.10).

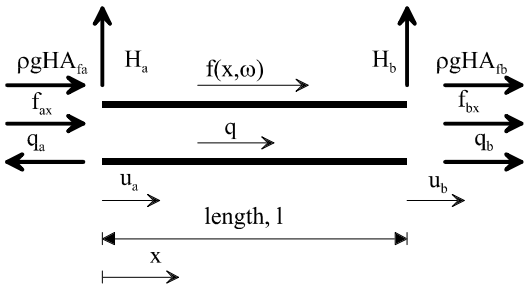

Figure 4.1: Definition of direction of the variables for one element

$$\begin{aligned} EA_p \int_a^b \mathbf{N}_x \mathbf{N}_x^T dx \mathbf{u}_x + \rho_p A_p \int_a^b \mathbf{N}\mathbf{N}^T dx \ddot{\mathbf{u}}_x \\ -A_p \rho_f g \frac{\nu R}{e} \int_a^b \mathbf{N}\mathbf{N}_x^T dx \mathbf{H} = \int_a^b \mathbf{N} f_x(x,t) dx \end{aligned} \tag{4.13}$$

These two equations have the Poisson coupling incorporated. The right hand side of Equation 4.12 is obtained as follows:

$$g\left[\delta \frac{\partial H}{\partial x}\right]_a^b = g\left[\mathbf{N}\frac{\partial H}{\partial x}\right]_a^b = \left(g\mathbf{N}\frac{\partial H}{\partial x}\right)_b - \left(g\mathbf{N}\frac{\partial H}{\partial x}\right)_a \tag{4.14}$$

Using the relation from Equation 3.20 ($\frac{\partial H}{\partial x} = -\frac{1}{A_f g}\frac{\partial Q}{\partial t}$) and the constraints for the polynomial functions ($n_i(x_j) = \delta ij$), Equation 4.14 reduces to

$$g\left[\mathbf{N}\frac{\partial H}{\partial x}\right]_a^b = -\frac{1}{A_f}\begin{bmatrix} 0 \\ 1 \end{bmatrix}\left(\frac{\partial Q}{\partial t}\right)_b + \frac{1}{A_f}\begin{bmatrix} 1 \\ 0 \end{bmatrix}\left(\frac{\partial Q}{\partial t}\right)_a \tag{4.15}$$

Now the direction of flow as given in Figure 4.1 ($Q_a = -Q$ and $Q_b = Q$) is applied:

$$g\left[\mathbf{N}\frac{\partial H}{\partial x}\right]_a^b = -\frac{1}{A_f}\begin{bmatrix} \frac{\partial Q}{\partial t} \\ \frac{\partial Q}{\partial t} \end{bmatrix} = -\frac{1}{A_f}\begin{bmatrix} \dot{Q}_a \\ \dot{Q}_b \end{bmatrix} \tag{4.16}$$

The boundary conditions in the form of the junction coupling also have to be incorporated. From Chapter 3.5 the junction coupling is the pressure forces and continuity at bends, T-connections etc.

The pressure forces are rather obvious, and are modelled as "external forces" acting on the structure. Looking at Figure 4.2 the forces acting on the pipe element when the pipe is free to move in x-direction but restricted in y-direction are:

$$f_{ha} = -\rho_f g A_{fa} H_a \quad ; \quad f_{hb} = \rho_f g A_{fb} H_b \tag{4.17}$$

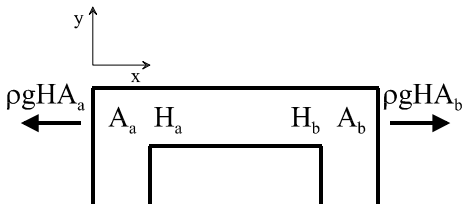

Figure 4.2: Pressure forces at junctions for an element with junction in both ends

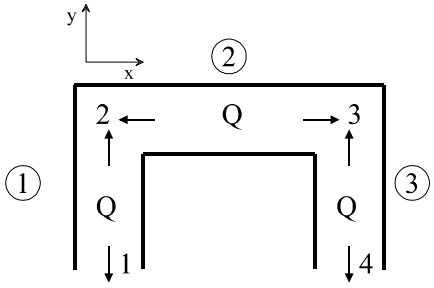

Figure 4.3: Piping system with 3 elements and 4 nodes showing continuity at nodes.

These forces are added to the external forces whenever the cross-sectional area changes. Since they are functions of the pressure they are put in the appropriate place on the left hand side of the equality sign.

The continuity at junctions is not that obvious. This is because of the way the matrices are constructed and the direction and choice of the variables. Considering the system in Figure 4.3 as a pure hydraulic system (no FSI), then, since the nodes are points (control volume equals zero) and the direction of the flow is *out* of each element, the following matrix equation describing the system must be valid[2]:

$$\mathbf{M}\begin{bmatrix}\ddot{H}_1\\ \ddot{H}_2\\ \ddot{H}_3\\ \ddot{H}_4\end{bmatrix}+\mathbf{K}\begin{bmatrix}H_1\\ H_2\\ H_3\\ H_4\end{bmatrix}=-\frac{\partial}{\partial t}\begin{bmatrix}Q_{11}\\ Q_{12}+Q_{22}\\ Q_{23}+Q_{33}\\ Q_{34}\end{bmatrix}= \tag{4.18}$$

$$-\frac{\partial}{\partial t}\begin{bmatrix}Q_{11}\\ Q_{12}-\tilde{Q}_{22}\\ Q_{23}-\tilde{Q}_{33}\\ Q_{34}\end{bmatrix}=-\frac{\partial}{\partial t}\begin{bmatrix}Q_{11}\\ 0\\ 0\\ Q_{34}\end{bmatrix}$$

where $\mathbf{M}$ and $\mathbf{K}$ are general 4x4 matrices describing the hydraulic system. The

[2]This matrix equation can be obtained from equation 4.12 by setting the Poisson number to zero.

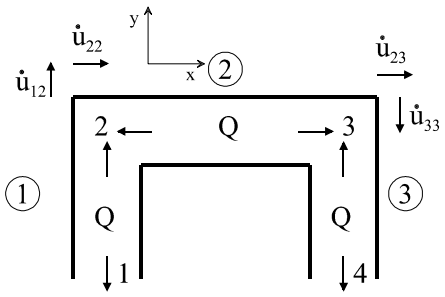

Figure 4.4: Piping system with 3 elements and 4 nodes. Constrained to move at node 1 and 4.

subscript Q_{ij} means "flow at element number i, node number j" and $\tilde{Q}_{ij} = -Q_{ij}$ similar to Equation 4.16 ($\tilde{Q}_{ij} = -Q_{ij}$ when on the left node of the element, positive direction of flow is in negative x-direction).

Now FSI is included, which means that the relation in Figure 3.5 must be added to the continuity relation on the right hand side of Equation 4.18. From Figure 3.5 and Figure 4.4 the continuity at junction 2 and 3 will be:

$$(Q_{12} - A_{f12}\dot{u}_{12}) - (\tilde{Q}_{22} - A_{f22}\dot{u}_{22}) = 0 \Rightarrow Q_{12} - \tilde{Q}_{22} = A_{f12}\dot{u}_{12} - A_{f22}\dot{u}_{22}$$

$$(Q_{23} - A_{f23}\dot{u}_{23}) - (\tilde{Q}_{33} - A_{f33}\dot{u}_{33}) = 0 \Rightarrow Q_{23} - \tilde{Q}_{33} = A_{f23}\dot{u}_{23} - A_{f33}\dot{u}_{33}$$

Inserting these relations into the right hand side of Equation 4.18 gives:

$$-\frac{\partial}{\partial t}\begin{bmatrix} Q_{11} \\ Q_{12} - \tilde{Q}_{22} \\ Q_{23} - \tilde{Q}_{33} \\ Q_{34} \end{bmatrix} = -\frac{\partial}{\partial t}\begin{bmatrix} Q_{11} \\ A_{f12}\dot{u}_{12} - A_{f22}\dot{u}_{22} \\ A_{f23}\dot{u}_{23} - A_{f33}\dot{u}_{33} \\ Q_{34} \end{bmatrix} = \tag{4.19}$$

$$\begin{bmatrix} -\dot{Q}_{11} \\ -A_{f12}\ddot{u}_{12} + A_{f22}\ddot{u}_{22} \\ -A_{f23}\ddot{u}_{23} + A_{f33}\ddot{u}_{33} \\ -\dot{Q}_{34} \end{bmatrix} \quad \begin{matrix} \text{rearranging} \\ A_f \text{ terms to the left side} \\ \Longrightarrow \end{matrix} \quad \begin{bmatrix} -\dot{Q}_{11} \\ 0 \\ 0 \\ -\dot{Q}_{34} \end{bmatrix}$$

The parts of the continuity relations that are functions of the displacements are set on the left hand side. The terms of $\ddot{u}$ must be transferred to the left hand side by setting the term with first index equal to 1 into the appropriate place of the first element and so on. For example, the term $-A_{f12}\ddot{u}_{12}$ becomes a A_{f12} term at the place in the mass matrix where it is multiplied with $\ddot{u}_{12}$. (see Equation 4.22 and Equation 4.25). Doing this also assures that the flow vector has zeroes everywhere except at nodes where flow enters or leaves the system.

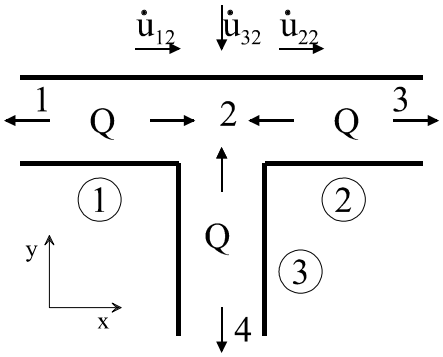

Figure 4.5: T connection, free to move only at node 2.

To show that this approach also is valid for branches and loops, consider the T-connection in Figure 4.5. The continuity at node 2 is described by:

$$(Q_{12} - A_{f12}\dot{u}_{12}) - (\tilde{Q}_{22} - A_{f22}\dot{u}_{22}) - (\tilde{Q}_{32} - A_{f32}\dot{u}_{32}) = 0$$

$$Q_{12} - \tilde{Q}_{22} - \tilde{Q}_{32} = A_{f12}\dot{u}_{12} - A_{f22}\dot{u}_{22} - A_{f32}\dot{u}_{32}$$

The hydraulic equations describing this system are:

$$\begin{gathered}\mathbf{M}\begin{bmatrix}\ddot{H}_1\\ \ddot{H}_2\\ \ddot{H}_3\\ \ddot{H}_4\end{bmatrix} + \mathbf{K}\begin{bmatrix}H_1\\ H_2\\ H_3\\ H_4\end{bmatrix} = \\ -\frac{\partial}{\partial t}\begin{bmatrix}Q_{11}\\ Q_{12}+Q_{22}+Q_{32}\\ Q_{23}\\ Q_{34}\end{bmatrix} = -\frac{\partial}{\partial t}\begin{bmatrix}Q_{11}\\ Q_{12}-\tilde{Q}_{22}-\tilde{Q}_{32}\\ Q_{23}\\ Q_{34}\end{bmatrix}\end{gathered} \tag{4.20}$$

thus the right hand side becomes:

$$-\frac{\partial}{\partial t}\begin{bmatrix}Q_{11}\\ Q_{12}-\tilde{Q}_{22}-\tilde{Q}_{32}\\ Q_{23}\\ Q_{34}\end{bmatrix} = -\frac{\partial}{\partial t}\begin{bmatrix}Q_{11}\\ A_{f12}\dot{u}_{12}-A_{f22}\dot{u}_{22}-A_{f32}\dot{u}_{32}\\ Q_{23}\\ Q_{34}\end{bmatrix} \tag{4.21}$$

Moving all the u terms to the left side assures continuity at node 2.

With all the couplings in place the equation for one element becomes (Equation

4.12 and Equation 4.13):

$$\begin{bmatrix} gA_f\mathbf{K}' & 0 \\ -\mathbf{C}_1 & EA_p\mathbf{K}' \end{bmatrix} \begin{bmatrix} \mathbf{H} \\ \mathbf{u} \end{bmatrix} + \begin{bmatrix} \frac{A_f g}{c_f^2}\mathbf{M}' & \mathbf{C}_2 \\ 0 & \rho_p A_p \mathbf{M}' \end{bmatrix} \begin{bmatrix} \ddot{\mathbf{H}} \\ \ddot{\mathbf{u}} \end{bmatrix} = \begin{bmatrix} -\dot{\mathbf{Q}} \\ \int_e \mathbf{N}\mathbf{f}(x,t)dx \end{bmatrix} \tag{4.22}$$

where the sub-matrices are defined as:

$$\mathbf{K}' = \int_a^b \mathbf{N}_x\mathbf{N}_x^T dx \qquad \mathbf{M}' = \int_a^b \mathbf{N}\mathbf{N}^T dx \tag{4.23}$$

$$\mathbf{C}_1 = \frac{A_p\rho_f g\nu R}{e}\int_a^b \mathbf{N}\mathbf{N}_x^T dx - \rho_f g \begin{bmatrix} -A_{fa} & \cdot & 0 \\ \cdot & 0_{n-1} & \cdot \\ 0 & \cdot & A_{fb} \end{bmatrix} \tag{4.24}$$

$$\mathbf{C}_2 = -2\nu A_f \int_a^b \mathbf{N}\mathbf{N}_x^T dx - \begin{bmatrix} A_{fa} & \cdot & 0 \\ \cdot & 0_{n-1} & \cdot \\ 0 & \cdot & -A_{fb} \end{bmatrix} \tag{4.25}$$

- $\mathbf{C}_1$ is the Poisson coupling from pressure to displacement and pressure based junction coupling.
- $\mathbf{C}_2$ is the Poisson coupling from displacement to pressure and the continuity based junction coupling.
- The Poisson coupling is distributed, i.e. it works along the pipe while the junction coupling only works at the nodes.
- The equation is valid also for branches and loops.

Note, different units in the matrices and the force vector.

4.2.2 Frequency-domain

The transformation to the frequency-domain is straightforward. Assuming harmonic motion Equation 4.22 is Laplace transformed to the frequency-domain [47, Svingen] as follows:

$$\begin{bmatrix} gA_f\mathbf{K}' & 0 \\ -\mathbf{C}_1 & EA_p\mathbf{K}' \end{bmatrix} \begin{bmatrix} \mathbf{h} \\ \mathbf{u} \end{bmatrix} + s^2 \begin{bmatrix} \frac{A_f g}{c_f^2}\mathbf{M}' & \mathbf{C}_2 \\ 0 & \rho_p A_p \mathbf{M}' \end{bmatrix} \begin{bmatrix} \mathbf{h} \\ \mathbf{u} \end{bmatrix} = \begin{bmatrix} -s\mathbf{q} \\ \int_e \mathbf{N}\mathbf{f}(x,\omega)dx \end{bmatrix} \tag{4.26}$$

where $s = j\omega$ and the sub-matrices are as defined in Equation 4.23 to Equation 4.25. This equation is used in the calculations of eigenvalues, eigenvectors and in frequency response analysis. Damping is assumed as stiffness-proportional Rayleigh damping [33, Petyt]. The damping matrix is therefore proportional to the first matrix in Equation 4.26.

$$\begin{bmatrix} gA_f\mathbf{K}' & 0 \\ -\mathbf{C}_1 & EA_p\mathbf{K}' \end{bmatrix} \begin{bmatrix} \mathbf{h} \\ \mathbf{u} \end{bmatrix} + s \begin{bmatrix} \beta_f\left(gA_f\mathbf{K}'\right) & \\ & \beta_p\left(EA_p\mathbf{K}'\right) \end{bmatrix} \begin{bmatrix} \mathbf{h} \\ \mathbf{u} \end{bmatrix} + s^2 \begin{bmatrix} \frac{A_f g}{c_f^2}\mathbf{M}' & \mathbf{C}_2 \\ & \rho_p A_p \mathbf{M}' \end{bmatrix} \begin{bmatrix} \mathbf{h} \\ \mathbf{u} \end{bmatrix} = \begin{bmatrix} -s\mathbf{q} \\ \int_e \mathbf{N}\mathbf{f}(x,\omega)dx \end{bmatrix} \tag{4.27}$$

where β_f and β_p are the fluid and structural frequency-dependent damping constants (see Chapter 5).

4.3 Complete element matrix

The equations in the previous chapter (Chapter 4.2.1) describe the fluid and the axial structural motion as well as all the FSI couplings involved. The complete element matrix must also include bending and torsion given by the equations in Chapter 3.3. The Finite Element discretization of these equations is straight forward and similar to the discretization of the extended waterhammer equations. The main difference is in the discretization of bending where third-order Hermitian polynomials are used [33]. The derivatives are then used as additional degrees of freedom. For bending the rotational displacement $\theta_{yz} = \frac{\partial w_{yz}}{\partial x}$ is the extra degree of freedom (see Appendix D). This means that a beam element with two nodes has four degrees of freedom. The complete element matrix will be:

$$\begin{bmatrix} \mathbf{K}_f & & & \\ -\mathbf{C}_1 & \mathbf{K}_a & & \\ & & \mathbf{K}_b & \\ & & & \mathbf{K}_t \end{bmatrix} \begin{bmatrix} \mathbf{h} \\ \mathbf{u}_a \\ \mathbf{u}_b \\ \mathbf{u}_t \end{bmatrix} + s \begin{bmatrix} \beta_f\mathbf{K}_f & & & \\ & \beta_p\mathbf{K}_a & & \\ & & \beta_p\mathbf{K}_b & \\ & & & \beta_p\mathbf{K}_t \end{bmatrix} \begin{bmatrix} \mathbf{h} \\ \mathbf{u}_a \\ \mathbf{u}_b \\ \mathbf{u}_t \end{bmatrix} + s^2 \begin{bmatrix} \mathbf{M}_f & \mathbf{C}_2 & & \\ & \mathbf{M}_a & & \\ & & \mathbf{M}_b & \\ & & & \mathbf{M}_t \end{bmatrix} \begin{bmatrix} \mathbf{h} \\ \mathbf{u}_a \\ \mathbf{u}_b \\ \mathbf{u}_t \end{bmatrix} = \begin{bmatrix} -s\mathbf{q} \\ \mathbf{f}_x \\ \mathbf{f}_b \\ \mathbf{m}_t \end{bmatrix} \tag{4.28}$$

For first order elements (linear elements) the element matrices will be of dimension 14 x 14 (see Figure 4.6). In a computer program it will be more practical to put all the indexes belonging to the same node in line in the "displacement" and "force" vector. The reason for this is to obtain consistence in the transformation presented

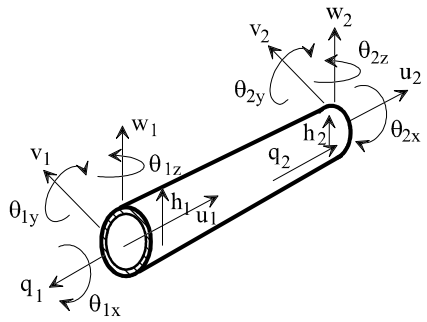

Figure 4.6: Degrees of freedom for a first order element.

in the next chapter (Chapter 4.4). The modified element equation will be on the form:

$$\mathbf{Ku}+s\mathbf{Du}+s^2\mathbf{Mu}=\mathbf{f} \tag{4.29}$$

where

$$\mathbf{u}^T=[u_{x1},u_{y1},u_{z1},\theta_{x1},\theta_{y1},\theta_{z1},h_1,u_{x2},u_{y2},u_{z2},\theta_{x2},\theta_{y2},\theta_{z2},h_2] \tag{4.30}$$

$$\mathbf{f}^T=[f_{x1},f_{y1},f_{z1},m_{x1},m_{y1},m_{z1},-sq_1,f_{x2},f_{y2},f_{z2},m_{x2},m_{y2},m_{z2},-sq_2] \tag{4.31}$$

and the force, moment and torsion terms in Equation 4.31 are made from the consistent load vector (integral formulation).

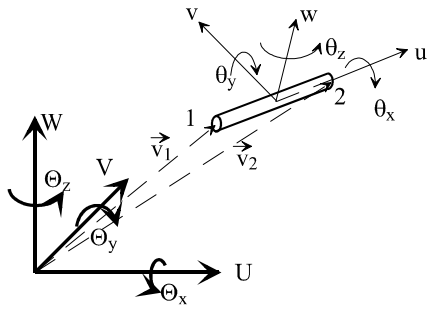

Figure 4.7: Transformation of a pipe element.

4.4 Global system

Since the geometry for each element is described in local coordinates, each element must be transformed to global coordinates (see Figure 4.7). This transformation is done with a so-called transformation matrix relating the local and global coordinates by cosine relations [33]. The transformation matrix is built using the vectors $\vec{v}_1$ and $\vec{v}_2$ from Figure 4.7 and an arbitrary vector $\vec{v}_3$ orienting the local yz-axes. The transformation is defined such that:

$$\mathbf{u} = \mathbf{RU} \quad and \quad \mathbf{f} = \mathbf{RF}$$

where capital letters are the global coordinates. The indexes belonging to pressure-pressure terms ($R_{7,7}$ and $R_{14,14}$) are set to 1, and the rest of the corresponding row and column are set to zero to assure that the pressure is not transformed. Using this relation in Equation 4.29:

$$\mathbf{KRU}+s\mathbf{DRU} + s^2\mathbf{MRU} = \mathbf{RF} \tag{4.32}$$

Equation 4.32 is pre-multiplied by the inverse transformation which is equal to the transposed matrix because of orthogonality:

$$\mathbf{R}^T\mathbf{KRU}+s\mathbf{R}^T\mathbf{DRU} + s^2\mathbf{R}^T\mathbf{MRU} = \mathbf{R}^T\mathbf{RF} = \mathbf{F} \tag{4.33}$$

thus giving the complete element matrix in global coordinates

$$\mathbf{K}_g\mathbf{U}+s\mathbf{D}_g\mathbf{U} + s^2\mathbf{M}_g\mathbf{U} = \mathbf{F} \tag{4.34}$$

It should be noted that this transformation also transforms the terms in the junction and Poisson coupling to appropriate global coordinates.

Assembling the global system matrices is done using standard procedures. For example, an element with global node numbers n_1 and n_2, then columns 1 to 7 are added into column $(7n_1 - 6)$ to $7n_1$ in the global matrices and columns 8 to 14 are added into columns $(7n_2 - 6)$ to $7n_2$. The rows are added in an identical manner.

4.5 Solving

4.5.1 Eigenvalues

Eigenvalues can be found in two ways

1. Setting the damping matrix and force vector to zero and solving the generalized eigenvalue problem ($\mathbf{K}_g\mathbf{U} = \omega^2\mathbf{M}_g\mathbf{U}$).

2. Setting only the force term to zero and do a determinant scan to find the resonant frequencies.

The first method is the easiest and fastest one. Highly efficient and accurate routines can be used [42, LAPACK], and both the eigenvalues (resonant frequencies) and eigenvectors (shape functions) are solved simultaneously, ($\det[\mathbf{K}_g - \omega^2\mathbf{M}_g] = 0$).

In some cases the damping matrix must be included. Valves, orifices etc. are all components included in the damping matrix, as shown in Chapter 6. A determinant scan is a method of obtaining the complex resonant-frequencies. According to linear algebra the resonant-frequencies are defined when the determinant of the *system matrix* is zero. The matrix Equation 4.34 have resonant-frequencies for ω where:

$$\det\left[\mathbf{K}_g + j\omega\mathbf{D}_g - \omega^2\mathbf{M}_g\right] = 0 \tag{4.35}$$

A scan is done by solving the determinant for a range of ω, and marking the frequencies where the determinant is zero or close to zero by a specified margin. When a desired number of frequencies are found, the corresponding eigenvectors are computed.

$$\left[\mathbf{K}_g + j\omega\mathbf{D}_g - \omega^2\mathbf{M}_g\right]\mathbf{U} = 0 \tag{4.36}$$

Since the trivial solution *always* is a solution, the eigenvectors are computed by setting an arbitrary index in the $\mathbf{U}$ vector equal to 1. The rest of the $\mathbf{U}$ vector is then found and each index will have relative values with respect to the one decided. The complex resonance frequencies will have the form:

$$\omega_c = \sigma + j\omega$$

where σ is the relative damping coefficient. This method can also be done in self-excitation analysis as described in [3, Brekke and Svingen] and [44, Svingen]. If σ has a positive value, the system is unstable (self-excitation).

4.5.2 Frequency response

Frequency response calculations are done with the use of Equation 4.34, setting all the numerical values in the force vector equal to zero except at the node where the

excitation is set. The matrix system:

$$\left[\mathbf{K}_g + s\mathbf{D}_g + s^2\mathbf{M}_g\right]\mathbf{U} = \mathbf{F}$$

is then solved for all frequencies of interest, and the results are the responses (amplitude and phase) for all nodes in the system. The excitation can for example be a pulsating pressure or flow. More interesting calculations can be done when other hydraulic components are included. In the calculations in Chapter 7.1 later in the thesis, an oscillating valve is used. In Chapter 6, other piping components are described.

4.6 Stationary and modal analysis

This chapter includes two additional extensions of the FEM discretization for use in stationary and dynamic hydraulic analysis. The method for stationary analysis have been presented by Brekke, but with some difference in deriving. Modal analysis in time-domain with FEM using the variables q and h have not been found in available literature, and is verified in Chapter 5 with experiments and calculations from literature.

4.6.1 Steady state solution

Stationary fluid analysis is obtained using the Allievi's equations with a stationary friction term. Exactly the same equations have been obtained by Professor Hermod Brekke at NTNU using the structure matrix method [lecture notes]:

$$\frac{\partial h}{\partial x} + \frac{1}{gA}\frac{\partial q}{\partial t} + \frac{f\,|q_0|}{2gDA^2}q = 0 \tag{4.37}$$

$$\frac{\partial q}{\partial x} + \frac{gA}{a^2}\frac{\partial h}{\partial t} = 0 \tag{4.38}$$

The time dependent terms are discarded and the derivative of Equation 4.37 is taken with respect to x.

$$\frac{\partial^2 h}{\partial x^2} + \frac{f\,|q_0|}{2gDA^2}\frac{\partial q}{\partial x} = 0 \tag{4.39}$$

$$\frac{\partial q}{\partial x} = 0 \tag{4.40}$$

The term $|q_0|$ is regarded as an iteration constant. Combining these equations:

$$\frac{\partial^2 h}{\partial x^2} = 0 \tag{4.41}$$

Applying Galerkin discretization in the same manner as presented in Chapter 4.2.1, and integrating from $x = 0$ to $x = L$:

$$\int_0^L \mathbf{N}_x \mathbf{N}_x^T dx \mathbf{h} = -\frac{f\,|q_0|}{2gDA^2}\mathbf{q} \tag{4.42}$$

Since for stationary flows the pressure drop is linear along a pipe, dividing each pipe into one element will give the exact results. After some algebra the following element matrix, or rather pipe matrix, is obtained:

$$\begin{bmatrix} k & -k \\ -k & k \end{bmatrix} \begin{bmatrix} h_1 \\ h_2 \end{bmatrix} = - \begin{bmatrix} q_1 \\ q_2 \end{bmatrix} \tag{4.43}$$

where

$$k = \frac{2gDA^2}{f\,|q_0|}$$

Assembling the system matrix is done in standard FEM manner, see for instance [77]. Since the system is nonlinear an iteration procedure must be done. One possible method of iteration is to guess the flow for each pipe. The pressures are calculated using the global system matrix. With the element equations new and (hopefully) more correct values of q is calculated. These values are then set into the iteration constant for a new calculation until some criteria are met.

4.6.2 Modal analysis

Modal analysis is a frequently used method in structural vibration analysis to calculate responses of a continuous system subjected to an arbitrary forcing condition [75]. In modal analysis the expansion theorem[3] is used to uncouple the coupled equation of motion. The main advantage by this uncoupling is that a matrix system reduces to a *set of uncoupled ordinary second order differential equations* that can easily be solved without using matrix solvers. In fact the whole solution can be made analytically when the function(s) on the right hand side is/are known.

Eigenvectors and eigenvalues for the undamped global system, Equation 4.44, are found and set into a $\mathbf{\Phi}$ and $\mathbf{\Lambda}$ matrix respectively.

$$-\omega^2 \mathbf{M}\mathbf{h} + \mathbf{K}\mathbf{h} = \dot{\mathbf{q}} \tag{4.44}$$

Each column, n, of $\mathbf{\Phi}$ is the eigenvector corresponding to the eigenvalue at index (n,n) in the diagonal eigenvalue (resonant frequency) matrix, $\mathbf{\Lambda}$. The generalized pressure is defined as:

$$\mathbf{h} = \mathbf{\Phi}\boldsymbol{\eta} \tag{4.45}$$

[3]The expansion theorem is based on the orthogonality of eigenvectors.

Setting Equation 4.45 into Equation 4.44 and pre-multiplying with the inverse (transposed because of orthogonality) eigenvector matrix gives:

$$\mathbf{\Phi}^T\mathbf{M}\mathbf{\Phi}\ddot{\boldsymbol{\eta}} + \mathbf{\Phi}^T\mathbf{K}\mathbf{\Phi}\boldsymbol{\eta} = \mathbf{\Phi}^T\dot{\mathbf{q}} \tag{4.46}$$

Here the eigenvector matrix is scaled[4] so that the diagonal matrix $\mathbf{\Phi}^T\mathbf{M}\mathbf{\Phi}$ becomes the identity matrix, $\mathbf{I}$. The system then becomes:

$$\mathbf{I}\ddot{\boldsymbol{\eta}} + \mathbf{\Lambda}\boldsymbol{\eta} = \mathbf{\Phi}^T\dot{\mathbf{q}} \tag{4.47}$$

This system is now completely uncoupled, and can readily be solved. A very important fact is that Equation 4.47 is equivalent to Equation 4.44. The physical pressure head is calculated using Equation 4.45. This function will be a sum of n sine functions.

When Rayleigh damping (see Chapter 5) is used, the eigenvector-matrix which diagonalizes the $\mathbf{K}$ and $\mathbf{M}$ matrices, also diagonalizes the $\mathbf{C}$ matrix due to proportionality.

$$\mathbf{C} = \alpha\mathbf{M} + \beta\mathbf{K}$$

$$\mathbf{\Phi}^T\mathbf{C}\mathbf{\Phi} = \mathbf{\Phi}^T\left[\alpha\mathbf{M} + \beta\mathbf{K}\right]\mathbf{\Phi} = \alpha\mathbf{\Phi}^T\mathbf{M}\mathbf{\Phi} + \beta\mathbf{\Phi}^T\mathbf{K}\mathbf{\Phi}$$

$$\mathbf{\Phi}^T\mathbf{C}\mathbf{\Phi} = \alpha\mathbf{I} + \beta\mathbf{\Lambda} \tag{4.48}$$

The complete system with stationary and frequency-dependent friction then becomes:

$$\mathbf{I}\ddot{\boldsymbol{\eta}} + \left(\alpha\mathbf{I} + \beta\mathbf{\Lambda}\right)\dot{\boldsymbol{\eta}} + \mathbf{\Lambda}\boldsymbol{\eta} = \mathbf{\Phi}^T(\dot{\mathbf{q}} + \alpha\mathbf{q}) \tag{4.49}$$

Strictly speaking it is necessary that α and β have the same values for all different pipes in the system to be able to uncouple all the equations, because the global damping matrix $\mathbf{\Phi}^T\mathbf{C}\mathbf{\Phi}$ is only diagonal as long as it is a sum of the *global* $\mathbf{M}$ and $\mathbf{K}$ matrices. How strict this requirement for similar α and β values for all the different pipes in a system with respect to accuracy is, is not known. The time-domain examples in Chapter 5 are calculated with modal analysis, and compared with calculations made with MOC. It is obvious from the derivation of the method that it is a method for analysis of "pure" dynamic systems (oscillations about a steady state solution, or linear systems), and not well suited for general transient calculations with non-linearities.

4.6.3 Direct solution with FSI

For general transient *time-domain* calculations of FSI in piping systems a direct solution similar to the one presented in [72, Xianglin et al.] is probably preferable

[4] $\mathbf{\Phi}$ is the *orthonormal* eigenvector matrix, and $\mathbf{\Lambda}$ is the eigenvalue matrix.

compared to a somewhat restrictive modal analysis. Here an ordinary FEM discretization must be done on the extended waterhammer equations. The solution process and discretization of Equation 4.50, Equation 4.51 and 4.52 can be done in many ways. An iteration procedure is described in [72, Xianglin].

$$\frac{1}{A_f}\frac{\partial q}{\partial t} + g\frac{\partial H}{\partial x} = -\frac{f\,|Q_{rel}|\,Q_{rel}}{4R} \tag{4.50}$$

$$\frac{1}{A_f}\frac{\partial q}{\partial x} + \frac{g}{c_f^2}\frac{\partial H}{\partial t} = 2\nu\frac{\partial^2 u_x}{\partial x \partial t} \tag{4.51}$$

$$-EA_p\frac{\partial^2 u_x}{\partial x^2} + \rho_p A_p\frac{\partial^2 u_x}{\partial t^2} = f_x(x,t) + A_p\rho_f g\frac{\nu R}{Ee}\frac{\partial H}{\partial x} + \frac{f\rho_f A_f\,|Q_{rel}|\,Q_{rel}}{4R} \tag{4.52}$$

4.7 Summary

The FEM discretization presented herein is based on ordinary Galerkin formulations. The coupled fluid and structural equations are discretized in a manner which makes analysis of large systems easy and straightforward. This is done by setting the flow and pressure variables in the same relative positions as in the Structure Matrix Method. Doing this assures that continuity at branches and loops is maintained, and also assures that the including of hydraulic piping elements as described in [2, Brekke] can be done with only minor modifications. Poisson and junction coupling is included.

Emphasis is made on frequency-domain FSI analysis, but extensions in using FEM for stationary modal analysis is given.

The flow vector $\mathbf{q}$ on the right hand side of the FSI matrix equations is multiplied with a factor $-s$. For pure hydraulic analysis it would be natural to divide by $-s$ on both sides of the equality sign to get all the s-dependent terms on the left hand side. By looking at Equation 4.27 one can see that this will cause different dependence on s for the fluid and structural matrices in the FSI analysis, and thus requiring global assembling of the matrices for every ω in a frequency response analysis. It will also be impossible to use standard eigenvalue routines because of inconsistent mass and stiffness matrices. Retaining the $-s$ on the right hand side in front of the $\mathbf{q}$ vector assures that the *global* fluid and structural matrices can be assembled *one time only* in a frequency-domain analysis, thus greatly improving calculation speed compared with global assembling for every frequency. It also makes it possible to use existing matrix eigenvalue solvers. Mathematically these two forms are of course equivalent.

Chapter 5

Friction

steady state friction given by the Moody chart does not give correct damping for oscillations of increasing frequency, and consequently some kind of frequency-dependent damping must be included.

Several scientists have been, and still are, working on this subject. In time-domain the work of Zielke [76] is being modified and extended for use in calculation of turbulent flow by Vardy and Brown [60]. Another approach is to assume that the transient friction is proportional to the instantaneous acceleration [60]. Eichinger [11] used a two-dimensional approach by calculating the friction at every cross section with the use of turbulence modelling and using MOC for the axial velocities. In the frequency-domain the work of Köngeter [25], making the frequency-dependent friction a function of frequency and amplitude, is well known. Unsteady turbulent friction in large diameter tunnels have been developed by Brekke [2]. Krus et al.[26] proposed a frequency-dependent friction model valid for both frequency and time-domain. An approach based on complex frequency-dependent wave speed is given in Wylie and Streeter [71].

A common denominator with all pipe friction models for turbulent flow (steady state *and* transient) is that they all must be based on experimental data and empirical equations (Moody chart and/or empirical formulas for steady state calculations). This is so, because the pipe flow equations are one-dimensional, while the turbulent friction is inherently a three-dimensional phenomenon. Just as in three-dimensional fluid flow where one divides clearly between the physical turbulence and turbulence models used to approximate the Reynolds stress tensor, one has to divide between physical transient friction and friction models in turbulent pipe flow. Within this content the Moody chart can be looked upon as a turbulence model for *steady state pipe flow*. Although this is a rather trivial observation [64, White],[1] it is important to note that it is a model *only* valid for steady state flow. The generation of

[1]Indeed the Moody friction is deduced from the turbulent stress term $-\rho\overline{u'v'}$ through the logarithmic law.

turbulent friction through *velocity- and pressure changes* is not modelled.

In this chapter a hydraulic friction model based on Rayleigh damping is presented. Both the steady state Moody friction and a dynamic friction term is modelled. For frequency-domain FSI calculations, a Rayleigh based frequency-dependent friction will greatly simplify the calculations because it can be used on both fluid and structure, and because Rayleigh damping does not complicate the solution process in any way. A physical interpretation is also given.

An analytical time-domain solution to the linearized Allievi's equations with frequency-dependent friction is found, and a discretization procedure for use with the Method of Characteristics (MOC) is presented.

5.1 Proportional damping

Proportional damping, or Rayleigh damping, is an accepted and widely used damping model for structural calculations [33]. For dynamic pipe flow calculations, Rayleigh damping is not used at all (at least not as a physical damping model to the authors knowledge). The reason for this is that Finite Element Analysis (FEA) is seldom used for transient pipe flow, thus other damping models have emerged.

Rayleigh damping consists of a linear combination of the mass and stiffness matrix:

$$\mathbf{C} = \alpha\mathbf{M} + \beta\mathbf{K} \tag{5.1}$$

The constants α and β generally have to be determined experimentally. The physical interpretation of Rayleigh damping in structural analysis is that the mass proportional term is the damping for solid body movement and is independent of frequency[2]. The stiffness proportional term is interpreted as the internal, or structural damping, and increases with increasing frequency.

Visualization of the frequency dependence in Rayleigh damping is best achieved with modal analysis. From Chapter 4.6.2 the flow equation using the generalized pressure vector is:

$$\mathbf{I}\ddot{\boldsymbol{\eta}} + (\alpha\mathbf{I} + \beta\boldsymbol{\Lambda})\,\dot{\boldsymbol{\eta}} + \boldsymbol{\Lambda}\boldsymbol{\eta} = \boldsymbol{\Phi}^T(\dot{\mathbf{q}} + \alpha\mathbf{q}) \tag{5.2}$$

where

$$\mathbf{h} = \boldsymbol{\Phi}\boldsymbol{\eta} \tag{5.3}$$

and $\boldsymbol{\Phi}$ and $\boldsymbol{\Lambda}$ are the eigenvector matrix and the diagonal eigenvalue matrix respectively. Since the system is uncoupled, each mode can be described by:

$$\ddot{\eta}_r + \alpha\dot{\eta}_r + \beta\omega_r^2\dot{\eta}_r + \omega_r^2\eta = Q_r \tag{5.4}$$

[2] Actually the mass proportional damping decreases with increasing frequency, but the general frequency dependence is very small compared to the stiffness proportional term.

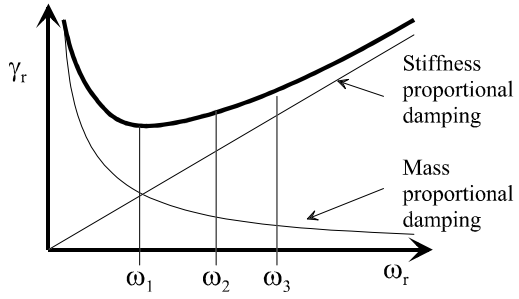

Figure 5.1: Typical variation of damping ratio as a function of the resonant frequency (exaggerated).

Then from basic vibration analysis with viscous damping:

$$\ddot{\eta}_r + 2\gamma_r\omega_r\dot{\eta}_r + \omega_r^2\eta = Q_r \tag{5.5}$$

where

$$2\gamma_r\omega_r = \alpha + \omega_r^2\beta \tag{5.6}$$

and γ_r is the modal damping ratio where the damping ratio is defined as the ratio of the damping constant to the critical damping constant. For each resonant frequency, or each mode, the damping ratio for the $r'th$ undamped resonant frequency is defined as [35]:

$$\gamma_r = \frac{\alpha}{2}\frac{1}{\omega_r} + \frac{\beta}{2}\omega_r \tag{5.7}$$

Looking at Equation 5.7 the only variable is the frequency, ω_r. A typical graph from Equation 5.7 is plotted in Figure 5.1 which shows that the damping ratio increases with increasing frequency, until the system eventually can become overdamped for the highest modes. Strictly speaking the graph in Figure 5.1 is only valid for systems that can be uncoupled, because it is impossible to find separate γ values for a coupled system (at least analytically). However it is obvious that a coupled system has the same variation in its sub-matrices with equal α and β values, thus the complete system will also have the same overall variation. The *friction or damping constant* for each mode is given in Equation 5.8:

$$c_r = \alpha + \omega_r^2\beta \tag{5.8}$$

5.2 Proportional fluid damping

Before deriving the proportional damping for hydraulics it is necessary to emphasize that the *main reason* for using this particular damping model is that it simplifies the FSI calculations *considerably*, because the same damping model is used for both fluid and structure. Another reason is that the results are good compared with experiments. It was first used by the author [45, Svingen], without paying very much attention to the physical interpretation or meaning. In fact, from [48, Svingen], the following, rather incorrect and unscientific, sentence can be found in the introduction chapter:

> "It should be noted that using Rayleigh damping [stiffness proportional] is more of an engineer's method of obtaining good results for practical calculations, than obtaining a mathematically correct damping model."

However, since computed results fit very well with experiments both in time and frequency-domain, there has to be *some* root in physics. By carefully reading the physical and mathematical fundamentals of liquid flow, indeed a physical interpretation is feasible[3]. In this chapter the damping model is first derived to show the details without any physical explanation. Physical interpretation and explanation are given afterwards.

It must also emphasized that frequency-dependent damping is a sub-part in this thesis. This means that although calculations are verified with experiments, and physical interpretations are found, a lot of future work remains both in the studying of general literature and in theoretical and experimental development.

5.2.1 FEM, waterhammer

Starting with the Navier-Stokes equations from Chapter 3.1 (momentum and continuity in x direction):

$$\frac{\partial \rho_f}{\partial t} + v_x \frac{\partial \rho_f}{\partial x} + \rho_f \frac{\partial v_f}{\partial x} = 0 \tag{5.9}$$

$$\rho_f \frac{\partial v_x}{\partial t} + \rho_f v_x \frac{\partial v_x}{\partial x} + \frac{\partial p}{\partial x} = F_x + \left(\kappa + \frac{1}{3}\mu\right) \frac{\partial}{\partial x}\left(\frac{\partial v_x}{\partial x}\right) + \mu\left(\frac{1}{r}\frac{\partial}{\partial r}\left(r\frac{\partial v_x}{\partial r}\right) + \frac{\partial^2 v_x}{\partial x^2}\right) \tag{5.10}$$

[3] Trying to deduce a physical explanation from a rather arbitrary model might seem as a questionable approach. However, a physical interpretation of the *model as such* is indeed possible, and is shown to be in fact deeply founded in both physics, and especially mathematics. The model itself does not explain the physical details of the transient damping, but approximates the effect of them. This is similar to turbulence modelling in three-dimensional flows.

Disregarding convective terms and assuming very low compressibility (see Chapter 3.1 and Appendix A), multiplying with $2\pi r$, integration with respect to r from 0 to R, and dividing by πR^2:

$$\frac{1}{K}\frac{\partial P}{\partial t} + \frac{\partial V}{\partial x} = 0 \tag{5.11}$$

$$\rho_f \frac{\partial V}{\partial t} + \frac{\partial P}{\partial x} = (2\mu + \lambda)\frac{\partial^2 V}{\partial x^2} + \mu \frac{2}{R}\frac{\partial v_x}{\partial r}\bigg|_{r=R} \tag{5.12}$$

where λ is the so called *second viscosity coefficient*, and has the following relation to the bulk viscosity [24, Karim and Rosenhead]:

$$\kappa = (2\mu + 3\lambda)/3 \tag{5.13}$$

The shear stress is described with the Darcy-Weisbach friction factor [64, White]:

$$\tau_0 = -\mu \frac{\partial v_x}{\partial r}\bigg|_{r=R} = \rho_f f \frac{V|V|}{8} \tag{5.14}$$

Using Equation 5.14 in Equation 5.12 gives the ordinary waterhammer equations. The only important viscosity term is the shear force τ_0. The bulk viscosity is disregarded by the use of Stokes hypothesis ($\kappa = -2/3\mu$). The equations are then linearized around steady state values:

$$\frac{1}{K}\frac{\partial P}{\partial t} + \frac{\partial V}{\partial x} = 0 \tag{5.15}$$

$$\frac{\partial V}{\partial t} + \frac{1}{\rho_f}\frac{\partial P}{\partial x} = -f\frac{|V_0|}{2R}V \tag{5.16}$$

FEM formulations are obtained as described in Chapter 4.2.1 by taking the derivative of Equation 5.16 with respect to x, and using Equation 5.15:

$$-\frac{1}{\rho_f}\frac{\partial^2 P}{\partial x^2} + \frac{1}{a^2\rho_f}\frac{\partial^2 P}{\partial t^2} + f\frac{|V_0|}{2Ra^2\rho_f}\frac{\partial P}{\partial t} = 0 \tag{5.17}$$

Applying FEM discretization in the same manner as described in Chapter 4.2.1:

$$\frac{1}{\rho_f}\int_e \mathbf{N}_x\mathbf{N}_x^T dx\mathbf{P} + \frac{1}{a^2\rho_f}\int_e \mathbf{N}\mathbf{N}^T dx\ddot{\mathbf{P}} + f\frac{|V_0|}{2Ra^2\rho_f}\int_e \mathbf{N}\mathbf{N}^T dx\dot{\mathbf{P}} = -\dot{\mathbf{V}} \tag{5.18}$$

or

$$\mathbf{M}\ddot{\mathbf{P}} + f\frac{|V_0|}{2R}\mathbf{M}\dot{\mathbf{P}} + \mathbf{K}\mathbf{P} = -\dot{\mathbf{V}} \tag{5.19}$$

These equations show that the damping matrix $f\frac{|V_0|}{2R}\mathbf{M}$ is proportional to the mass matrix by the factor $f\frac{|V_0|}{2R}$, thus the mass proportional term in the Rayleigh damping

model evolves automatically from the ordinary waterhammer equations. This means that the steady state friction is in fact *inverse* proportional to the frequency in accordance with Figure 5.1. One should note that this relation is *not* because of the FEM discretization, but an effect of the steady state friction model itself. This effect is also described in [4, Brekke et al.].

Frequency-dependent friction is obtained by adding stiffness proportional damping.

$$\mathbf{M}\ddot{\mathbf{P}}+f\frac{|V_0|}{2R}\mathbf{M}\dot{\mathbf{P}}+\beta\mathbf{K}\dot{\mathbf{P}}+\mathbf{K}\mathbf{P}=-\dot{\mathbf{V}} \tag{5.20}$$

Here β is an arbitrary constant that must be set to give suitable damping ratios for each mode. The frequency-domain version of Equation 5.20 will be:

$$s^2\mathbf{M}\mathbf{P}+f\frac{|V_0|\,s}{2R}\mathbf{M}\mathbf{P}+\beta s\mathbf{K}\mathbf{P}+\mathbf{K}\mathbf{P}=-s\mathbf{V} \tag{5.21}$$

No mathematical or physical interpretation of the stiffness proportional damping has yet been presented, only that it will, in accordance to Figure 5.1 and Equation 5.7, produce damping that increases with increasing frequency [75, Zaveri and Phil].

> A small "error" in the damping model is introduced when applying the boundary condition $\frac{\partial P}{\partial x}\Big|_a^b$ in Equation 5.19, Equation 5.20 and Equation5.21, since according to Equation 5.16 $\left(\frac{1}{\rho_f}\frac{\partial P}{\partial x}=-\frac{\partial V}{\partial t}-f\frac{|V_0|}{2R}V\right)$ also at the boundaries, and not only $-\frac{\partial V}{\partial t}$. In the FEM damping model the effect of steady state friction at the boundaries is neglected. This simplification is done only with this particular FEM discretization using pressure at the left hand side for one reason only: It simplifies the FSI calculations considerably. This simplification is not necessary using the flow (Q or V) on the left hand side or when using FEM or any other methods for pure hydraulic calculations (i.e. Structure Matrix Method). Anyhow, this simplification have no effect what so ever on the frequency-dependent term as shown in Chapter 5.6.

5.2.2 Mathematical properties

Looking at Equation 5.20 it is clear that the stiffness proportional term ($\mathbf{K}\dot{\mathbf{P}}$) is a $\frac{\partial^3 P}{\partial x^2 \partial t}$ term in Equation 5.17 (The $\mathbf{K}$ matrix stem from a $\frac{\partial^2}{\partial x^2}$ term). Doing the derivation to obtain Equation 5.17 in reverse order one can see that this corresponds to a $\frac{\partial^2 V}{\partial x^2}$ term in Equation 5.16. The modified waterhammer equations will then be:

$$\frac{1}{K}\frac{\partial P}{\partial t}+\frac{\partial V}{\partial x}=0 \tag{5.22}$$

$$\frac{\partial V}{\partial t}+\frac{1}{\rho_f}\frac{\partial P}{\partial x}=-f\frac{|V_0|}{2R}V+\frac{\lambda_f}{\rho_f}\frac{\partial^2 V}{\partial x^2} \tag{5.23}$$

The stiffness proportional damping is seen to come from an "artificial bulk viscosity term" in the waterhammer equations. The mathematical properties of frequency-dependent *stiffness proportional* damping is therefore exactly the same as ordinary bulk viscosity: A frequency-dependent dissipation term [65, White], [31, Willard et al.].

5.2.3 Solution procedure with MOC

The similarities to linear viscoelastic analysis can bee seen when looking at the mathematical equivalent formulation of Equation 5.22 and Equation 5.23:

$$\frac{\partial V}{\partial t} + \frac{1}{\rho_f}\frac{\partial P}{\partial x} = -f\frac{|V_0|}{2R}V \tag{5.24}$$

$$\frac{1}{K}\frac{\partial P}{\partial t} + \frac{\partial V}{\partial x} + \frac{\lambda_f}{K}\frac{\partial^2 V}{\partial x \partial t} = 0 \tag{5.25}$$

which can be regarded as a kind of linear "viscoelastic hydraulic equations". Proof of this relation is presented in Appendix C. The importance of this, in the author's point of view, is that these equations can be solved with MOC in a similar manner (in principle) as for *soil dynamics* as described in [71, Wylie and Streeter].

Substituting the pressure with the pressure head and the bulk modulus with the wave-propagation-speed/density relation and at the same time retaining the original nonlinear steady state damping term, gives the starting point for the MOC procedure:

$$g\frac{\partial h}{\partial x} + \frac{\partial V}{\partial t} + f\frac{|V|\,V}{4R} = 0 \tag{5.26}$$

$$\frac{\partial h}{\partial t} + \frac{a^2}{g}\frac{\partial V}{\partial x} + \frac{\lambda_f}{\rho_f g}\frac{\partial^2 V}{\partial x \partial t} = 0 \tag{5.27}$$

The term $\frac{\lambda_f}{\rho_f g}\frac{\partial^2 V}{\partial x \partial t}$ is approximated as follows:

$$\frac{\lambda_f}{\rho_f g}\frac{\partial^2 V}{\partial x \partial t} \approx \frac{\lambda_f}{\rho_f g \Delta t}\left(\frac{\partial V}{\partial x} - \left(\frac{\Delta V}{\Delta x}\right)_{t-\Delta t}\right)$$

$$\frac{\lambda_f}{\rho_f g}\frac{\partial^2 V}{\partial x \partial t} \approx \frac{\lambda_f}{\rho_f g \Delta t}\frac{\partial V}{\partial x} - \frac{\lambda_f}{\rho_f g \Delta t}\left(\frac{\Delta V}{\Delta x}\right)_{t-\Delta t} \tag{5.28}$$

Using Equation 5.28 in Equation 5.27 gives two equations that can be transformed to ordinary differential equations:

$$g\frac{\partial h}{\partial x} + \frac{\partial V}{\partial t} + f\frac{|V|\,V}{4R} = 0 \tag{5.29}$$

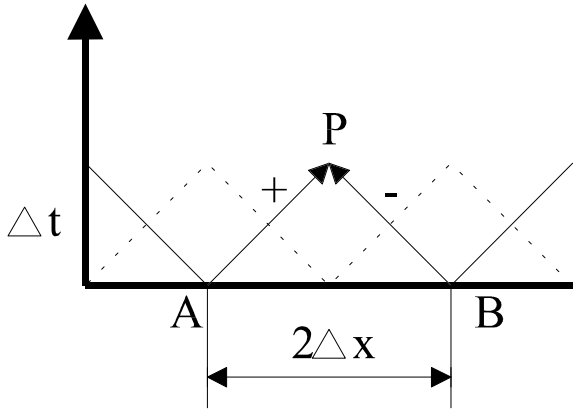

Figure 5.2: Characteristic grid

$$\frac{\partial h}{\partial t} + \frac{a_m^2}{g}\frac{\partial V}{\partial x} - \frac{\lambda_f}{\rho_f g \Delta t}\left(\frac{\Delta V}{\Delta x}\right)_{t-\Delta t} = 0 \tag{5.30}$$

where the modified wave propagation speed, a_m, is defined as:

$$a_m = \sqrt{a^2 + \frac{\lambda_f}{\rho_f \Delta t}} \tag{5.31}$$

The transformed equations are:

$$\frac{dx}{dt} = \pm a_m \tag{5.32}$$

$$\frac{dh}{dt} \pm \frac{a_m}{g}\frac{dV}{dt} \pm \frac{a_m}{g}\frac{f\,|V|\,V}{4R} - \frac{\lambda_f}{\rho_f g \Delta t}\left(\frac{\Delta V}{\Delta x}\right)_{t-\Delta t} \tag{5.33}$$

Integrating these equations along the characteristic lines while substituting the velocity, V, with the flow Q, gives the algebraic equations, see Figure 5.2:

$$H_P - H_A + \frac{a_m}{gA}(Q_P - Q_A) + \frac{f\Delta x}{2gDA^2}Q_P\,|Q_A| - \frac{\lambda_f}{2\Delta x \rho_f g A}(Q_B - Q_A) = 0 \tag{5.34}$$

$$H_P - H_B - \frac{a_m}{gA}(Q_P - Q_B) - \frac{f\Delta x}{2gDA^2}Q_P\,|Q_B| - \frac{\lambda_f}{2\Delta x \rho_f g A}(Q_B - Q_A) = 0 \tag{5.35}$$

The pipe dividing is given as:

$$\Delta x = \Delta t \sqrt{a^2 + \frac{\lambda_f}{\rho_f \Delta t}} \tag{5.36}$$

Often the time steps are calculated explicit. The time steps are found by reorganizing Equation 5.36:

$$\Delta t = \frac{-\frac{\lambda_f}{\rho_f} + \sqrt{\left(\frac{\lambda_f}{\rho_f}\right)^2 + (2a\Delta x)^2}}{2a^2} \tag{5.37}$$

The time marching procedure is almost exactly the same as for traditional calculations. The only difference is that the dynamic friction terms in Equation 5.34 and Equation 5.35 are added in. Since the dynamic friction terms are calculated using values from the last time step, no iteration of any kind is needed, thus the speed of calculation nearly equals that of a traditional calculation. This particular discretization with the proposed damping model has not been found in the available literature. Examples using this discretization can be found in Chapter 5.3. (Vennatrø [62] used this *damping model*, but with a different discretization, based on Equation 5.22 and Equation 5.23, resulting in an iteration procedure).

5.2.4 The second viscosity coefficient

Before going further on with the physical interpretation it is worthwhile to discuss the ordinary bulk viscosity, or more precisely, the second viscosity coefficient. The second viscosity coefficient have been known for a long time, but the usual treatment of it is not to treat it at all. Stoke (1845) assumed that it should be equal to $-2/3\mu$, thus making the bulk viscosity (Equation 5.13) disappear. Assuming incompressible flow ($divV = 0$) will also make it disappear. Later experimental research has found that Stoke's hypothesis is only valid for ideal monatomic gases and that the second viscosity coefficient is *positive* and indeed much greater than μ (see review paper by Karim and Rosenhead [24]). In water the second viscosity term is approximately $3\sim4$ times the value of the shear viscosity depending on the temperature. In other liquids the difference is much greater (in Benzene the ratio λ/μ is 130 to 150).

The physical properties of the bulk viscosity is that it is a frequency-dependent dissipation term [24, Karim and Rosenhead]. To explain physically what the bulk viscosity is, one must go down to atomic level. Consider a shock wave causing two atoms to collide. In a monatomic ideal gas the molecules will only have translation after the collision, while the molecules in a poly-atomic fluid will have both rotation and translation. During and just after the shock the poly-atomic fluid will be in a state of thermodynamic non-equilibrium because of the rotational degrees of freedom. The process of equilibration is assumed to be an irreversible (dissipative) one controlled by the second viscosity coefficient [31, Willard et al.] [37, Schlichting].

The effect from bulk viscosity is negligible for most practical flow situation (including liquid pipe flow where shear forces are dominant), but very important for energy absorption and attenuation of acoustic waves at high frequencies (over 10^4

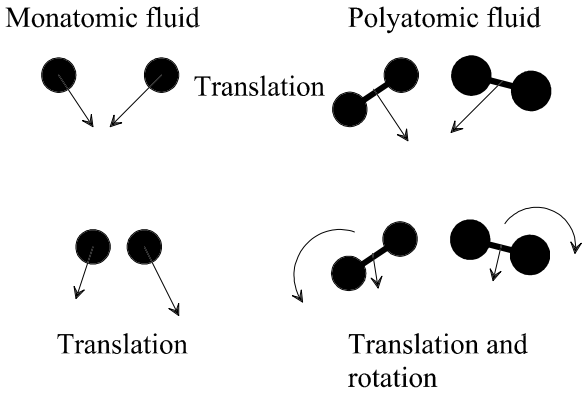

Figure 5.3: Physical explanation of bulk viscosity

Hz), and for calculation of attenuation of shock-waves in liquids and poly-atomic gases [37, Schlichting].

5.2.5 Model versus physical explanation

The process of modelling a physical relation on one hand and explaining the physical details on the other must not be confused. It is emphasized here because using *stiffness proportional damping (artificial bulk viscosity) is a model*, not a physical explanation, of frequency-dependent damping. In the same manner as the viscosity coefficients models the extremely complex intermolecular motions and dissipation, the artificial bulk viscosity models the complex three-dimensional transient and turbulent shear flows and dissipation.

Physical explanations are vital for understanding the details. However, these details often produce extremely complex dynamics, and consequently have to be modelled with easier equations that include only the overall effects to produce equation sets that can be solved within the limits of ordinary computers. Using artificial bulk viscosity for transient and oscillatory pipe friction is such a model.

5.2.6 Damping model

There is no doubt that the frequency-dependent damping found in hydraulic piping systems stem mainly from shear forces because of alternating turbulent velocity profile in the cross section as described by several authors, [76, Zielke] [11, Eichinger] among others. Modelling this profile can, of course, be done using two dimensions and turbulence models [11, Eichinger], but the disadvantage is the enormous amount of computer power compared to a one-dimensional approach. One-dimensional approaches based on Zielke's model and/or instantaneous accelerations are still in the

developing stages but seems like very promising time domain models [60, Vardy and Brown].

From Chapter 5.2.4 it is obvious that the bulk viscosity or the second viscosity is negligible compared to the shear forces, for the frequencies of importance in piping systems (typical in the order of 0-200 Hz). *The overall physical properties however, are of great interest.* By comparing bulk viscosity and frequency-dependent hydraulic pipe friction, the following similarities can be seen:

- Both forms of attenuation are frequency-dependent.
- Dissipation increases with increasing frequency [25, Köngeter] [2, Brekke].
- For slow transients the frequency dependence is negligible [60, Vardy and Brown]. Looking at Equation 5.22 one can see that $\frac{\partial V}{\partial x}$ approaches zero under these circumstances, and consequently $\frac{\partial^2 V}{\partial x^2}$ will also be small.
- Shock waves (waterhammer) will clearly have a large $\frac{\partial V}{\partial x}$ an consequently large $\frac{\partial^2 V}{\partial x^2}$ following the wave.

Because of these similarities the following propositions are made:

Proposition 1 *Using artificial bulk viscosity to obtain frequency-dependent friction in turbulent pipe flow is a mathematical model based on overall physical properties of attenuation of waves.*

The actual cause of the frequency-dependent damping and attenuation, the turbulent alternating velocity profile, is therefore not a part of the model as such, but merely a physical explanation of what is modelled (similar to ordinary viscosity).

The main properties of this damping model will essentially be the same as for general stiffness proportional damping in addition to the three last terms:

- Very easily included in the calculations when using FEM.
- Can be used in direct solution techniques in time and frequency-domain, or in modal analysis.
- Frequency-dependent friction is modelled directly into the governing equations, thus valid in both time and frequency-domain.
- The damping constant will most likely be a function of relative roughness, viscosity and the Reynolds number (Re_d) in a very similar manner as for steady state friction (see page 60).

- Included as an artificial bulk viscosity term in the momentum equation of Allievi's equations:

$$\frac{1}{K}\frac{\partial P}{\partial t} + \frac{\partial V}{\partial x} = 0 \tag{5.38}$$

$$\frac{\partial V}{\partial t} + \frac{1}{\rho_f}\frac{\partial P}{\partial x} = \frac{\lambda_f}{\rho_f}\frac{\partial^2 V}{\partial x^2} - f\frac{V\,|V|}{4R} \tag{5.39}$$

5.2.7 Non-dimensional analysis and analytical solution

A clearer view of the equations is obtained by making them non-dimensional. The steady state friction in Equation 5.4 is linearized, and the following non-dimensional parameters are used:

$$\frac{\partial}{\partial t_*} = \frac{L}{a}\frac{\partial}{\partial t} \quad \frac{\partial}{\partial x_*} = L\frac{\partial}{\partial x} \quad P_* = \frac{1}{a^2\rho_f}P \quad V_* = \frac{1}{a}V \quad \left(\omega_* = \frac{L}{a}\omega\right) \tag{5.40}$$

The equations then become:

$$\frac{\partial P_*}{\partial t_*} + \frac{\partial V_*}{\partial x_*} = 0 \tag{5.41}$$

$$\frac{\partial V_*}{\partial t_*} + \frac{\partial P_*}{\partial x_*} = \frac{\lambda_f}{\rho_f La}\frac{\partial^2 V_*}{\partial x_*^2} - \frac{f\,|V_0|\,L}{2Ra}V_* \tag{5.42}$$

With this choice of variables the constants in front of the damping terms control the equations. Similar relations can be found for the ordinary waterhammer equations without the frequency dependent friction term in [70, Wylie], although other non-dimensionalizing quantities were used. The choice of variables here are quite standard, except for P_* and V_* relating pressure and velocity to the wave propagation velocity. The reason for doing this is to retain valid equations also for zero mean flow and mean pressure (acoustics).

An interesting parameter is the pipe length L. For long pipes the steady state friction term will be dominant while the transient parameter will dominate the solution for shorter pipes. This can be explained by the fact that long pipes have lower resonant-frequencies than short pipes, thus the effect of the artificial bulk viscosity will start at a higher relative resonant-frequency number.

In time domain it is obvious that a long pipe will have larger steady state pressure loss than a short pipe, considering that they have the same friction per unit length. The transient friction however, will travel with the velocity change $\frac{\partial^2 V_*}{\partial x_*^2}$ (for example a pressure wave). When integrating the instantaneous losses due to the transient friction along the two pipes at any given moment in time, they *must* be equal regardless of the length of the pipe, thus the ratio:$\frac{\text{dynamic friction}}{\text{pipe length}}$, will be larger for short pipes than for long pipes. This relation can be visualized by considering two equal pressure waves propagating at equal speed in one long and one short pipe (see

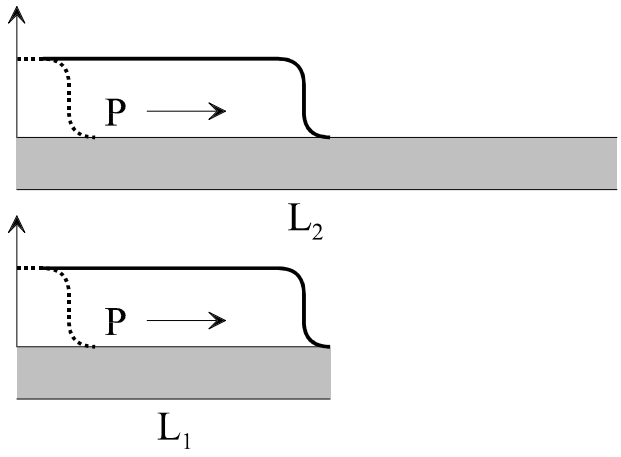

Figure 5.4: Two equal pressure waves traveling in two pipes of different lengths.

Figure 5.4). When the wave reach the end of the short pipe, the wave in the long pipe still has some distance to go before reaching its end. Since obviously the total amount of pressure loss due to the waves is equal in the two pipes at that moment (see also Figure 5.5 and Figure 5.6), the shorter pipe would have lost more pressure in relative terms with respect to the total length than the longer pipe.

Combining the Equation 5.41 and Equation 5.42 will give two equivalent wave-like equations[4]:

$$-\frac{\partial^2 P_*}{\partial t_*^2}+\frac{\partial^2 P_*}{\partial x_*^2}-\frac{f\left|V_0\right|L}{2Ra}\frac{\partial P_*}{\partial t_*}+\frac{\lambda_f}{\rho_f La}\frac{\partial^3 P_*}{\partial x_*^2 \partial t_*}=0 \tag{5.43}$$

$$-\frac{\partial^2 V_*}{\partial t_*^2}+\frac{\partial^2 V_*}{\partial x_*^2}-\frac{f\left|V_0\right|L}{2Ra}\frac{\partial V_*}{\partial t_*}+\frac{\lambda_f}{\rho_f La}\frac{\partial^3 V_*}{\partial x_*^2 \partial t_*}=0 \tag{5.44}$$

Analytical solutions are found by the method of separation of variables. A solution to Equation 5.43 is assumed to be on the form

$$P_*(x,t)=\tilde{P}(x)\tilde{T}(t) \tag{5.45}$$

Inserting this into Equation 5.43 gives:

$$-\tilde{P}\frac{d^2\tilde{T}}{dt^2}+\frac{d^2\tilde{P}}{dx^2}\tilde{T}-\alpha\tilde{P}\frac{dT}{dt}+\beta\frac{d^2\tilde{P}}{dx^2}\frac{d\tilde{T}}{dt}=0 \tag{5.46}$$

[4]Since they are non-dimensional they are in fact equal. Subtracting one equation from the other will result in the equation $0=0$. (The physical interpretations are of course different, as well as the boundary conditions).

where $\alpha_* = \frac{f|V_0|L}{2Ra}$ and $\beta_* = \frac{\lambda_f}{\rho_f La}$. It is impossible to separate $\tilde{P}$ and $\tilde{T}$ on each side of the equality sign and consequently a trial-and-error procedure has to be performed. From the chapter on modal analysis (Chapter 4.6.2), it was found that the modal damping ratio was $\gamma_r = \frac{\alpha}{2}\frac{1}{\omega_r} + \frac{\beta}{2}\omega_r$, and it should therefore be natural to assume that the damping for the analytical time-dependent part, $\tilde{T}$, will be similar and that the x-dependent part will have a sine shape. Indeed a solution that satisfies Equation 5.43 is found by inspection to be[5]:

$$\tilde{P}(x) = A_1 \cos(\omega_* x_*) + A_2 \sin(\omega_* x_*) \tag{5.47}$$

$$\tilde{T}(t) = B_1 e^{(-\gamma+\sqrt{\gamma^2-1})_*\omega_* t_*} + B_2 e^{(-\gamma-\sqrt{\gamma^2-1})_*\omega_* t_*} \tag{5.48}$$

where

$$\gamma_* = \frac{\alpha_*}{2}\frac{1}{\omega_*} + \frac{\beta_*}{2}\omega_* \tag{5.49}$$

The constants are determined by the boundary and initial conditions. The general solution will be (considered the resonant-frequencies are found from Equation 5.44 with the particular boundary conditions):

$$\begin{aligned} P_*(x,t) = \sum_{r=1}^{\infty} \Big[&(A_1 \cos(\omega_r x)_* + A_2 \sin(\omega_r x)_*) * \\ &\left(B_{r1} e^{(-\gamma+\sqrt{\gamma^2-1})_*\omega_{*r} t_*} + B_{r2} e^{(-\gamma-\sqrt{\gamma^2-1})_*\omega_{*r} t_*} \right) \Big] \end{aligned} \tag{5.50}$$

$$\gamma_* = \frac{f\,|V_0|\,L}{2Ra}\frac{1}{2\omega_{*r}} + \frac{\lambda_f}{\rho_f La}\frac{\omega_{*r}}{2} \tag{5.51}$$

Although the analytical solution will be somewhat impractical for general calculations because of the large amount of work to determine the boundary and initial conditions, it shows some important properties concerning the damping.

- For low non-dimensional frequencies the solution is underdamped ($\gamma_*^2 < 1$).
- Increasing the frequencies increases the damping until eventually the system becomes overdamped ($\gamma_*^2 > 1$) for very high frequencies.
- λ_f have to be determined to give proper frequency-dependent damping (experiments).
- The pipe length, L, is an important parameter for the relative effect of transient damping with respect to resonant-frequencies.
- Setting λ_f to zero gives the analytical solution to the ordinary waterhammer equations with linearized steady state friction.

[5] The solution was found by "intelligent guessing" and trial and error.

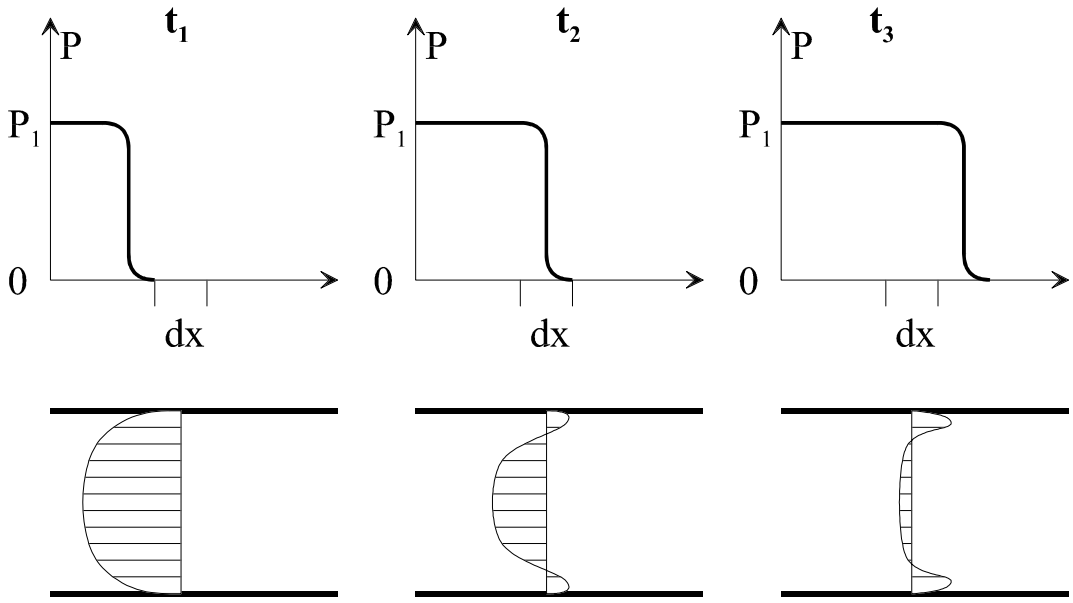

Figure 5.5: Traveling pressure wave with corresponding velocity profile.

5.2.8 Physical interpretation

Mathematically the damping term is the same as bulk viscosity. Consequently the physical interpretation has to be *analogous* to the physical interpretation of bulk-viscosity, or more precisely, the second viscosity coefficient as given in Chapter 5.2.4. In Figure 5.5 a traveling pressure wave is drawn where dx is a small unit of pipe. The figure simulates the pressure and velocity profile in a pipe for three time steps after a total closure of a valve. The velocity profiles are drawn for a mid-pipe section in accordance with computations and measurements in [11, Eichinger]. By looking at the velocity profile for time step t_3 one can se that it is in a state of non-equilibrium with strong shear forces. This means that a substantial amount of pressure energy has been used to make this velocity profile (this is just another way of saying that the shear forces at the wall have increased). Considering three-dimensional (already) turbulent pipe flow, it is clear that this velocity profile will cause even more turbulence , see Figure 5.6. The process of equilibration, which in this case will be the process of averaging the turbulence across the cross section, thus making a more or less even velocity profile, will obviously be a dissipative *and* irreversible one. Analogous to the second viscosity coefficient, this dissipative process of equilibration is controlled by the damping coefficient, λ_f. The amount of fluid energy that dissipates during the equilibration process is of course proportional to the amount of energy needed to make the corresponding velocity profile. Therefore, the damping coefficient, λ_f, has a relation to the shear forces caused by this velocity

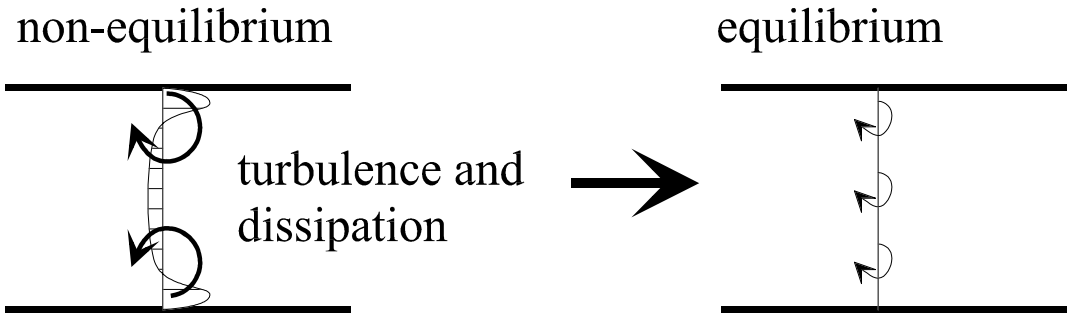

Figure 5.6: Equilibration of turbulence caused by velocity profile.

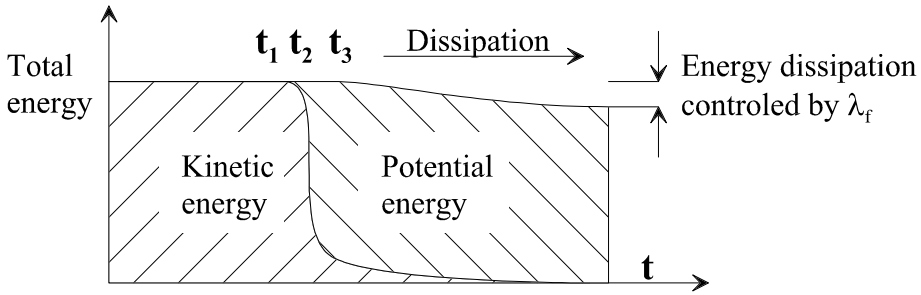

Figure 5.7: Total energy in a pipe cross section during the passing of a pressure wave.

profile through energy considerations. In other words, the damping coefficient λ_f, has no "knowledge" of the transient shear forces, but is an estimation of the energy lost in the process of making them. Figure 5.7 shows the kinetic and the potential energy (in the form of pressure) for the three time steps in Figure 5.5 in addition to the dissipation. The long tail of kinetic energy can be interpreted as the remaining shear forces, and is consistent with research presented in [60, Vardy and Brown].

By looking at the governing equations (Equation 5.52 and Equation 5.53):

$$\frac{1}{K}\frac{\partial P}{\partial t} + \frac{\partial V}{\partial x} = 0 \tag{5.52}$$

$$\frac{\partial V}{\partial t} + \frac{1}{\rho_f}\frac{\partial P}{\partial x} = \frac{\lambda_f}{\rho_f}\frac{\partial^2 V}{\partial x^2} - f\frac{V\,|V|}{4R} \tag{5.53}$$

one can see that $\frac{\partial^2 V}{\partial x^2}$ is proportional to $-\frac{1}{K}\frac{\partial^2 P}{\partial t \partial x}$. In other words the damping is proportional to the rate of change of pressure per unit time per unit length. The damping term will therefore only have a value as long as the flow is in a phase of dynamic change, and will not affect the steady state solution. A more physical

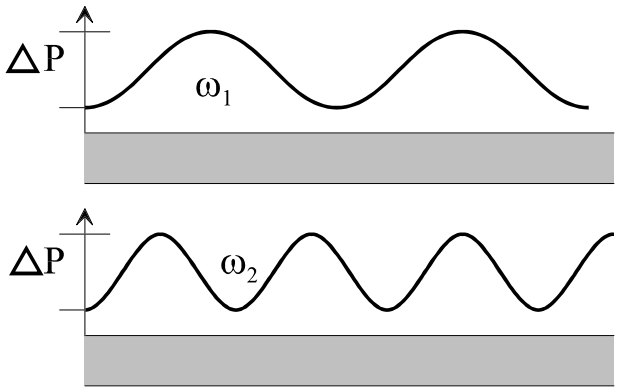

Figure 5.8: Increasing the frequency while retaining the same amplitude.

interpretation of this is that the amount of energy lost through turbulent dissipation is proportional to the steepness of a pressure wave, and the speed of which this wave changes.

A frequency-domain view is somewhat clearer, where, from Equation 5.52: $\frac{\partial^2 V}{\partial x^2} = -\frac{j\omega}{K}\frac{\partial P}{\partial x}$. Considering constant frequency, the only way to increase $\frac{\partial^2 V}{\partial x^2}$, and thus increase the amount of damping, is to increase the amplitude, which is natural from a physical point of view[6]. Increasing the frequency and at the same time retaining a constant amplitude will obviously also increase $\frac{\partial P}{\partial x}$, because more peaks would be made for the same length of pipe (see Figure 5.8).

Based on the argumentations in this chapter, the following proposition is made:

Proposition 2 *The physical interpretation of the proposed damping coefficient λ_f, is a parameter controlling the amount of fluid energy that is dissipated during the equilibration of a non-equilibrium (turbulent) velocity profile caused by fluid fluctuations in time and space (pressure wave), hence it controls the transient damping.*

[6]This should not be confused with any relations to the steady state flow or the steady state friction.

5.2.9 Dimensional analysis

With the use of dimensional analysis it can be found which physical parameters (is most likely to) affect the damping coefficient λ_f. The choice of variables are made with the constraint that *the flow-amplitude and frequency dependence is automatically included* in the equations as explained in the previous section. With this constraint it is natural to assume that λ_f has the following relation:

$$\lambda_f = F\left(d,\, \epsilon,\, \mu,\, V_0,\, \rho\right) \tag{5.54}$$

It is a function of diameter, roughness, viscosity, velocity and density. The only "questionable" parameter is the velocity, which could be the steady state velocity as given in Equation 5.54 or, perhaps more likely, the instantaneous velocity[7].

By using *Buckingham pi theorem*, three pi groups are found:

$$\prod_1 = \frac{\lambda_f}{\mu} \tag{5.55}$$

$$\prod_2 = \frac{\epsilon}{d} \tag{5.56}$$

$$\prod_3 = \frac{\rho V_0 d}{\mu} \tag{5.57}$$

With these pi groups Equation 5.54 reduces to:

$$\frac{\lambda_f}{\mu} = F\left(\frac{\epsilon}{d},\, \frac{\rho V_0 d}{\mu}\right) = F\left(\frac{\epsilon}{d},\, Re_d\right) \tag{5.58}$$

Thus, the dynamic damping coefficient is a function of viscosity, relative roughness and the Reynold's number.

[7] Being dependent on the steady state velocity, or the "starting velocity", is very fortunate from a calculation point of view, and does indeed give adequate results. However, from a physical point of view, the damping coefficient should be a function of the instantanious velocity, requiering calculation of "new" λ_f values at each time step.

5.3 Verifications

The main objective with the verification is to show that the derived damping model is *capable* of calculating correct transient and oscillatory friction. Emphasis is made on the qualitative observations and not so much on determination of the λ_f value with respect to diameter, roughness and Re. The reason for this is that exact determination of damping constants for different pipes is outside the scope- and time-frame for this thesis, and is consequently part of future work. However, some leads to the numerical values of the constant, λ_f, for some specific pipes are given.

5.3.1 Time-domain

For the time-domain verifications experiments and calculations found in Peter Eichinger's dissertation are used [11] for comparison with calculations with the proposed damping model. Time-domain FEM calculations with frequency-dependent friction are performed with modal analysis as presented in Chapter 4.6.2. Time-domain MOC calculations are performed with the discretization technique presented in Section 5.2.3.

Experimental data and calculation found in Eichinger's thesis of total closure ofthe valve for the system given in Figure 5.9 can be found in Figure 5.10. This figure shows calculations made with MOC combined with a two dimensional finite difference approach using the $k - \epsilon$ turbulence model [11], and calculations made with an ordinary MOC procedure with steady state friction, as well as experimental data.

Figure 5.11 shows calculations performed by the author using FEM (modal analysis) and the proposed dynamic friction factor (artificial bulk viscosity). The calculations were performed with a program made in the interactive programming environment Maple. In the FEM model 31 first-order elements were used. The calculation shows that the frequency is correct, and also the amplitude. The shape of the calculated amplitudes are rounded as found in the experiments, but show a bit too much sinusoidal look after the first couple of oscillations. The dynamic friction factor, λ_f, was found to be 700,000.0. This may seem very much, but when comparing the stiffness matrix and the damping matrix, $\mathbf{C} = \beta\mathbf{K}$, one finds that the value of β is only 0.00038. (No steady state friction is included).

In Figure 5.12 the result from a calculation done by the author with MOC and the proposed dynamic friction factor is plotted. A FORTRAN program for a single pipeline was made for these calculations. The pipe was divided into 30 segments. The steady state friction is also included in this calculation. The dynamic friction factor for this calculation was found to be the same as for the calculations with FEM, ($\lambda_f = 700,000.0$, see Figure 5.11).

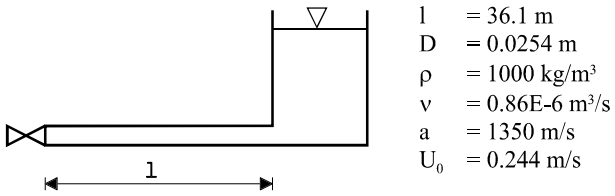

Figure 5.9: Characteristics of the system for full closure of valve, turbulent $Re = 7200$.

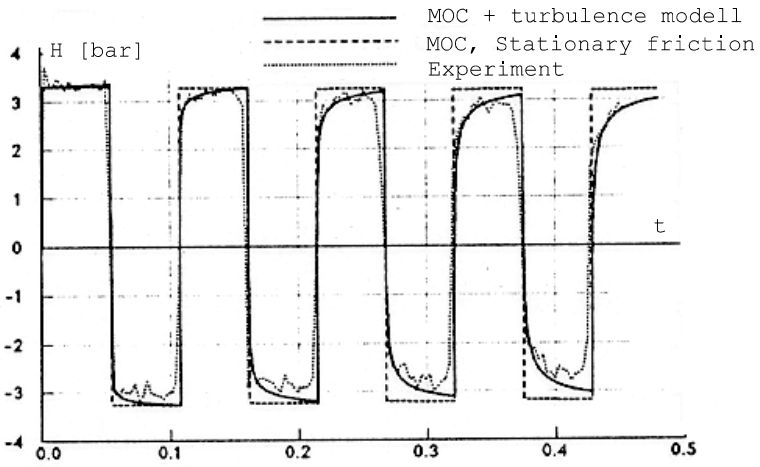

Figure 5.10: Calculations and experiment of pressure pulses after total closure of valve (Eichinger's dissertation). $Re = 7200$.

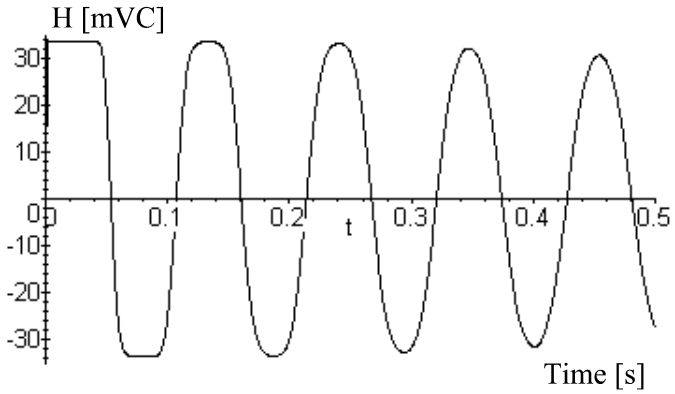

Figure 5.11: Calculation of sudden closure with the proposed dynamic friction factor using FEM and modal analysis. $Re = 7200$.

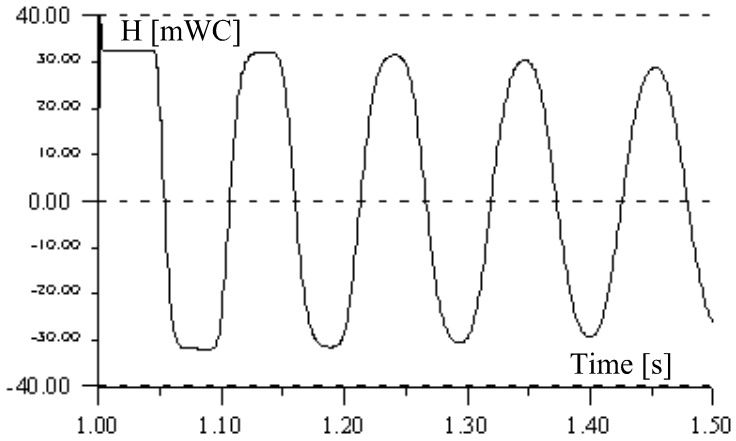

Figure 5.12: Calculation of sudden closure with the proposed dynamic friction factor using MOC. Note- starting time is 1 s. $Re = 7200$.

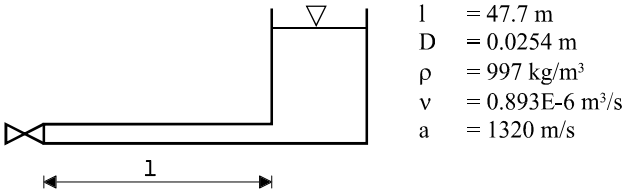

Figure 5.13: Piping system for experiment with attenuation of pressure waves, turbulent Re=5300.

An experiment with longer duration to show the attenuation over a period of time is shown in Figure 5.13, Figure 5.14 ,Figure 5.15 and Figure 5.16. Figure 5.14 (from Eichinger's thesis) shows clearly that steady state friction gives too little attenuation compared with experiments. Calculations with Eichinger's model, Figure 5.14, and the calculations with the proposed dynamic friction model performed by the author, Figure 5.15 and Figure 5.16, show excellent agreement with experiments. Also with the calculations in Figure 5.15 and Figure 5.16 the λ_f values was found to be 700,000.0.

The FEM and MOC calculations presented here (Figure 5.11, Figure 5.12, Figure 5.15 and Figure 5.16) are very similar. They show that the proposed dynamic friction factor (frequency dependent damping model) can be used with both discretization techniques.

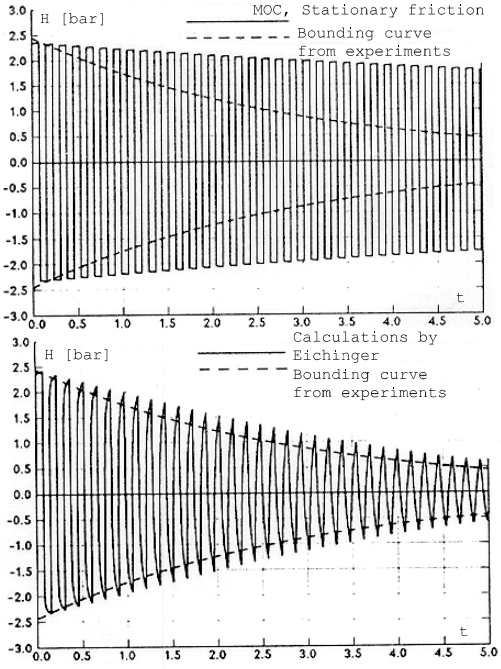

Figure 5.14: Experimental data and calculations with MOC and Eichinger's model. Turbulent (Re=5300).

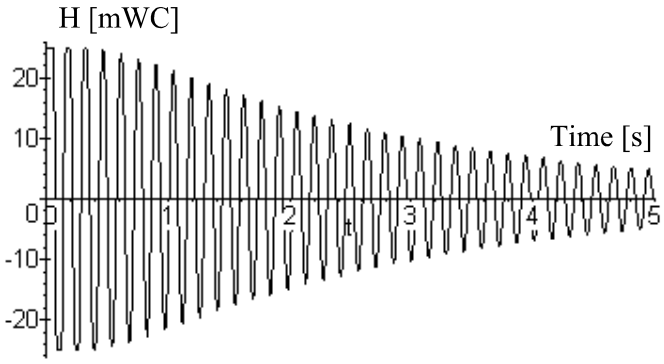

Figure 5.15: Calculation of sudden closure with the proposed dynamic friction factor using FEM and modal analysis. $Re = 5300$.

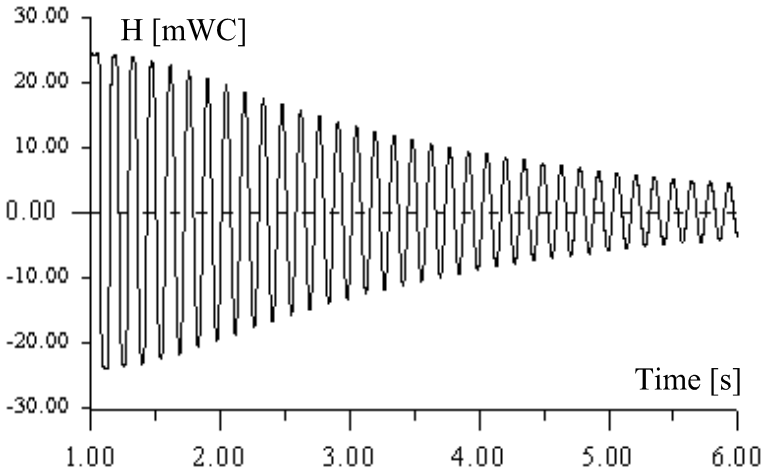

Figure 5.16: Calculation of sudden closure with the proposed dynamic friction factor using MOC. Note- starting time is 1 s. $Re = 5300$.

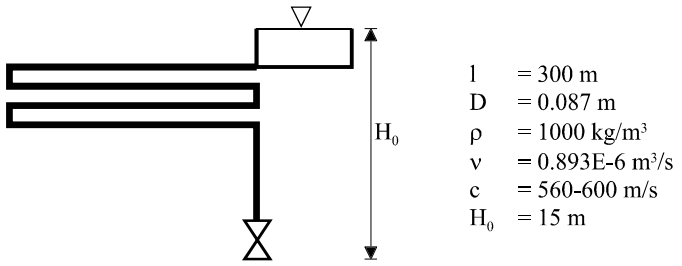

Figure 5.17: Experimental setup for frequency-domain verification

5.3.2 Frequency-domain

Frequency-domain experiments on *single straight pipelines* with turbulent mean flow have not been found by the author in the available literature[8]. It is also troublesome to compare the model with other models found in literature (i.e. [2, Brekke]), because these models are based on empirical friction factor functions of frequency, amplitude etc. added to the steady state friction factor. Comparison of these models is performed with these friction factors. The model presented here is based more fundamentally on the mathematics of the governing equations, thus no relevant friction factor as expressed in other models can be found. Verifications are achieved using the structure matrix method as described in the next chapter and with experiments and calculations found in [44, Svingen]. The Structure Matrix Method is used because analytical functions can be found for a single pipe line. Frequency-domain verifications are also included with the experiments and calculations of FSI using FEM in Chapter 8.1. It can be included here that the λ_f value for the 80 mm diameter smooth stainless steel pipe with water as used in the FSI experiment was approximately $34,000.0$.

The experiments[9] from [44, Svingen] were done with a 300m (corroded) galvanized steel pipe as shown in Figure 5.17. The valve characteristics are approximated with the polynomial $Q(y) = 0.5y - 20.4y^2$ for $H_0 = 15m$. The non-dimensional transfer from pressure head to valve opening was then measured and calculated. For an opening $y_0 = 3mm$ and amplitude $y_{amp} = 0.5mm$, the Nyquist diagram from the experiments is given in Figure 5.18. Calculations taken from [44] using Köngeter's damping model [25], together with calculations using the proposed damping model are in Figure 5.19. The figure shows that excellent frequency-dependent damping can be approximated. The λ_f value was found to be 250,000 (in comparison with

[8]Frequency-dependent friction is a part of the ongoing research at the Water Power Laboratory at NTNU. Experimental apparatus are now being built for future research.

[9]The pipe itself have a very high roughness due to corrosion as well as a lot of bends. This makes it unsuitable for exact determination of friction factors. However, it is well suited to show the general frequency-dependent damping behavior, and therefore to verify the proposed model.

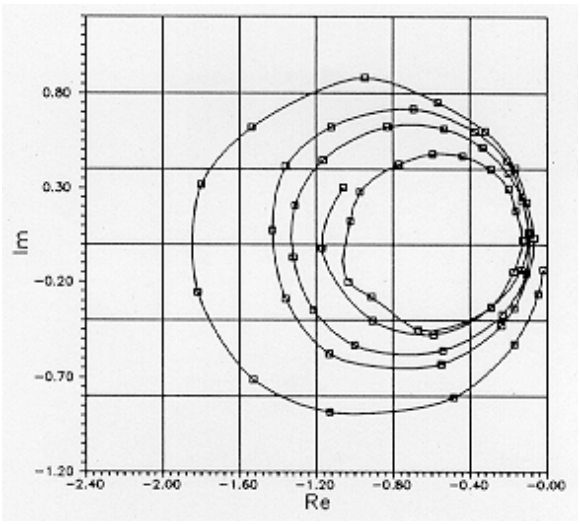

Figure 5.18: Nyquist diagram from experiments on the 300m piping system

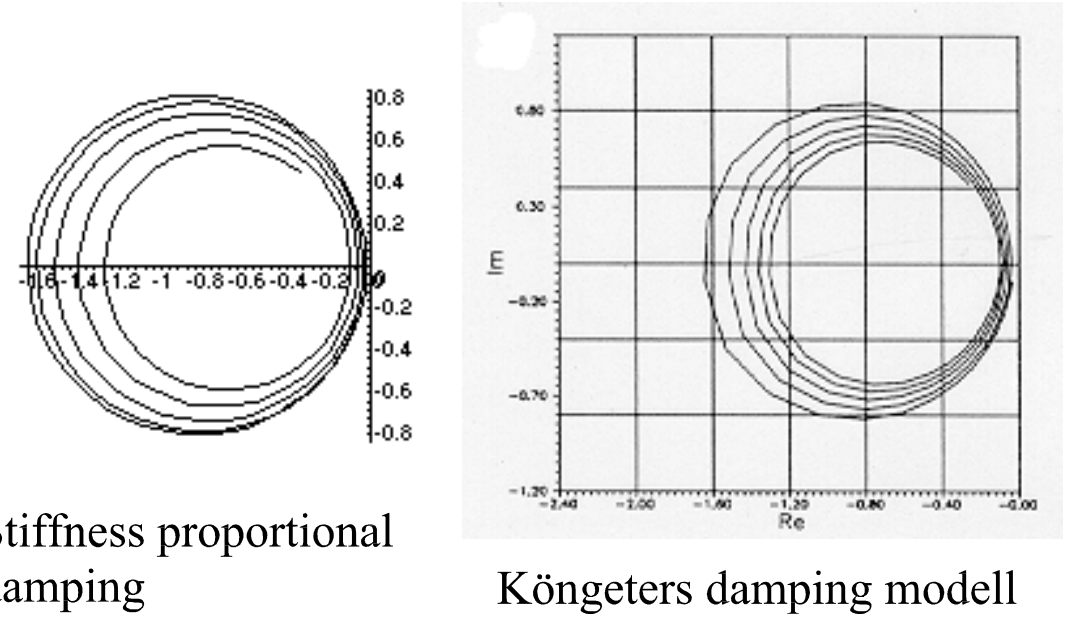

Figure 5.19: Nyquist diagrams from calculations using stiffness proportional damping (artificial bulk viscosity) compared with Köngeter's damping model.

Köngeter's model), which corresponds to a **C** matrix 0.007 times the **K** matrix. This is 7.3 times the λ_f value found for the smooth stainless steel pipe in the FSI experiments which is a strong indication that the value is a function of the roughness.

5.4 The Structure Matrix Method

In the previous chapter (Chapter 5.3) the Structure Matrix Method [2] was used because of the exactness of an analytical solution. The starting point is the Laplace transformed version of Equation 5.44 (non-dimensional variables):

$$-s^2 V_* + \frac{\partial^2 V_*}{\partial x_*^2} - \frac{f\,|V_0|\,Ls}{2Ra} V_* + \frac{\lambda_f s}{\rho_f La}\frac{\partial^2 V_*}{\partial x_*^2} = 0 \tag{5.59}$$

which is equivalent to:

$$\frac{\partial^2 V_*}{\partial x_*^2} = \frac{s^2 + \frac{f|V_0|Ls}{2Ra}}{1 + \frac{\lambda_f s}{\rho_f La}} V_* \tag{5.60}$$

A general solution to this equation is

$$V_* = A_1 e^{zx} + A_2 e^{-zx} \tag{5.61}$$

where

$$z = \sqrt{\frac{s^2 + \frac{f|V_0|Ls}{2Ra}}{1 + \frac{\lambda_f s}{\rho_f La}}} \tag{5.62}$$

The procedure of making the pipe matrix involves a substantial amount of algebra and is essentially the same as described in [2, Brekke] and [73, Xinxin], or as with the Transfer Matrix Method. The only difference is that the starting point of the derivation is with the flow and not the pressure as the free variable. This is because of the term $\frac{\partial^2 V_*}{\partial x_*^2}$ making the derivation through the pressure very hard to grasp compared with using the flow. The pipe matrix equation becomes:

$$\begin{bmatrix} -\frac{s}{z}\frac{1}{\tanh z} & \frac{s}{z}\frac{1}{\sinh z} \\ \frac{s}{z}\frac{1}{\sinh z} & -\frac{s}{z}\frac{1}{\tanh z} \end{bmatrix} \begin{bmatrix} P_{*1} \\ P_{*2} \end{bmatrix} = \begin{bmatrix} V_{*1} \\ V_{*2} \end{bmatrix} \tag{5.63}$$

In general piping analysis it is often more convenient to use the pressure head and the flow (as in Chapter 5.3). Making the pressure head and flow non-dimensional while keeping the dimensions of t and x one obtains the structure matrix used in Chapter 5.3:

$$Q^* = \frac{q}{q_0} \quad H^* = \frac{h}{h_0} \tag{5.64}$$

$$\frac{s}{2h_w az}\begin{bmatrix} -\dfrac{1}{\tanh(Lz/a)} & \dfrac{1}{\sinh(Lz/a)} \\ \dfrac{1}{\sinh(Lz/a)} & -\dfrac{1}{\tanh(Lz/a)} \end{bmatrix}\begin{bmatrix} H_1^* \\ H_2^* \end{bmatrix} = \begin{bmatrix} Q_1^* \\ Q_2^* \end{bmatrix} \tag{5.65}$$

$$z = \sqrt{\frac{s^2 + \frac{f|q_0|}{DA}s}{1 + \frac{\lambda_f s}{a^2\rho_f}}} \quad h_w = \frac{q_0 a}{2gAh_0} \tag{5.66}$$

5.5 The Transfer Matrix Method

The transfer matrix with this damping model can be obtained in essentially the same manner as the structure matrix. Rearranging Equation 5.63:

$$\begin{bmatrix} P_{*1} \\ V_{*1} \end{bmatrix} = \begin{bmatrix} \cosh(z) & \dfrac{z}{s}\sinh(z) \\ \dfrac{s}{z}\sinh(z) & -\cosh(z) \end{bmatrix}\begin{bmatrix} P_{*2} \\ V_{*2} \end{bmatrix} \tag{5.67}$$

or as the equivalent inverse form:

$$\begin{bmatrix} P_{*2} \\ V_{*2} \end{bmatrix}\begin{bmatrix} \dfrac{\cosh z}{Z_t} & z\dfrac{\sinh z}{sZ_t} \\ s\dfrac{\sinh z}{zZ_t} & -\dfrac{\cosh z}{Z_t} \end{bmatrix}\begin{bmatrix} P_{*1} \\ V_{*1} \end{bmatrix} \tag{5.68}$$

where

$$Z_t = 2\cosh^2 z - 1 \tag{5.69}$$

and z is given by Equation 5.62.

5.6 Simplifications with FEM

As mentioned on page 48 a small error in the damping model is introduced when applying the boundary conditions in the particular FEM discretization used herein. Going back to Equation 5.41 and Equation 5.42 one can see that two equivalent wave equations (Equation 5.43 and Equation 5.44) can be made. When using Equation 5.44 the conditions at the boundaries can be obtained easily and correctly from Equation 5.41 ($\frac{\partial V_*(x_*=0,x_*=1)}{\partial x_*} = \frac{\partial P_*(x_*=0,x_*=1)}{\partial t_*}$). However, in the FSI analysis the use of pressure on the right hand side will cause problems with the junction coupling because of the continuity relations. When using Equation 5.43 the boundary relation for $\frac{\partial P_*(x_*=0,x_*=1)}{\partial x_*}$ must be taken from Equation 5.42. Although this is fully possible, it will cause recomputing of the global stiffness and mass matrices in the FSI analysis for every frequency because the hydraulic parts of the matrices would be divided by extra functions of $j\omega$. Disregarding the extra terms causes no such recomputing.

The frequency domain FEM formulation of Equation 5.43, including the boundary relation due to partial integration, is:

$$\left(s^2 + \alpha_* s\right) \mathbf{M}_* \mathbf{P}_* + \left(1 + \beta_* s\right) \mathbf{K}_* \mathbf{P}_* = \left(1 + \beta_* s\right) \left[N \frac{\partial P_*}{\partial x_*} \right]_0^1 \tag{5.70}$$

The $\frac{\partial P_*}{\partial x_*}$ relation must be obtained from Equation 5.42. However, Equation 5.42 have the term $\frac{\partial^2 V_*}{\partial x_*^2}$ which must be taken care of. This is done with the relation from Equation 5.60, thus Equation 5.70 becomes:

$$\begin{gathered} \left(s^2 + \alpha_* s\right) \mathbf{M}_* \mathbf{P}_* + \left(1 + \beta_* s\right) \mathbf{K}_* \mathbf{P}_* = \\ \left(1 + \beta_* s\right) \left(-s - \alpha_* + \beta_* \frac{s^2 + \alpha_* s}{1 + \beta_* s} \right) \mathbf{V}_* \end{gathered} \tag{5.71}$$

Rearranging Equation 5.71 causes *cancellation of all the β_* terms on the right side*, and the equation becomes the non-dimensional hydraulic FEM equation without the damping simplifications at the boundaries:

$$\frac{s}{(s + \alpha_*)} \left[s^2 \mathbf{M}_* \mathbf{P}_* + \alpha_* s \mathbf{M}_* \mathbf{P}_* + \beta_* s \mathbf{K}_* \mathbf{P}_* + \mathbf{K}_* \mathbf{P}_* \right] = -s \mathbf{V}_* \tag{5.72}$$

whereas the simplified version similar to Equation 5.21 is:

$$\left[s^2 \mathbf{M}_* \mathbf{P}_* + \alpha_* s \mathbf{M}_* \mathbf{P}_* + \beta s \mathbf{K}_* \mathbf{P}_* + \mathbf{K}_* \mathbf{P}_* \right] = -s \mathbf{V} \tag{5.73}$$

where

$$\alpha_* = \frac{f \left| V_0 \right| L}{2Ra} \quad \beta_* = \frac{\lambda_f}{\rho_f L a} \tag{5.74}$$

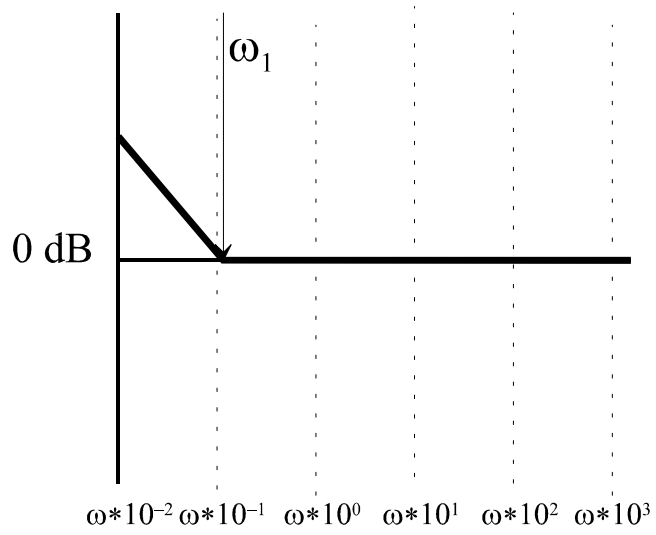

Figure 5.20: Bode diagram of the damping error due to simplification.

Frequency range	**Damping**
$0 \rightarrow \omega_{*1} = \frac{1}{2} f \left\|v_0\right\| \frac{L}{Ra}$	too little
$\omega_{*1} = \frac{1}{2} f \left\|v_0\right\| \frac{L}{Ra} \rightarrow \infty$	exact

Table 5.1: Frequency range of damping

The simplified version is obtained by neglecting the α_* term in the fraction in front of the parenthesis in Equation 5.72. When considering a pipe with the same non-dimensional velocity oscillation, the relation of correct pressure versus simplified pressure (Equation 5.72 and 5.73) is:

$$\frac{\frac{s}{(s+\alpha_*)} P_c}{P_s} = 1$$

$$\frac{P_c}{P_s} = \frac{s + \frac{1}{2} f \left\|v_0\right\| \frac{L}{Ra}}{s} \tag{5.75}$$

This function is zero for the non-dimensional frequency $\omega_* = \frac{1}{2} f \left\|v_0\right\| \frac{L}{Ra}$, has a pole at $\omega_* = 0$, and a gain of $\left(\frac{1}{2} f \left\|v_0\right\| \frac{L}{Ra}\right)^{-1}$. According to control theory [18, Haugen] the bode diagram (asymptotes) as given in Figure 5.20 can be drawn. The different damping from the diagram are listed in Table 5.1. (To obtain dimensional frequencies one must multiply with $\frac{a}{L}$).

As an example the frequency for the system in Figure 5.17 will be: $\omega_1 \approx 0.017 Hz$. For the FSI experiment the frequency will be: $\omega_1 \approx 0.012 Hz$. This shows that the simplified damping is mathematically correct for all practical frequency-domain

calculations (In the FSI experiments in Chapter 7.1 the starting frequencies were $4,5Hz$). Only for very low frequencies for long pipes will the simplification produce an error by producing too little steady state damping, thus requiring the non-simplified model to be used. One should also note that the *frequency dependent* damping is correct for all frequencies (no simplification is done).

Usually, in structural calculations only stiffness proportional damping is used [33, Petyt]. Doing this also for the flow equations ($f = 0$ in Equation 5.75), one can see that the mathematically correct damping is produced.

5.7 Summary

In this chapter the special frequency-dependent friction model used in the FSI calculations is proposed, explained and verified. It is shown that the same friction model can be used in both time and frequency-domain using FEM, SMM, TMM or MOC. The model is still in the *early development stages*, thus further experiments and research are needed to make it an applicable model. Especially the investigation of the friction factor λ_f and its relation to other piping parameters (viscosity, relative roughness and Reynold's number) has to be undertaken. However, it is clear that the model introduces minimal extra computational effort both for frequency- and time-domain calculations using either FEM, SMM or MOC. The closest related damping models found in literature are the model using complex wave-speed found in [71, Wylie and Streeter] and the model proposed in [26, Krus et al.].

A considerable amount of this chapter has been used to give a physical interpretation seen in relation to turbulent, transient pipe flow. The physical interpretation is found to be a relaxation process due to the increased friction because of rapid change in velocity profile in a pipe. The fact that it is relaxation process fundamentally based on the governing equations means that *the flow-amplitude and frequency dependence is automatically included*. An important practical aspect of this is that no iteration is needed in the calculations. Mathematically the model introduces an artificial viscosity term in the equations.

In relation to FEM the model is ordinary Rayleigh damping, making frequency-dependent FSI calculations easy and consistent. In the discretization used herein for the FSI calculation a simplification is done. This simplification affect *only the steady state damping term* by producing too little steady state friction in the extreme lower end of the frequency range (far below any of the starting frequencies used for the experiments in this thesis). This is done only to avoid recalculation of the matrices for each frequency (In the calculations only stiffness proportional damping is used).

The frequency-dependent damping in the FSI calculations is regarded as "internal", that is -no *direct* interaction is caused by the damping. This is consistent with research done by other authors in which the interaction caused by friction

forces is negligible compared with the Poisson and junction coupling [8, de Jong] [56, Tijsseling and Lavooij].

Analytical solution to the waterhammer equations with the proposed frequency-dependent damping is found. The solution is valid in time-domain.

Chapter 6

System elements

Two of the main parts of the objective of this thesis is to be able to include all the hydraulic system components developed for the Structure Matrix Method [73, Xinxin], and to include supports and surrounding structure. This chapter explains how this is achieved along with some other extensions.

6.1 Hydraulic components

In [2, Brekke] and [73, Xinxin] a whole range of different components ranging from simple throttles to complete hydro-turbines including the governor is derived for use with SMM. The specific derivation of these matrices is therefore not presented here, but only an explanation of the small changes needed for FSI analysis using the FEM program.

As an example, the matrix for a valve, is used. The valve is chosen because it is used for the experiments in this thesis. The matrix equation as given in [73, Xinxin] is:

$$\begin{bmatrix} -\frac{1}{2} & -\mu_{y0} & \frac{1}{2} \\ 0 & \frac{1}{k_q} & 0 \\ \frac{1}{2} & \mu_{y0} & -\frac{1}{2} \end{bmatrix} \begin{bmatrix} h_1 \\ y \\ h_2 \end{bmatrix} = \begin{bmatrix} q_1 \\ y_{ex} \\ q_2 \end{bmatrix} \tag{6.1}$$

which is obtained from the Taylor expansion of the equation:

$$Q = \mu(Y)\sqrt{2g\left(H_2 - H_1\right)} \tag{6.2}$$

where Y is the valve opening, μ is the flow coefficient as a function of Y, and H_1 and H_2 are the pressure heads at each side of the valve. $\mu_{y0} = \left(\frac{\partial \mu}{\partial y}\right)_0$ and k_q is the relation from the valve excitation y_x and the actual valve opening y (often equal to one). The variables in the matrix are non-dimensional:

$$h = \frac{H}{H_0} \quad q = \frac{Q}{Q_0} \quad y = \frac{Y}{Y_0} \tag{6.3}$$

In the discretization for the FSI program, the flow vector on the right hand side in Equation 4.28 is multiplied with a factor $-s$ for convenience reasons. Doing this with Equation 6.1 one obtains a matrix that can be placed directly into the FSI program:

$$-s \begin{bmatrix} -\frac{1}{2} & -\mu_{y0} & \frac{1}{2} \\ 0 & \frac{1}{k_q} & 0 \\ \frac{1}{2} & \mu_{y0} & -\frac{1}{2} \end{bmatrix} \begin{bmatrix} h_1 \\ y \\ h_2 \end{bmatrix} = \begin{bmatrix} -sq_1 \\ -sy_{ex} \\ -sq_2 \end{bmatrix} \tag{6.4}$$

All the other components, including pumps and turbines as described in [73, Xinxin], can be obtained in exactly the same manner. In some cases it is more convenient not to have non-dimensional variables, however this is done in a rather trivial manner using Equation 6.3.

In relation to FSI one can think of circumstances where the valve can move together with the pipe. This happened unintentionally in the FSI experiments and modifications had to be done as described in [49, Svingen]. Actually, making a valve support rigid with respect to FSI forces is a hard task requiring massive measures in both strength and mass. For the experiments in this thesis the original valve supports consisting of two $100 \times 100 \times 9$ mm H beams, was replaced with two $300 \times 300 \times 11$ mm H beams, along with some major modifications to the design to make it more stiff. It is therefore safe to say that in general a valve is *always* free to move to some extent.

A moving valve can be modelled in many different ways according to the type of valve and the support conditions. An example showing the general modifications is given here for a short thick walled end of line valve free to move in axial direction with respect to the pipe.

The hydraulic part will be as in Equation 6.4 with additional boundary conditions similar to Equation 4.19[1]:

$$\begin{bmatrix} -(A_0 + A_{ex}(\omega))s^2 u_1 \\ \\ (A_0 + A_{ex}(\omega))s^2 u_2 \end{bmatrix} - s \begin{bmatrix} -\frac{1}{2}\frac{Q_0}{H_0} & -\mu_{y0}\frac{Q_0}{Y_0} & \frac{1}{2}\frac{Q_0}{H_0} \\ 0 & \frac{1}{k_q}\frac{Q_0}{Y_0} & 0 \\ \frac{1}{2}\frac{Q_0}{H_0} & \mu_{y0}\frac{Q_0}{Y_0} & -\frac{1}{2}\frac{Q_0}{H_0} \end{bmatrix} \begin{bmatrix} h_1 \\ y \\ h_2 \end{bmatrix} = \begin{bmatrix} -sq_1 \\ -sy_{ex} \\ -sq_2 \end{bmatrix} \tag{6.5}$$

where $A_{ex}(\omega)$ represents the oscillating area change due to the valve opening and A_0 is the steady state opening. (For an end of line valve the displacement u_2 is of course nonexistent because u_1 will be the last node of the pipe).

The equation of motion for this valve with an oscillating opening area will simply be:

$$s^2 m u_1 = f_1 + A_1(\omega)\rho g h_1 \tag{6.6}$$

[1] In the calculations, Q_o was approximated with the relation $Q_0 = \mu(Y)_0\sqrt{2g\,(H_2 - H_1)_0}$.

which is equal to an added mass term (the total mass of the valve) at the last node of the pipe.

6.2 Supports and surrounding structure

To include supports and surrounding structure is rather straightforward. Because the program is based on the Finite Element Method which is virtually the only method used in structural calculations today, literally *every kind of surrounding structure and support* regardless of the complexity can be included in a painless manner by simply adding them into the global matrices in exactly the same way as the pipes themselves.

Indeed this point is one of the main advantages of the discretization presented in this thesis.

6.3 Bends and elbows

Correct treatment of bends requires the use of three-dimensional structural software. The reason for this is that bends inherit very complex strain-stress relations. A treatment of bends using geometrically nonlinear finite elements can be found in [23, Jonsson].

However, for a general piping software nonlinear three-dimensional calculation must be disregarded to keep the computations to a reasonable level. The usual method is to model the bends as short pipe segments with a bending stiffness (EI_p) that is decreased by a so-called flexibility factor [12, Everstine]. The flexibility factors used herein are the ones developed by von Kármán in 1911, and can be found in [8, de Jong]:

$$f_L = 1.65\frac{\overline{R}^2}{er_c}$$

where $\overline{R}$ is the mean radius of the pipe, e is the wall thickness and r_c is the radius of curvature of the bend. The constraints to this formula is that $\frac{r_c}{\overline{R}} > 1.7$, $r_c\gamma > 2\overline{R}$ where γ is the elbow angle in radians, and that there are no flanges or other stiffeners in a distance R on either side of the bend. It should be noted that the effect of the flexibility factor on the overall response decreases when the elbows are short compared with the lengths of the pipes (i.e. long slender pipes).

6.4 Acoustic sources

In recent years the research on acoustical *sources* in piping systems has been a field of growing importance. Graf and Ziada [16] mention several cases of flow induced

vibrations due to shear instabilities at branches. The excitation mechanisms causing this phenomena are at present not well understood, and further research in this field is likely to occur. A treatment of two coaxial closed side branches is found in [16], and an analytical treatment of the flow past a deep cavity can be found in [10, Durgin and Graf].

6.5 Summary

In this chapter it is shown how to include hydraulic components described in [2, Brekke] and [73, Xinxin] ranging from throttles to hydro-turbines by doing some minor modification to the matrices. It is also shown how to modify these matrices if moving boundary conditions must be applied. Since the pipes themselves are structures modelled with FEM, including surrounding structure is no different than the assembling of global piping matrices. The flexibility factors of elbows are given a brief introduction.

Chapter 7

Experimental arrangement and computer program

7.1 Experimental Arrangement

In order to verify and improve the computer program an experimental piping rig was built. When doing an experiment of any kind, it is important to isolate the details that are subjects of research. Consequently the rig was built with long slender thin-walled pipes, in order to be sure that FSI (junction and Poisson coupling) was of dominance. The philosophy when designing the system was to purify the fluid structure interaction *in the pipes only*, i.e. disturbances from external sources and effects from supports should be minimized as much as possible. Making the boundary conditions simple and clean was therefore stressed.

7.1.1 Layout

The experimental apparatus consists of an L shaped piping system with constant water level, i.e. constant head upstream, and a specially designed valve downstream. The valve discharges into atmosphere. The pipes are thin walled and long compared to the diameter. Hydraulic pressures and structural accelerations are measured at several places in the system.

A schematic sketch showing the overall dimensions are given in Figure 7.1 and the properties are listed in Table 7.1. Key points are rigid supports only at the upstream and downstream ends, causing the system to be extremely movable, and thus enhance the FSI effects. Because of the extreme slenderness the system changes shape when filled with water (especially in the reach marked as number 3 in Figure 7.1). The exact detailed dimensions of the water filled system are found in Figure 7.2 with corresponding coordinates in Table 7.2 (the same coordinates are used in the computer program).

7.1.2 Calibrations

Calibration of the pressure transducers was performed at the beginning of each day with experimental work by first reading the voltage at zero pressure (no water), and then reading the pressure when the system was filled with water and there where no flow in the system. The height from the transducer at the valve and to the top of the water level was previously measured to be 9.82m, and transducers where calibrated according to this[1].

Accelerometers where calibrated by setting them on a wheel and rotating the wheel to obtain $\pm 1g$.

7.1.3 Other components and details

- The stationary pressure head measured from the transducer at the valve is 9.82m.
- The pipes are welded together.
- The water quality is ordinary tap which discharges to atmosphere at the valve.
- Pressure transducers are of type "Entran EPX-M51W-7A" which are flush mounted.
- Accelerometers are of type "Entran EGAS-FS-50D". These are extremely small, weighing only 1/2 gram. They are attached with double-sided tape or a special wax, and can therefore be freely moved around.
- Transducers and accelerometers are driven by an "HBM MGA MA 10 DC" amplifier transmitting amplified signals to a frequency response analyzer: "SOLARTRON/Schlumberger 1253 Gain-Phase Analyzer". Pictures of the system are shown in Figure 7.3.

[1] Accelerometers and pressure transducers were calibrated from the factory. For the transducers no measurable nonlinearities where found. The accelerometers had a bandwidth from zero to one thousand Hz.

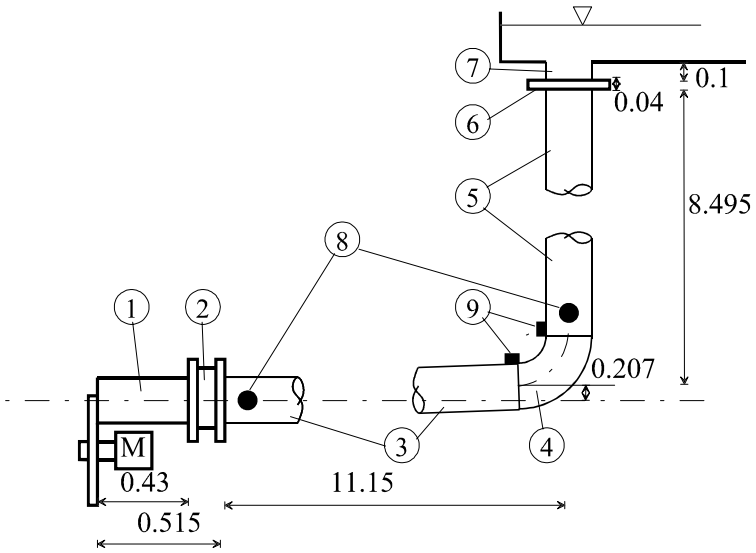

Figure 7.1: A sketch showing the overall dimensions of the piping system. Properties are given in Table 7.1.

Number	**Dimension [mm]**	**Description [SI units]**
1	D100, d80	Stainless steel, $\rho = 7840$, $E = 2.0 * 10^{11}$, $\nu = 0.3$
2	D≈200, d80	Shutdown valve, bolted between DIN 2576 80 PN10 flanges
3	D83, d80	Stainless steel, $\rho = 7840$, $E = 2.0 * 10^{11}$, $\nu = 0.3$
4	D84, d80, R130	Bend, stainless steel, $\rho = 7840$, $E = 2.0 * 10^{11}$, $\nu = 0.3$
5	D83, d80	Stainless steel, $\rho = 7840$, $E = 2.0 * 10^{11}$, $\nu = 0.3$
6	D200, d80	DIN 2576 80 PN10 flange and steel flange 80 PN 10
7	D100, d80	Steel, $\rho = 7840$, $E = 2.1 * 10^{11}$, $\nu = 0.3$
8	-	Entran pressure transducer
9	-	Entran accelerometer

Table 7.1: Material properties of the system, D and d are outer and inner diameters

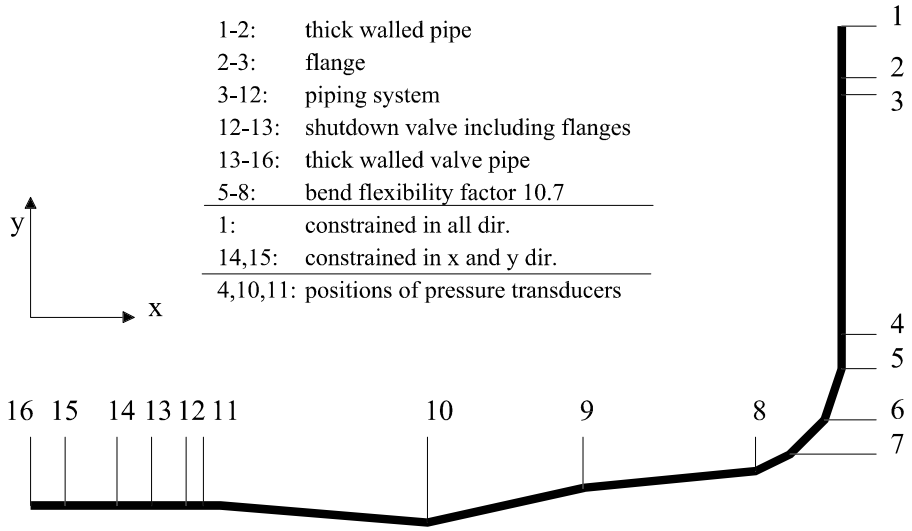

Figure 7.2: Measurements of water filled system (note- not to scale).

Coordinate	**x**	**y**
1	11.665	8.842
2	11.665	8.742
3	11.665	8.702
4	11.665	0.437
5	11.665	0.337
6	11.648	0.267
7	11.6	0.223
8	11.535	0.207
9	7.465	0.1
10	5.545	-0.03
11	0.615	0.0
12	0.515	0.0
13	0.43	0.0
14	0.3	0.0
15	0.1	0.0
16	0.0	0.0

Table 7.2: Coordinates of the system

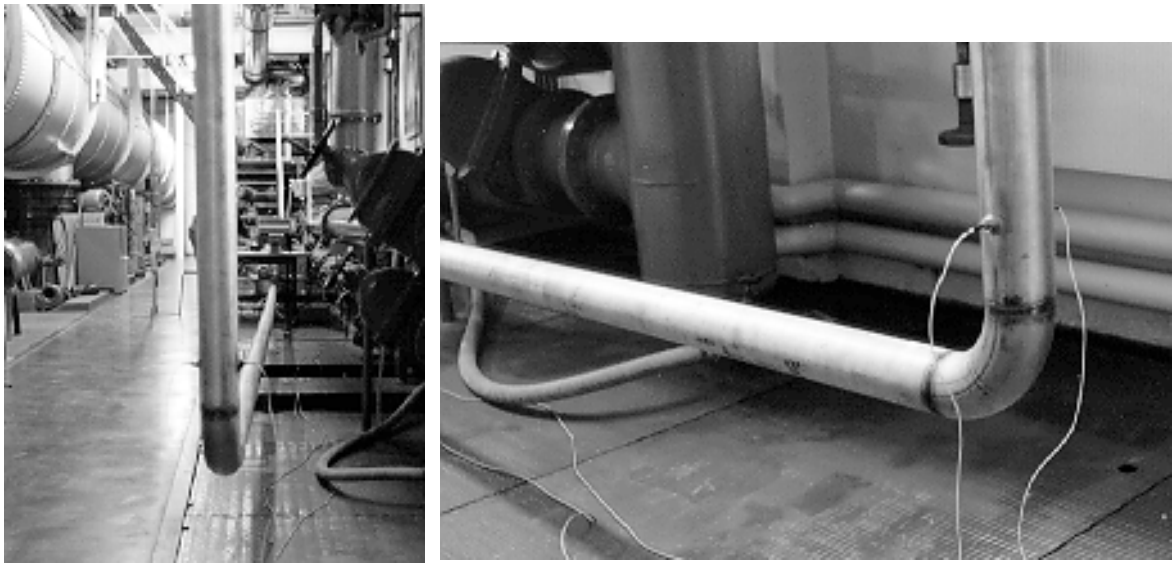

Figure 7.3: Pictures of the piping system. a) showing the horizontal reach and b) showing the bend with transducers.

7.1.4 Disc valve

In order to make sinusoidal valve movements with constant amplitudes over a wide range of frequencies, ($f = 0 \sim 300Hz$), a specially designed valve was made. Pictures of the valve are shown in Figure 7.4 ,Figure 7.5 and Figure 7.6. The valve consists of:

- A short pipe with a 80 by 10 mm sluice opening.
- A rotating teflon[2] disk (thickness 2 mm), with three sine functions superpositioned on the periphery partially covering the sluice.
- An electric motor driven by a three-phase "SIEMENS SIMOVERT MICRO MASTER" frequency converter making the speed of the motor adjustable from 0 to 6000 rpm. in 6.0 rpm. intervals (0.1 Hz), (see Figure 7.7).

With three sine functions on the periphery, the valve opening is adjustable in a range from 0 to 300 Hz. in intervals of 0.3 Hz. To obtain stability at high speed the disk was sandwiched between two steel plates. A digital counter was also connected to the motor to obtain the exact frequency (rpm), because a small deviation from the input to output frequency was measured. The steady state opening and thus the relative amplitude is adjustable by opening and closing a "gate" on the opposite side of the disk. Absolute amplitudes can be adjusted by changing the disk. By varying the number of superpositioned sine functions the top end of the frequency range can be adjusted. The formula describing the shape of the disk is:

$$r = r_0 + A\sin(n\theta)$$

where r is the radius, r_0 is the mean radius, A is the amplitude, n is the number of sine functions per revolution ($n \geq 2$) and θ is the angle. In Figure 7.8 a typical disk is shown.

The first disk was made "by hand", but was found to be too inaccurate. It is this disk that is shown in Figure 7.5. Three new disks with amplitudes of 5, 2.5, and 1.5 mm were made. These three disks were made on a CNC machine at HiST in Trondheim with an accuracy of approximately ± 0.004 mm.

[2] polytetrafluorethylene

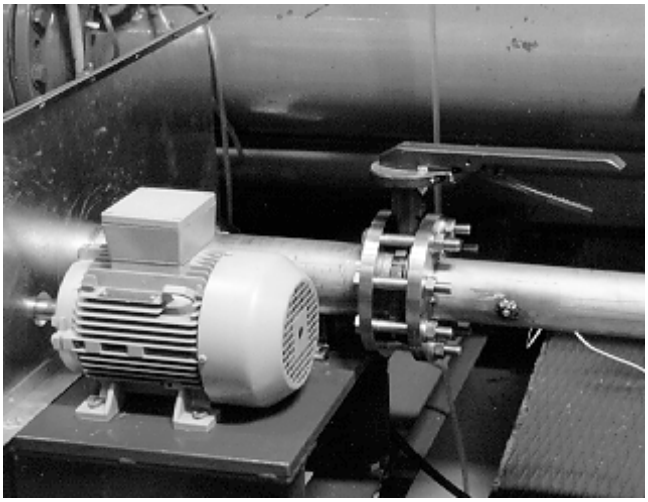

Figure 7.4: The rotating disk valve (back view).

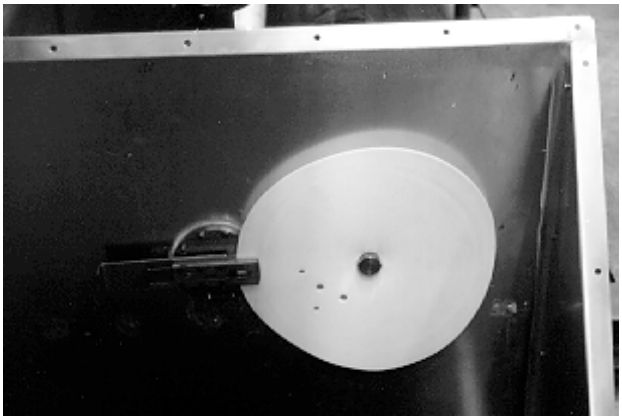

Figure 7.5: Front view of the valve showing the disk and valve opening.

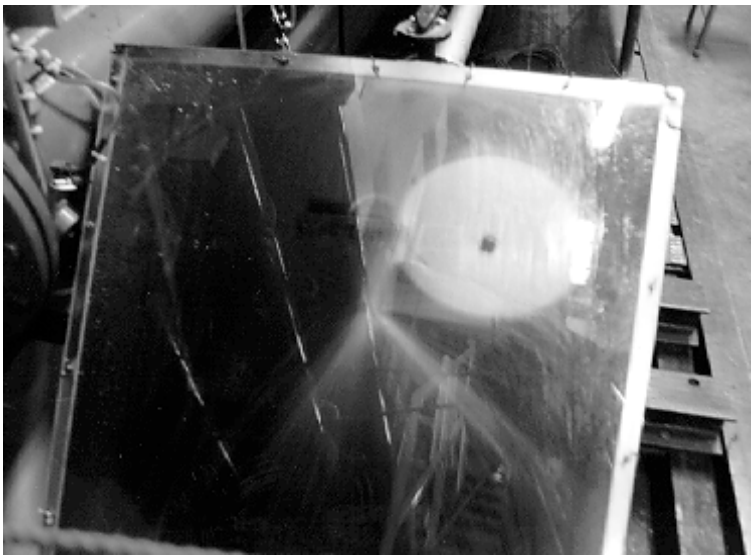

Figure 7.6: Picture of the valve in operation.

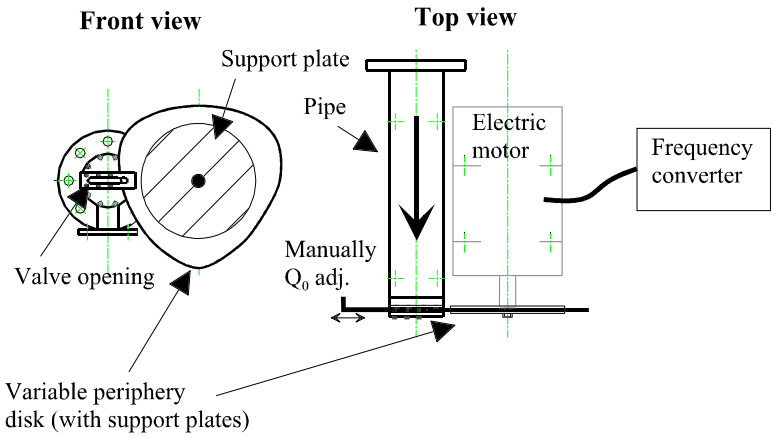

Figure 7.7: A sketch showing the design of the valve.

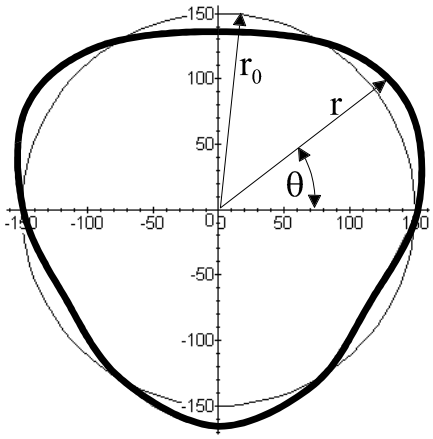

Figure 7.8: Disk with three sine functions (fat line), exaggerated.

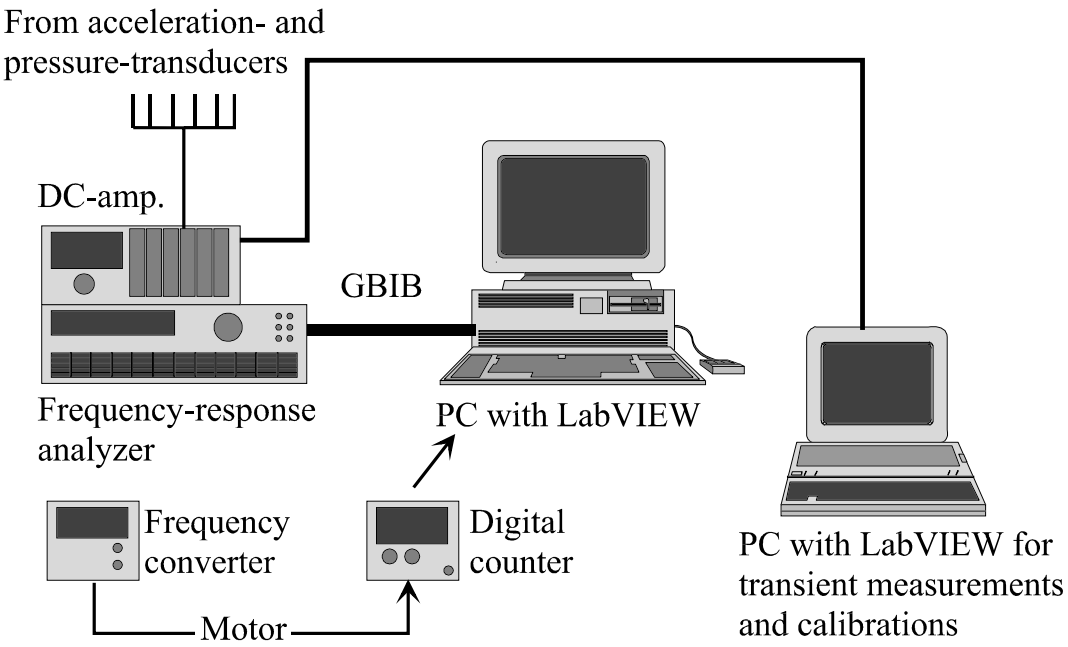

Figure 7.9: Data acquisition system

7.1.5 Data acquisition system

The gain-phase analyzer was controlled with PC and LabVIEW through a GPIB communication port. A program was made in the LabVIEW environment that could control all the functions of the gain-phase analyzer as well as showing all the results graphically and saving them for later use, see Figure 7.9.

The gain-phase analyzer was used in the "single channel mode" which means that only one channel at a time was measured (normally two channels are used to obtain the transfer function H_2/H_1 between these channels). The reason for measuring only one channel was that the disk mounted on the motor was controlled by the frequency converter and not by the gain-phase analyzer, thus the frequency of the valve (three times that of the motor) had to be "manually" fed into the gain-phase analyzer. In this experiment it is the transfer function from pressure and acceleration to the valve opening that is of interest, and since the exact amplitude and frequency of the valve are known, there were no need to measure it by the gain-phase analyzer. When using the "single channel mode" the measured signal is divided by unity, thus the amplitude and phase are restored when the frequency and amplitude of the excited signal are known. The practical consequence of this was the manual "feeding" of frequencies read from the counter. However, this was (partly) compensated for by

the use of LabVIEW[3].

The experiments were done by setting the frequency of the valve opening by adjusting the frequency converter accordingly, and to measure the frequency response (amplitude) of the pressure transducers and accelerometers. Amplitudes and steady state openings are given together with the results in Chapter 8.1.

7.2 Computer program

Making a general program from scratch requires a lot of work, and has been the most laborious part of this thesis. The program is coded with a mixture of C++ and FORTRAN. The main body of the program was coded with the use of objects (Object Oriented Programming, OOP) in C++. For the solvers (Real/Complex eigenvalues and Real/Complex matrix solver) existing FORTRAN routines were used [42, LAPACK]. An explanation and tutorial to object oriented programming in C++ can be found in [43, Stroustrup]. How to mix FORTRAN and C++ is slightly machine and compiler-dependent. The compilers used herein[4] were Watcom C/C++ and Watcom FORTRAN (32 bit compilers), and the compiled FORTRAN and C++ codes are linked together with the Watcom linker. Explanations of how to mix the two languages using WATCOM are found in the user manuals [63].

7.2.1 Object Oriented Programming

Standard programming languages have two types of generalized structures. One type is used to hold or gather data. In FORTRAN, `common` blocks are used for this purpose while the more versatile `struct` is used in C. The other structure-type is used to perform operations on these data (`function` and `subroutine`).

Object Oriented Programming (OOP) introduces a new type of structure, namely *objects*, or more precisely a `class` (`class` is the name of the structure-type, as in `struct` or `function`, while the word object is used to describe the "physical" entities when these classes are made in the computer's memory). The most obvious characteristics of these objects is that they have *both* data and functions/subroutines. These functions and subroutines are called *methods*. This means that different entities "knows" what they can do. For example a matrix object may have methods to make the inverse, the transposed, multiply with other matrices etc.

Two versions of a program that multiplies two matrices, uses the resulting matrix in a matrix solution, and print the solution, are shown in pseudo-code in Figure 7.10 and Figure 7.11. Using standard programming one needs one subroutine for

[3]Mounting three pickups on the disk/motor and setting the gain-phase analyzer in "sync" mode (synchronizing the analyzer to the valve opening), was not done because of time and founding limits.

[4]The program was developed on a UNIX workstation, and was moved to PC platform later.

multiplication, one for solving and one for printing. It is also necessary to remember all the arguments for these subroutines. In the object oriented version one can see that all the code relating to multiplication, solution and printing can be hidden within the *matrix class*. No calls to external subroutines (often with a large number of arguments) are needed. The practical consequences of this is that large programs become much easier to grasp, and more importantly: much easier to debug, because all the functions and subroutines are completely independent of the main program code. (The FORTRAN routines used in the FEM computer program are made as methods within matrix objects, and are completely hidden from the main program).

Another important thing about OOP is *abstraction* and *inheritance*. Abstraction means that one can make classes that have no defined data or methods, only the names of these methods. An abstract matrix class could for instance have an undefined method called solve. Then one could make two different matrix classes (Real and Complex) that *inherit* and define the method solve. Further down in the hierarchy one could make specialized matrices (FEM stiffness matrices) that inherit one or both of the methods depending on the matrix. With this approach it is possible to make abstract and quasi-abstract levels at the top, and make more concrete code that inherits the definitions further down the hierarchy. The advantage is that it is very easy to extend existing programs to include new routines and structures and only relatively small modifications at the bottom levels are needed to change existing structures. In the examples in Figure 7.10 and Figure 7.11 one would have to change the main program to be able to print complex matrices using standard programming (print and cprint). In the object oriented version this is not necessary because the print routine is inside the object itself, thus the same main program can be used.

```
Matrix A(n,m);
Matrix B(m,n);
Matrix C(n,n);
Matrix D(n,1);
   mult(A,n,m,B,n,m,C);
   solve(C,D,n);
   print(D,n,1);
end;
```

Figure 7.10: Pseudo-code using standard programming.

```
Matrix A(n,m);
Matrix B(m,n);
Matrix D(n,1)
   D.solve(A*B);
   D.print;
end;
```

Figure 7.11: Pseudo-code using object oriented programming.

7.2.2 Program pseudo-code

When using OOP standard flow charts are not right tool to describe the program flow. The most obvious reason for this, is that there are practically no *program flow* to describe. This is realized when remembering that all the methods needed to perform operations on data within a specific class, also are inside this class. Thus designing a program will be a task of deciding which classes to make, what kind of data they shall have, the methods to operate on the data and how these classes shall communicate with other classes. The communication process between classes is the other reason for not using flow charts. Therefore in OOP, so-called pseudo-codes are used both to describe the program and as a program design tool[5].

An overview of the main classes and methods of the FEM FSI program used in this thesis is given below:

```
Start Program
   Make pipe_base
   Make FEM_structures from pipe_base
   Solve FEM_structures
   Make output from (FEM_structures and pipe_base)
   Write output
End program
```

When reading the pseudo-code the *nouns* are the objects (classes) in the program, the *verbs* related to the nouns are the methods, while the *prepositions* relating two or more classes defines the data transfer between these classes. This program therefore consists of three main classes at the top level (in addition to the program itself):

- pipe_base
  - make
- FEM_structures (all the FEM matrices, stiffness etc.)
  - make
  - solve
- output.
  - make
  - write

[5]Making a flow chart descibing the same overall functionality can of course be done, but this chart will not be helpful in making a good object oriented program.

In addition data has to be transferred from pipe_base to output and FEM_structures, and from FEM_structures to output.

Each of these top level classes are then divided in a hierarchical manner into subclasses down to the code itself. The pipe_base reads data from a input-file, do some calculations (number of elements, lengths, moments of inertia etc.) and sets up a database of the piping network. FEM_structures reads data from pipe_base and make the global FEM matrices. The global system is then solved (eigenvalue or frequency response, depending on the input). The output reads from pipe_base and FEM_structures and writes the solution to various files. When the program ends the data structures are destroyed (deleted in memory)[6]. Specialized matrix classes were made, and most of the classes in FEM_structures were based on (inherited), methods and data structures from these matrix classes.

[6] The program consists of approximately. 6600 lines of C++ code and 14300 lines of FORTRAN (matrix solvers, LAPACK).

Chapter 8

Experimental and numerical results

8.1 Introduction

The main objectives of this chapter are, (in relation to the general points on page 4), to verify the computer code by comparison with experimental data. A minor objective is also to show that the proposed damping model can be used with success for FSI calculations. This Chapter contains only the results. Discussions are given in the next chapter.

All the experimental results are obtained from frequency response analysis of pressure and acceleration recordings obtained from the system described in section 7.1 using the valve with various relative amplitudes and with three different discs.

8.2 Experimental results

The experiments were made using three different valve characteristics, discs with: $5.0mm$ amplitude, $2.5mm$ amplitude and $1.5mm$ amplitude. With each of these discs different valve openings (Y_0) were set. Pressure and accelerations were measured.

8.2.1 2.5 mm amplitude

Two different series of experiments were performed, $Y_0 = 10mm$ and $Y_0 = 15mm$.

- Figure 8.1, Figure 8.3 and Figure 8.5 show pressure amplitudes from the experiment and from calculations without coupling to have a comparison with the calculations with coupling (FSI). Valve parameters for these figures are: $Y_0 = 15.0mm$ ($A_0 = 150mm^2$), $P_0 = 93.2 \pm 1.0KPa$ at the valve.
- Figure 8.2, Figure 8.4 and Figure 8.6 show the calculations with the same parameters as above, but with FSI included. Damping as explained in Chapter 5 is also included.
- Results for $Y_0 = 10mm$ are given in Figure 8.7 to Figure 8.10, where Figure 8.9 and Figure 8.10 are accelerations in x and y directions at the bend.
- In Figure 8.26 and Figure 8.27 comparisons between acceleration calculations with and without FSI are shown. The calculations without FSI are done by setting the Poisson ratio to zero, and using only the pressure-based coupling (one way coupling at junction from pressure to structure as shown in Figure 4.2). In Svingen [45] this relation is shown where the calculations will be uncoupled, but done simultaneously.

8.2.2 5 mm amplitude

Parameters for the valve with this disk were: $Y_0 = 38.3mm$ ($A_0 = 383mm^2$), $P_0 = 92.2 \pm 1.0KPa$ (at the valve). The amplitude was $5.0mm$.

- Results from calculations and experiments are in Figure 8.11 to Figure 8.16. The calculations are done with and without damping.
- Figure 8.28 to Figure 8.30 are comparisons between acceleration-calculations with and without FSI.

8.2.3 1.5 mm amplitude

Two series were performed also with this amplitude: $Y_0 = 4.5mm$, $P_0 = 94.0 \pm 1.0KPa$ and $Y_0 = 13.9mm$, $P_0 = 91.2 \pm 1.0KPa$. The amplitude of the valve was $1.5mm$.

- Figure 8.17 to Figure 8.22 show the pressure for the two steady-state valve openings.
- Figure 8.23 to Figure 8.25 show accelerations for $Y_0 = 13.9mm$.

8.3 Numerical results

The results from the computer program are obtained with a system that has the properties as given in Figure 7.1 and Figure 7.2 and in Table 7.1 and Table 7.2. Details concerning the numerical procedures and discretization can be found in Chapter 3 to Chapter 6. Timoshenko beam theory was used to model the bending of the pipes.

8.3.1 Computer representation of experimental arrangement

The experimental system was represented in the computer program as follows (see Figure 7.1 and Figure 7.2):

Nodes 1-5 ordinary pipe elements with appropriate thickness.

Nodes 5-8 pipe elements with flexibility factor (10.7).

Nodes 8-12 ordinary pipe elements with appropriate thickness.

Nodes 12-13 thick-walled ordinary pipe elements.

Nodes 13-16 ordinary pipe elements with appropriate thickness.

8.3.2 Eigenvalues of the system

Eigenvalues of the system shown in Figure 7.1 was calculated without the valve matrix just to give an idea of the frequencies involved and to see the differences with and without FSI. In Table 8.1 the first 31 resonant-frequencies for uncoupled, Poisson coupling, junction coupling and both couplings can be found.

Mode #	**Uncoupled**	**Poisson**	**Junction**	**Both**
1	2.0	2.0	2.0	2.0
2	3.6	3.6	3.6	3.6
3	6.0	6.0	6.0	6.0
4	10.3	10.3	10.3	10.3
5	12.4	12.4	12.4	12.4
6	19.8	19.8	19.7	19.6
7	22.2	22.2	22.1	22.1
8	29.1 F	29.2 (F)	26.8 (F)	27.2 (F)
9	31.3	31.3	31.3	31.2
10	36.2	36.2	36.2	36.2
11	43.8	43.8	43.2	42.7
12	54.1	54.0	54.1	53.9
13	58.3 F	57.2 (F)	57.1 (F)	56.0 (F)
14	59.5	59.5	60.5	60.3
15	74.1	74.3	73.9	73.2
16	79.9	78.9	79.0	76.7
17	87.9 F	84.7 (F)	82.1 (F)	79.1 (F)
18	96.5	96.6	96.4	96.4
19	100.8	101.7	101.7	102.3
20	111.6	113.8	107.4	106.2
21	117.7 F	117.8 (F)	120.3 (F)	120.1 (F)
22	120.5	121.0	121.7	121.4
23	136.0	137.5	137.3	137.4
24	137.8	139.1	137.8	139.7
25	148.2 F	145.3 (F)	149.7 (F)	147.9 (F)
26	158.0	158.7	158.0	158.2
27	171.7	171.6	171.6	171.6
28	179.6 F	176.9 (F)	182.6 (F)	182.7 (F)
29	184.0	184.1	188.6	189.8
30	207.4	207.4	207.5	207.2
31	211.6 F	208.2 (F)	211.7 (F)	208.5 (F)

Table 8.1: The first 31 resonant frequencies calculated with various couplings. F represents fluid modes [Hz].

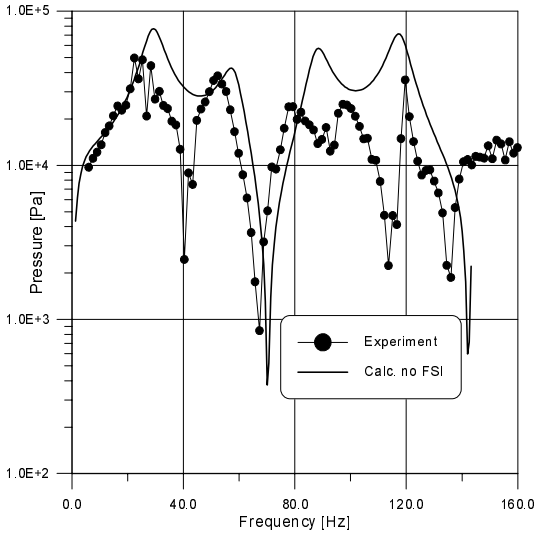

Figure 8.1: Pressure at bend (node 4). Y_0=15mm, Y_{ex}=2.5mm. Calculations: no FSI, no damping.

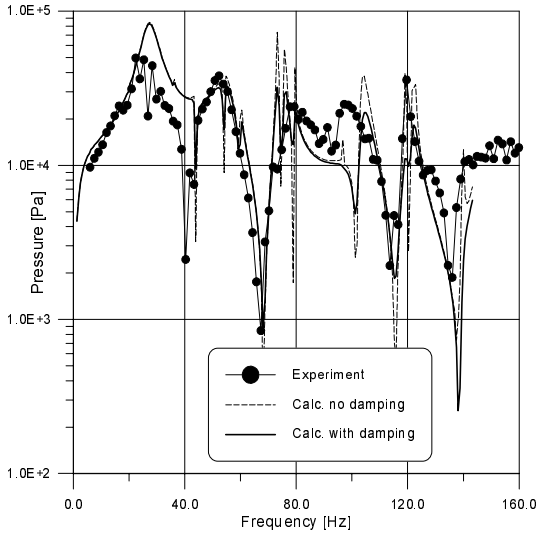

Figure 8.2: Pressure at bend (node 4). Y_0=15mm, Y_{ex}=2.5mm. Calculations: FSI , damping/no damping.

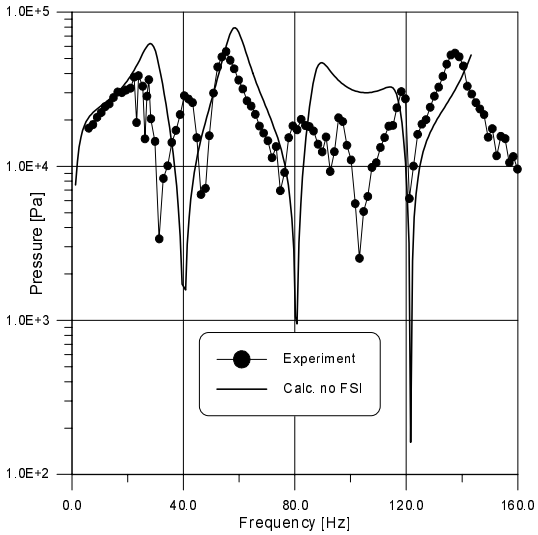

Figure 8.3: Pressure at midpoint (node 10). Y_0=15mm, Y_{ex}=2.5mm. Calculations: no FSI, no damping.

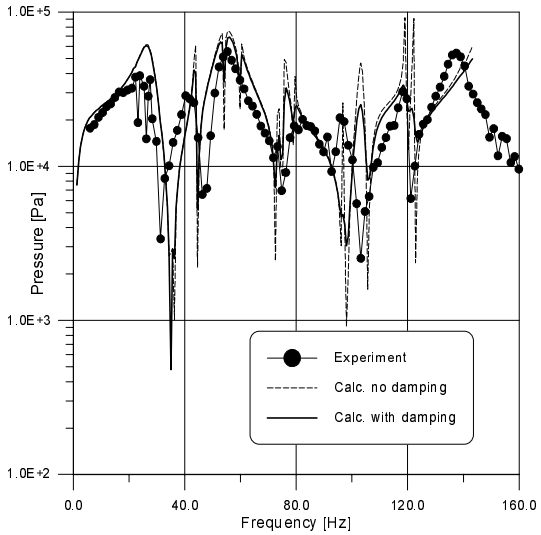

Figure 8.4: Pressure at midpoint (node 10). Y_0=15mm, Y_{ex}=2.5mm. Calculations: FSI, damping/no damping.

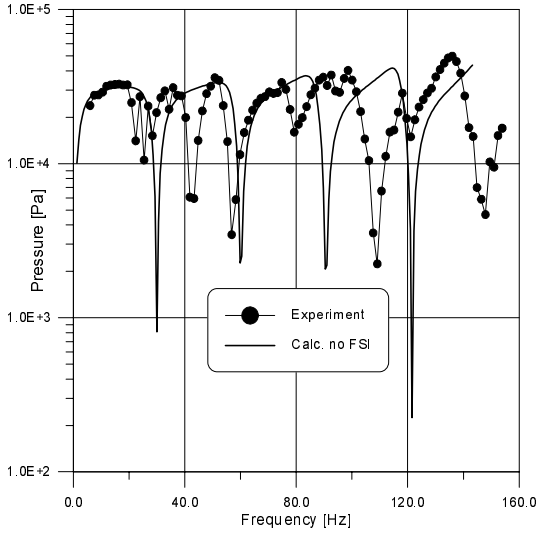

Figure 8.5: Pressure at valve (node 11). Y_0=15mm, Y_{ex}=2.5mm. Calculations: no FSI, no damping.

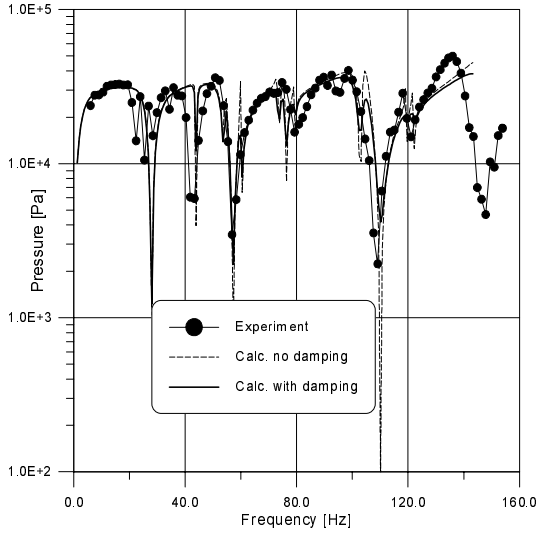

Figure 8.6: Pressure at valve (node 11). Y_0=15mm, Y_{ex}=2.5mm. Calculations: FSI, damping/no damping.

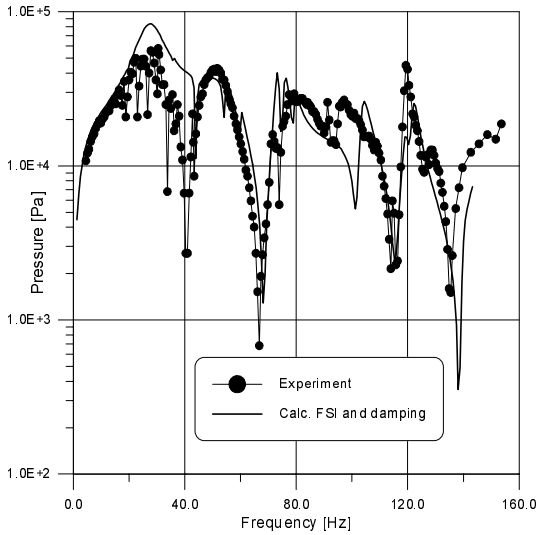

Figure 8.7: Pressure at bend (node 4). Y_0=10mm, Y_{ex}=2.5mm. Calculations: FSI, damping.

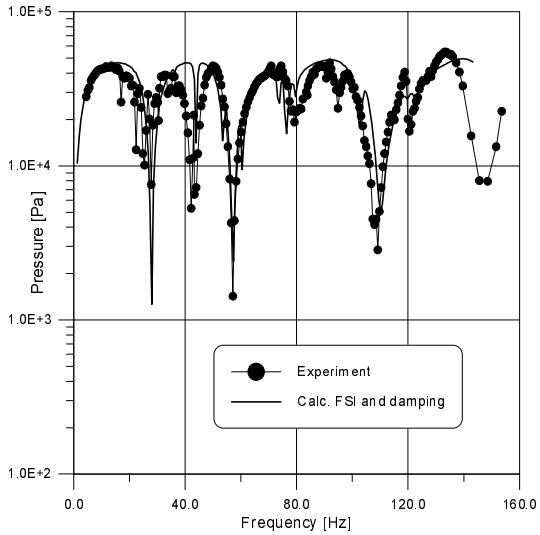

Figure 8.8: Pressure at valve (node 11). Y_0=10mm, Y_{ex}=2.5mm. Calculations: FSI, damping.

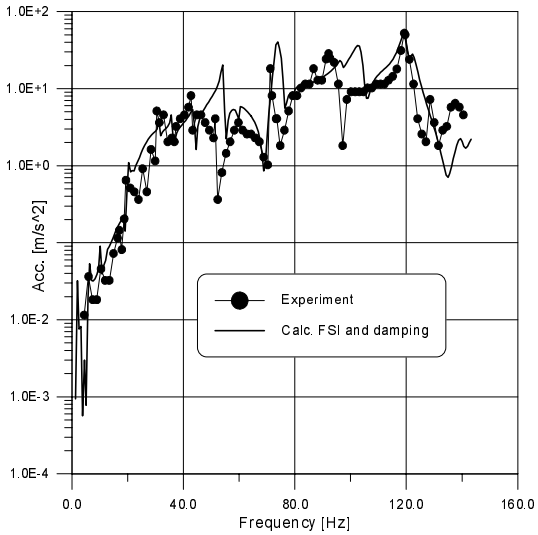

Figure 8.9: Acceleration in x-dir. at bend (node 5). Y_0=10mm, Y_{ex}=2.5mm. Calculations: FSI, damping.

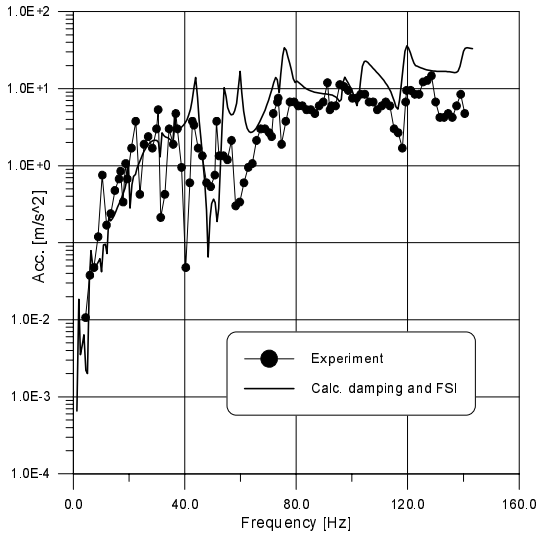

Figure 8.10: Acceleration in y-dir. at bend (node 8). Y_0=10mm, Y_{ex}=2.5mm. Calculations: FSI, damping.

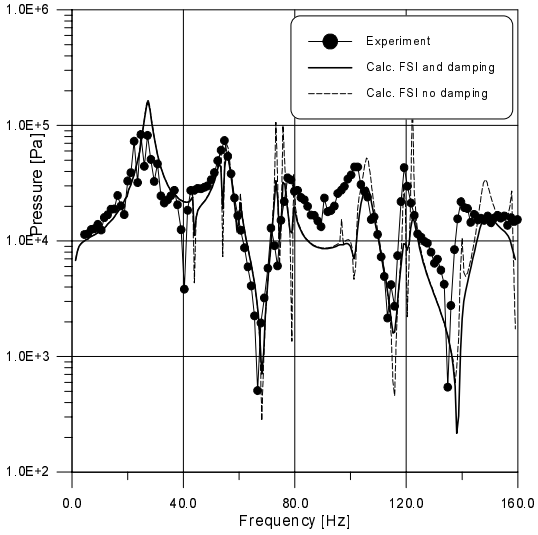

Figure 8.11: Pressure at bend (node 4). Y_0=38.3mm, Y_{ex}=5.0mm. Calculations: FSI, damping/no damping.

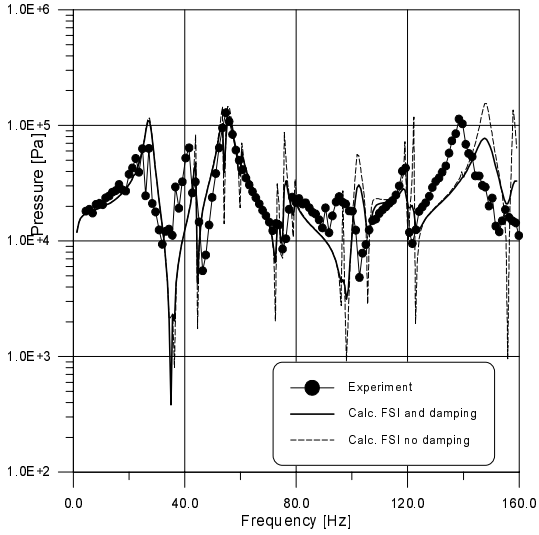

Figure 8.12: Pressure at midpoint (node 10). Y_0=38.3mm, Y_{ex}=5.0mm. Calculations: FSI, damping/no damping.

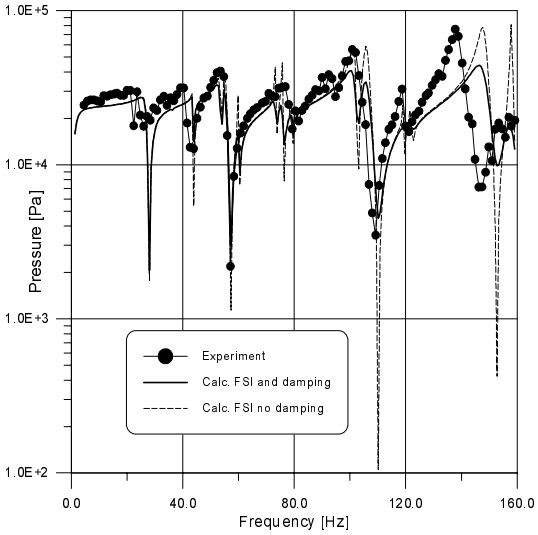

Figure 8.13: Pressure at valve (node 11). Y_0=38.3mm, Y_{ex}=5.0mm. Calculations: FSI, damping/no damping.

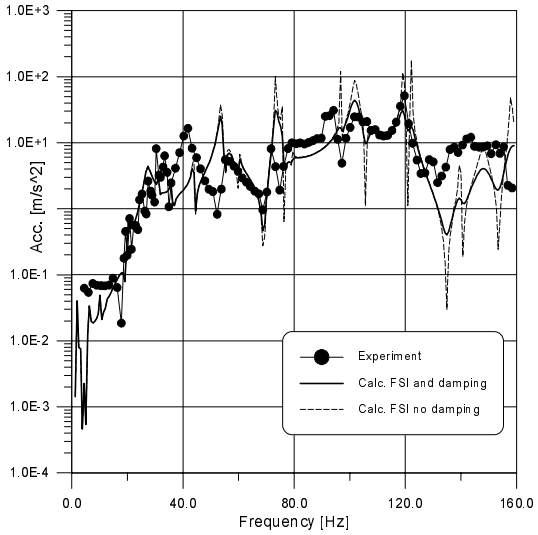

Figure 8.14: Acceleration in x-dir. at bend (node 5). Y_0=38.3mm, Y_{ex}=5.0mm. Calculations: FSI, damping/no damping.

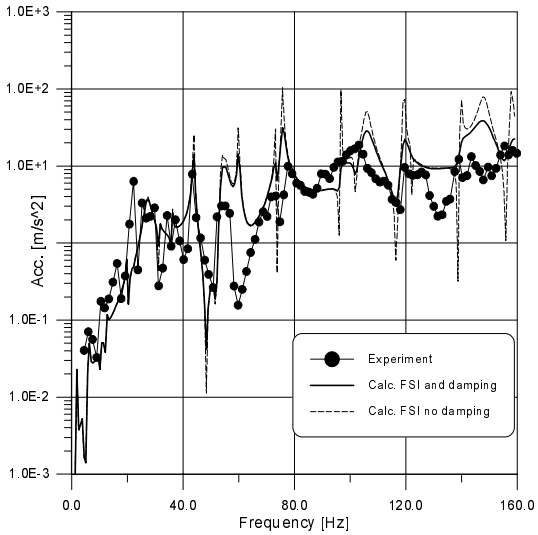

Figure 8.15: Acceleration in y-dir. at bend (node 8). Y_0=38.3mm, Y_{ex}=5.0mm. Calculations: FSI, damping/no damping.

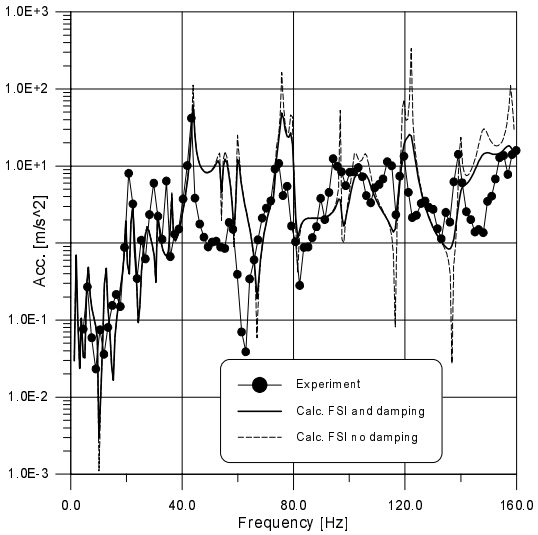

Figure 8.16: Acceleration in y-dir. at midpoint (node 10). Y_0=38.3mm, Y_{ex}=5.0mm. Calculations: FSI, damping/no damping.

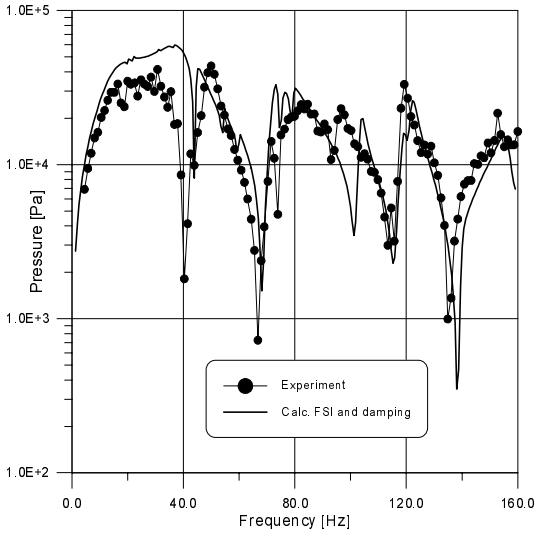

Figure 8.17: Pressure at bend (node 4). Y_0=4.5mm, Y_{ex}=1.5mm. Calculations: FSI, damping.

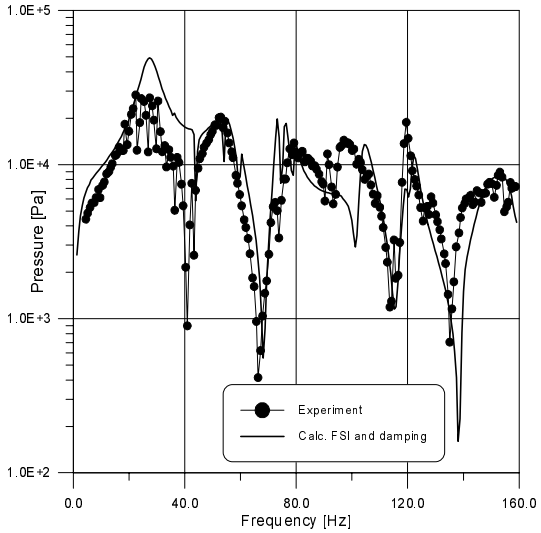

Figure 8.18: Pressure at bend (node 4). Y_0=13.9mm, Y_{ex}=1.5mm. Calculations: FSI, damping.

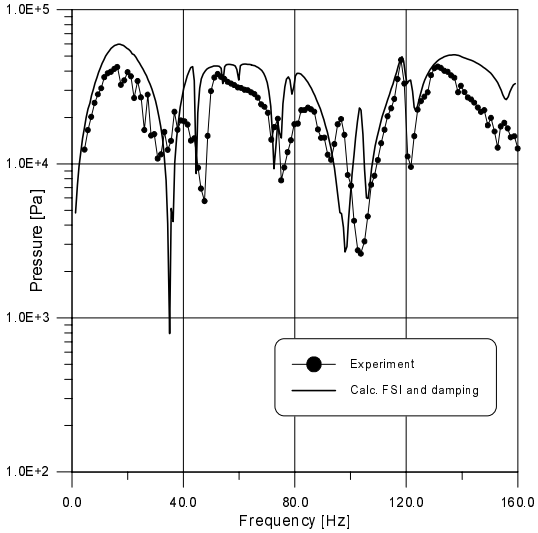

Figure 8.19: Pressure at midpoint (node 10). Y_0=4.5mm, Y_{ex}=1.5mm. Calculations: FSI, damping.

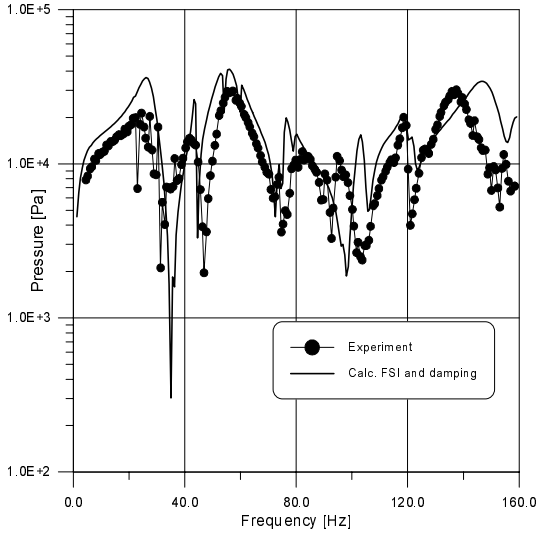

Figure 8.20: Pressure at midpoint (node 10). Y_0=13.9mm, Y_{ex}=1.5mm. Calculations: FSI, damping.

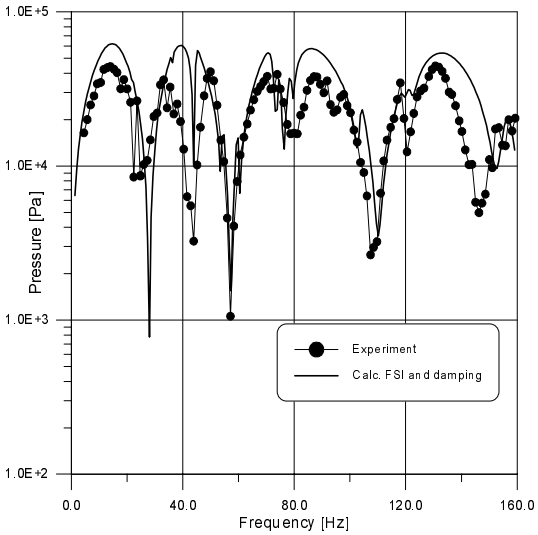

Figure 8.21: Pressure at valve (node 11). Y_0=4.5mm, Y_{ex}=1.5mm. Calculations: FSI, damping.

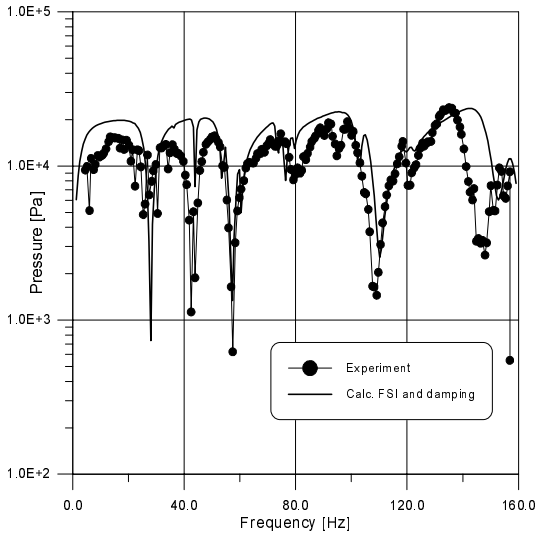

Figure 8.22: Pressure at valve (node 11). Y_0=13.9mm, Y_{ex}=1.5mm. Calculations: FSI, damping.

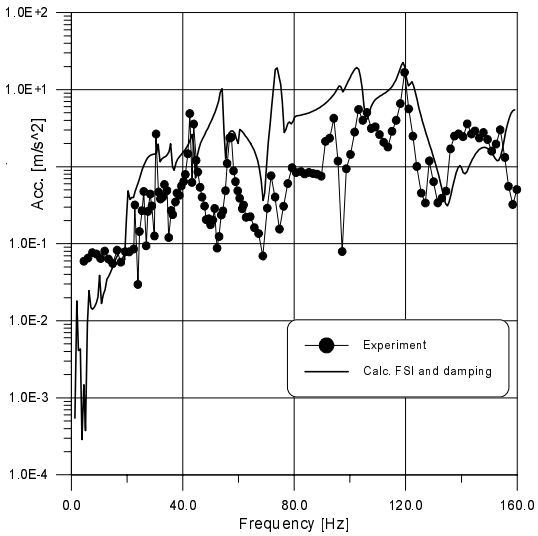

Figure 8.23: Acceleration in x-dir. at bend (node 5). Y_0=13.9mm, Y_{ex}=1.5mm. Calculations: FSI, damping.

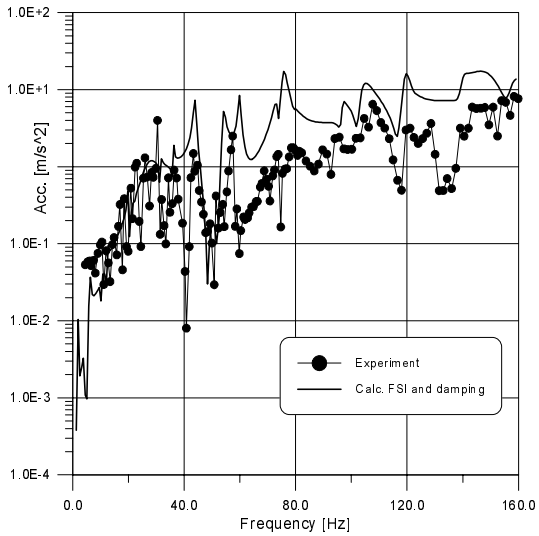

Figure 8.24: Acceleration in y-dir. at bend (node 8). Y_0=13.9mm, Y_{ex}=1.5mm. Calculations: FSI, damping.

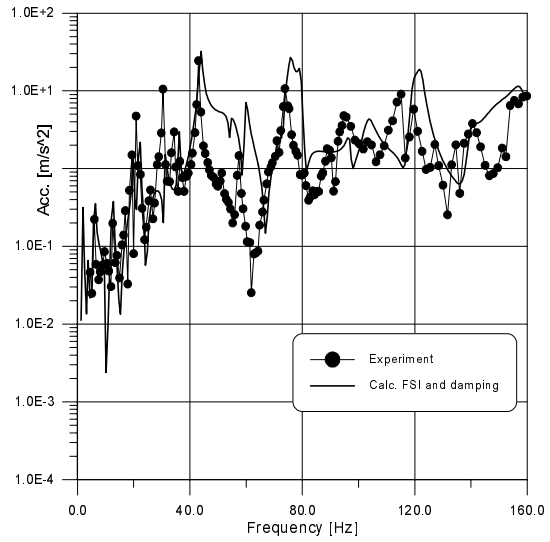

Figure 8.25: Acceleration in y-dir. at midpoint (node 10). $Y_0 = 13.9mm$, $Y_{ex} = 1.5mm$. Calculations: FSI, damping.

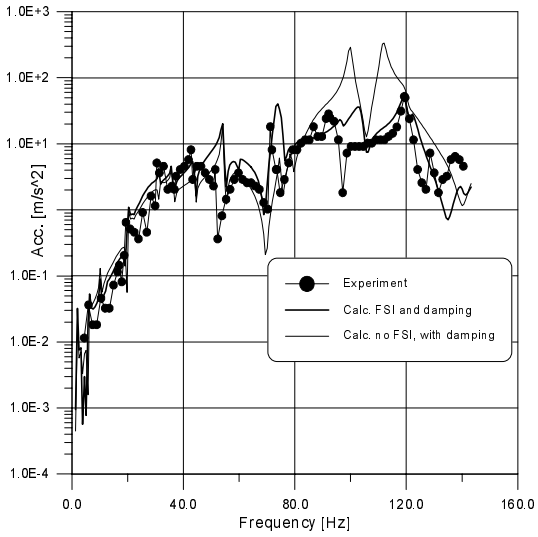

Figure 8.26: Acceleration in x-dir. at bend (node 5). Y_0=10mm, Y_{ex}=2.5mm. Calculations: FSI/no FSI, damping.

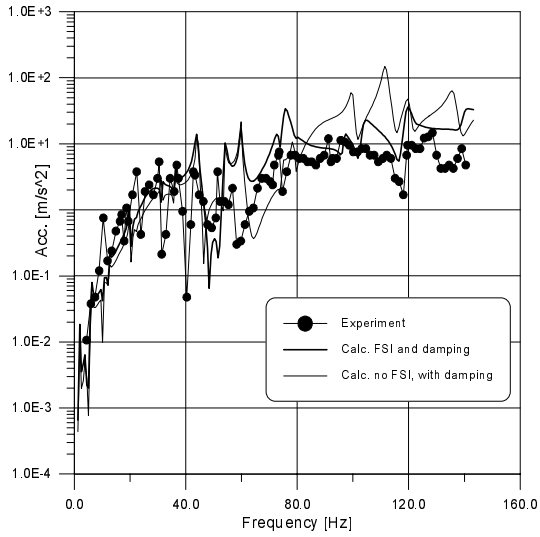

Figure 8.27: Acceleration in y-dir. at bend (node 8). Y_0=10mm, Y_{ex}=2.5mm. Calculations: FSI/no FSI, damping.

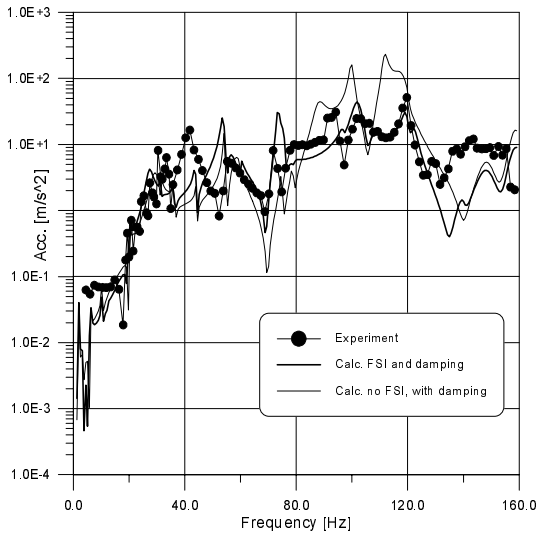

Figure 8.28: Acceleration in x-dir. at bend (node 5). Y_0=38.3mm, Y_{ex}=5.0mm. Calculations: FSI/no FSI, damping.

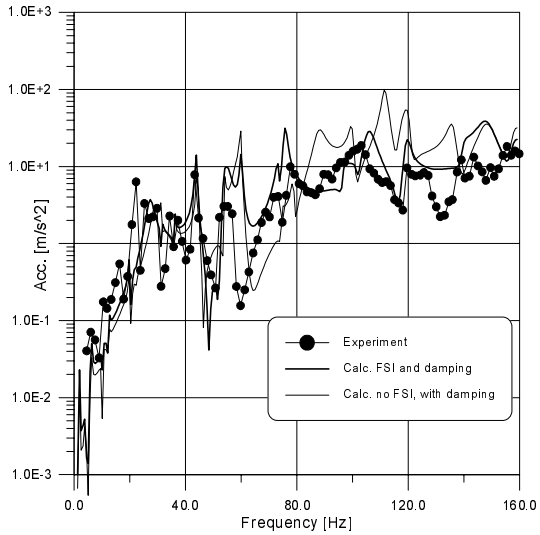

Figure 8.29: Acceleration in y-dir. at bend (node 8). Y_0=38.3mm, Y_{ex}=5.0mm. Calculations: FSI/no FSI, damping.

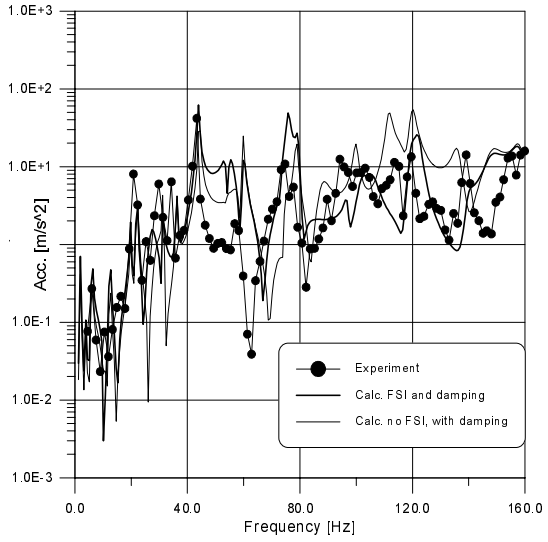

Figure 8.30: Acceleration in y-dir. at midpoint (node 10). $Y_0 = 38.8mm$, $Y_{ex} = 5.0mm$. Calculations: FSI/ no FSI, damping.

Chapter 9

Discussion

9.1 Eigenvalues

The resonant-frequencies presented in Table 8.1 indicate that the difference between the various couplings are in general small. Larger deviations can be found in the fluid resonant-frequencies than in the structural ones, which are literally identical below 70 Hz. The largest difference in fluid frequency between the uncoupled and the fully coupled calculations is at mode number 17. At this frequency a pressure anti-node is approximately at the bend, and it is also close to the first longitudinal frequency of the horizontal pipe. However, it is the author's opinion that great care should be taken when looking at the resonant-frequencies alone. This is because the size of the pressure amplitudes can be large also between the pressure resonant-frequencies because of the FSI effects.

The reason for this lies in the mathematical fundamentals of eigenvalue analysis. To be able to see the relative size of the pressure amplitudes between the pressure resonant-frequencies (at structural frequencies between the fluid frequencies), one must also look at the eigenvectors. Since both fluid and structure are involved with different units, the eigenvector matrix should be *both* non-dimensional *and* orthonormal, to be able to extract this kind of information from it. Non-dimensionality and orthonormality are no criteria to be able to do this. However, to extract this information with a reasonable amount of work, and more importantly, be able to visualize the results, it is an obvious advantage. Currently the program calculates eigenvectors (orthogonal), but the non-dimensionality and orthonormality are not yet implemented.

9.2 Frequency response

The frequency response calculations reveal much more information than the eigenvalue analysis because the exact amplitude can be calculated.

9.2.1 FSI

The effect of FSI is clearly seen in Figure 8.1 to Figure 8.6. The uncoupled calculations deviate significantly from the experiments. The size of the amplitudes are more or less the same, but the peaks are placed at different frequencies. The shapes are also different.

The calculations with FSI show very good agreement with all the experiments. In Figure 8.3 and Figure 8.4 one can see that there is a pressure peak in the experiment at 40 Hz. The uncoupled analysis has actually a node at that frequency, while the analysis with FSI correctly predict the peak. A similar situation happens at approximately 90 Hz in Figure 8.5 and Figure 8.6.

9.2.2 The valve characteristics

Looking at the different figures (especially Figure 8.17 to Figure 8.22) one can see that different steady state valve openings (Y_0) have a large effect on the amplitudes. This emphasizes the importance of being able to model other hydraulic piping components besides the pipes with a high level of accuracy.

9.2.3 Accelerations

The measured and calculated accelerations with FSI show very good agreement, even though the agreement is not as good as for the pressure amplitudes. All the major acceleration peaks are correctly predicted by the program. Looking at Figure 8.14 one can see that the main peaks measured are at approximately 30, 40, 75, 100 and 120 Hz. These peaks, as well as their sizes, are predicted by the program.

The calculations without FSI (Figure 8.26 to Figure 8.30) shows good agreement up to about 90 Hz. In the range from 90 to 120 Hz the uncoupled calculations have much *larger* amplitudes than both experiments and calculations with FSI.

9.2.4 Damping

By looking at the figures showing calculations with and without damping, it is very obvious that correct *frequency-dependent damping* is essential in obtaining the correct maximum amplitudes for both accelerations and pressures. The damping model used herein as explained in Chapter 5 shows very promising results. To obtain

these results, it is necessary to choose an appropriate value for the damping constant, λ_f, for the corresponding pipe. It is therefore obvious that specialized experiments and field measurements are needed to find the relations to other piping parameters (roughness, diameter and Re_0 number). Good correspondence with experiments was found with an λ_f-value of $34,000.0$, (smooth stainless steel pipe with inner diameter of 80 mm).

9.3 Findings

The importance of being able to model the valve (and other hydraulic piping components) is seen in Figure 8.17 to Figure 8.22. The peaks are more or less at the same frequencies, but the shapes have changed. An extreme case is found in Figure 8.13 where the peaks are grown together to almost a continuous peak all the way from 4.5 to 100 Hz.

A very interesting observation is found in Figure 8.26 to Figure 8.30, where actually the calculations without FSI have *larger* amplitudes than the ones with FSI. These unrealistic peaks from the calculations without FSI occur around the axial resonant-frequencies of the two reaches. Looking at Figure 8.26 one can see that the acceleration calculated without FSI at 100Hz, is approximately *10 times larger* than the one measured and the one calculated with FSI. The same phenomenon can be observed at 110 Hz. These peaks are largest in x-direction at the bend, but can also be found in the y-direction (Figure 8.27). A similar finding in *time-domain* can be found in [56, Tijsseling and Lavooij]. At the midpoint of the horizontal reach this effect is much smaller. The pressure amplitudes at the bend at these frequencies are also much smaller for the experiments and calculations with FSI compared to the calculations without FSI (see Figure 8.1 and Figure 8.3).

On the basis of these experiments *only*, it is difficult to give an explanation to the reason for this damping effect due to FSI. The author believes that this particular system have characteristic fluid- and structural eigenvalues that make this damping effect, and that other systems may have characteristics that lead to amplifications of the acceleration amplitudes. This explanation is strengthened by [53, Tijsseling] where the effects of interaction, both in the pressures and in the stresses/accelerations are reported to be strongly system-dependent. It *is* clear that this effect in the calculations with FSI is *not* due to the proposed damping model used. This can be seen by comparing Figure 8.14 and Figure 8.28.

Physically an uncoupled analysis (coupling only from fluid to structure) violates the energy conservation. In an uncoupled calculation, all the fluid energy is transferred to the structure, but no energy is transferred back to the fluid. Besides, the fluid transfers all its energy and still retains all of it, which of course is physically impossible. The large differences between uncoupled calculations compared with

experiments and FSI calculations (both pressures and accelerations) can therefore be explained (at least in an overall picture) by the law of energy conservation, and indeed strengthens the importance of being able to calculate the correct responses in a piping system.

9.4 Discrepancies

Although the agreements with calculations and experiments are very good, some discrepancies can be found. In the pressure amplitudes the calculations deviates from the experiments in the range 20 to 40 Hz. This deviation is most obvious at the bend (see for instance Figure 8.7). The calculated amplitudes are too large, and the small short amplitudes found in the experiment are not found in the calculations. There may be several reasons for this. The reason most likely is that the system is not discretized with sufficient accuracy. Because the system changed shape when filled with water, measurements had to be done "by hand" with an accuracy of maximum $\pm 1\ cm$. The shape of the system was also difficult to discretize because of the curved horizontal reach (see Figure 7.2). The pipe curved both ways with relatively small deviations, and it was difficult to find the exact spots where the curves changed. This reach was therefore approximated with three pipe lengths with 5 elements each. The effect of this approximation is reflected in the bending vibrations because the variable $(\frac{\partial w}{\partial x})$ describing the bending angle as well as the direction of w will be slightly inaccurate at the connection points of the shorter pipe lengths, as shown in Figure 9.1. By looking at the accelerations in y direction (for example Figure 8.10, Figure 8.15 and Figure 8.16) one can find these short amplitudes. Another reason *might* be that even though the valve support was modified by greatly adding both stiffness and mass [49, Svingen], it still moved enough to affect the vibrations.

In the figures (Figure 8.17 to Figure 8.22) one can see that the calculated pressure amplitudes in general are too large compared to the ones measured. This disagreement extends throughout the frequency range, thus, a possible reason could be the valve matrix. As mentioned in Chapter 6 the steady state flow through the valve was not measured[1], but approximated with the relation:

$$Q_0 = \mu(Y)_0 \sqrt{2g\left(H_2 - H_1\right)_0}$$

$H_{1,0}$ and Y_0 were known (atmospheric pressure and steady state valve opening respectively). H_2 is the pressure just in front of the valve, and was measured with the pressure transducer by averaging the signal over one minute using LabVIEW. The inaccuracy connected to this steady state pressure measurement was that the

[1] The reason for not measuring the steady state flow was the design of the valve, optimized for perfect sine functions.

transducer was very close to the shutdown valve (0.10 m), thus, any disturbances to the flow made by the valve, was picked up by the transducer. The parameter μ was approximated as the discharge area which is consistent with the loss coefficients ($\zeta < 0.03$) for a bellmouth when $r/D_h \geq 0.2$. (see [20]). For this valve the smallest value of r/D_h was 0.8, giving a hydraulic loss of maximum 0.02mWC (r is the radius of the bellmouth and D_h is the hydraulic diameter).

This discrepancy is *only* seen for the experiments with the 1.5 mm amplitude discs. The clearance between the disk end the pipe-end (water side) of the valve was 0.1 mm, thus some water would always go between the disc and the pipe-end instead of going straight out. The relative effect of this leakage is greater for a disc with small amplitude than a disc with a large amplitude.

Anyhow, the experiments with this disc are used to show the difference between a large steady-state opening and a small steady-state opening, so the discrepancies in this respect are less important, although it emphasizes the importance of accurate modelling.

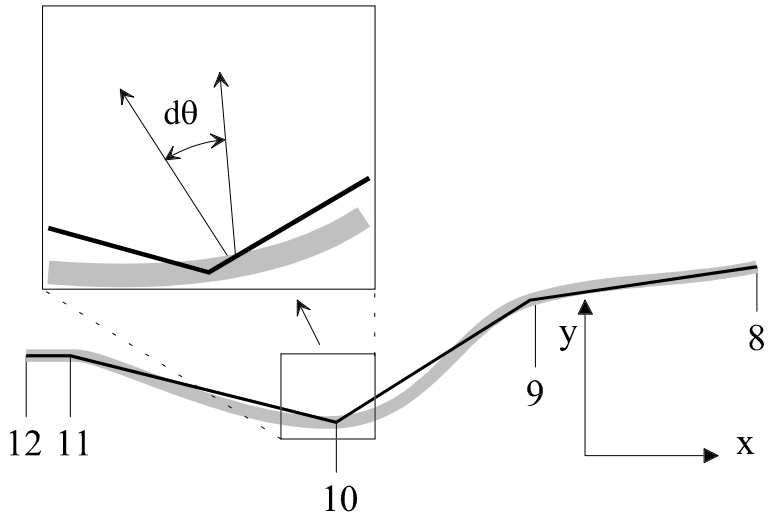

Figure 9.1: Error in discretization of the horizontal pipe-reach, (exaggerated).

9.5 Summary

Very good agreement between experiment and calculations are found, both for the pressure amplitudes and the accelerations. Calculations without FSI deviate quantitatively and qualitatively by large amounts at various frequencies.

Axial acceleration-calculations without FSI give (at least in this particular case), maximal accelerations 10 times larger than of those measured and calculated with FSI. This suggests that piping designs based on vibration calculations without FSI, can in fact be much too conservative than necessary.

The pressure amplitudes change when the valve changes its characteristics. This shows the importance of being able to include a good representation of the valve in the calculations. Other hydraulic piping components (pumps, turbines etc.) have similar effects on the amplitudes.

As an example one can think that the valve in the experiment (Figure 7.1) is replaced with a pump which has a given blade passing frequency of 90 Hz. For the simplicity and purpose of this example, one can assume that the pump characteristics are the same as the valve characteristics. By using a calculation without FSI one gets the impression that this frequency will be an excellent one because (from Figure 8.5) the pressure response has a node at this place. The experiment and the calculations with FSI (Figure 8.6) show that the opposite is the case, namely a pressure peak. This pump will therefore cause large vibrations in the system, especially at the pump supports, and *only* a calculation with FSI will reveal it. For larger systems with loops and branches, the differences between calculations with and without FSI, will presumably be even larger.

An eigenvalue analysis reveals a lot of information about the system. However, the author believe that it should be used with care because large pressure amplitudes can be excited at frequencies where no actual fluid resonant-frequency (in a mathematical and physical sense) exists. These pressure amplitudes are made solely due to the FSI effects. The pressure peak at 90 Hz in Figure 8.6 is not predicted by looking at the resonant frequencies, but is predicted by the frequency response calculations.

The damping model seems to predict the frequency-dependent damping with good accuracy, and it is very easy to include in the calculations. To be able to use it for any given pipe and flow, further experimental and theoretical work are needed to find the corresponding λ_f values.

9.6 Further work

The author has great belief in the FEM discretization, and further work will include further development of the computer code. More specifically the program will be extended from two-dimensional to three-dimensional piping network, and codes for

elastic boundary conditions will be included. Research in developing the damping model, to be able to use it for any given pipe, is also needed.

In general more experimental work is needed, both laboratory work and field measurements, to give a broader basis for further enhancements of computer codes and general design criteria.

Experimental and theoretical research in the field of acoustical sources as mentioned in Chapter 6.4 is also very important.

Fatigue analysis is a field where frequency response calculations often are preferable when statistical input data are used. The same statistical fatigue analysis techniques as used for marine risers and pipelines, as described in [27, Larsen], can also be used for general piping systems. In [28, Larsen and Passano] and [27, Larsen], time- and frequency-domain calculations have been compared and the conclusion was that frequency-domain calculations can be used with a high degree of confidence even for nonlinear input (short-crested waves). Development of statistical fatigue analysis calculation for use in general piping systems based on the research done in marine riser analysis [9, Demirbilek] will be the next logical step.

Appendix A

Neglecting convective terms

The two-dimensional Navier-Stoke's equations from Chapter 3 (continuity and momentum, Equation 3.1, Equation 3.2 and Equation 3.3) are:

$$\frac{\partial \rho}{\partial t} + v_x \frac{\partial \rho}{\partial x} + v_r \frac{\partial \rho}{\partial r} + \rho_f \frac{\partial v_x}{\partial x} + \frac{\rho}{r}\frac{\partial}{\partial r}\left(r v_r\right) = 0 \tag{A.1}$$

$$\begin{aligned} \rho \frac{\partial v_x}{\partial t} + \rho v_x \frac{\partial v_x}{\partial x} + \rho v_r \frac{\partial v_x}{\partial r} + \frac{\partial p}{\partial x} = F_x + \\ \left(\kappa + \frac{1}{3}\mu\right)\frac{\partial}{\partial x}\left(\frac{\partial v_x}{\partial x} + \frac{1}{r}\frac{\partial\left(r v_r\right)}{\partial r}\right) + \mu\left(\frac{1}{r}\frac{\partial}{\partial r}\left(r\frac{\partial v_x}{\partial r}\right) + \frac{\partial^2 v_x}{\partial x^2}\right) \end{aligned} \tag{A.2}$$

$$\begin{aligned} \rho \frac{\partial v_r}{\partial t} + \rho v_x \frac{\partial v_r}{\partial x} + \rho v_r \frac{\partial v_r}{\partial r} + \frac{\partial p}{\partial r} = F_r + \\ \left(\kappa + \frac{1}{3}\mu\right)\frac{\partial}{\partial r}\left(\frac{\partial v_x}{\partial x} + \frac{1}{r}\frac{\partial\left(r v_r\right)}{\partial r}\right) + \mu\left(\frac{1}{r}\frac{\partial}{\partial r}\left(r\frac{\partial v_r}{\partial r}\right) + \frac{\partial^2 v_r}{\partial x^2}\right) \end{aligned} \tag{A.3}$$

Introducing Stokes hypothesis [65]: $\left(\kappa + \frac{1}{3}\mu\right) = 0$, and $\frac{\partial \rho}{\partial p} = 1/a^2$ where $a^2 = K/\rho$ (neglecting the external body forces F_x):

$$\frac{1}{a^2}\frac{\partial p}{\partial t} + \frac{1}{a^2} v_x \frac{\partial p}{\partial x} + \frac{1}{a^2} v_r \frac{\partial p}{\partial r} + \rho \frac{\partial v_x}{\partial x} + \rho \frac{\partial v_r}{\partial r} + \frac{v_r}{r} = 0 \tag{A.4}$$

$$\rho \frac{\partial v_x}{\partial t} + \rho v_x \frac{\partial v_x}{\partial x} + \rho v_r \frac{\partial v_x}{\partial r} + \frac{\partial p}{\partial x} = \mu\left(\frac{1}{r}\frac{\partial v_x}{\partial r} + \frac{\partial^2 v_x}{\partial r^2} + \frac{\partial^2 v_x}{\partial x^2}\right) \tag{A.5}$$

$$\rho \frac{\partial v_r}{\partial t} + \rho v_x \frac{\partial v_r}{\partial x} + \rho v_r \frac{\partial v_r}{\partial r} + \frac{\partial p}{\partial r} = \mu\left(\frac{1}{r}\frac{\partial v_r}{\partial r} + \frac{\partial^2 v_r}{\partial r^2} + \frac{\partial^2 v_r}{\partial x^2}\right) \tag{A.6}$$

The following non-dimensional variables are used:

$$\frac{\partial}{\partial t_*} = \frac{L_0}{V_0}\frac{\partial}{\partial t} \quad \frac{\partial}{\partial x_*} = L_0\frac{\partial}{\partial x} \quad \frac{\partial}{\partial r_*} = L_0\frac{\partial}{\partial r} \quad \frac{1}{r_*} = L_0\frac{1}{r}$$

$$v_{x*} = \frac{v_x}{V_0} \quad v_{r*} = \frac{v_r}{V_0} \quad p_* = \frac{p}{\frac{1}{2}\rho_{f0}V_0^2} \quad a \approx a_0 \quad \rho = \rho_0$$

A.1 Continuity

The continuity equation (Equation A.4) now becomes:

$$\begin{gathered}\frac{V_0}{L_0}\frac{\rho_0 V_0^2}{2a_0^2}\frac{\partial p_*}{\partial t_*} + \frac{V_0\rho_0 V_0^2}{2L_0 a_0^2}v_{x*}\frac{\partial p_*}{\partial x_*} + \frac{V_0\rho_0 V_0^2}{2L_0 a_0^2}v_{r*}\frac{\partial p_*}{\partial r_*} + \\ \frac{\rho_0 V_0}{L_0}\frac{\partial v_{x*}}{\partial x_*} + \frac{\rho_0 V_0}{L_0}\frac{\partial v_{r*}}{\partial r_*} + \frac{V_0}{L_0}\frac{v_{r*}}{r_*} = 0\end{gathered} \tag{A.7}$$

$$\frac{V_0^2}{2a_0^2}\frac{\partial p_*}{\partial t_*} + \frac{V_0^2}{2a_0^2}v_{x*}\frac{\partial p_*}{\partial x_*} + \frac{V_0^2}{2a_0^2}v_{r*}\frac{\partial p_*}{\partial r_*} + \frac{\partial v_{x*}}{\partial x_*} + \frac{\partial v_{r*}}{\partial r_*} + \frac{1}{\rho_0}\frac{v_{r*}}{r_*} = 0$$

$$\frac{M_0^2}{2}\frac{\partial p_*}{\partial t_*} + \frac{M_0^2}{2}v_{x*}\frac{\partial p_*}{\partial x_*} + \frac{M_0^2}{2}v_{r*}\frac{\partial p_*}{\partial r_*} + \frac{\partial v_{x*}}{\partial x_*} + \frac{\partial v_{r*}}{\partial r_*} + \frac{1}{\rho_0}\frac{v_{r*}}{r_*} = 0 \tag{A.8}$$

where the Mach number is defined as: $M_0 = V_0/a_0$. The following relations can be found in Equation A.8 when considering very small Mach numbers, $M_0^2 \ll 1$, typical for liquid pipe flow:

Term		**Order**	**Smallness**
$\frac{M_0^2}{2}v_{x*}\frac{\partial p_*}{\partial x_*}$	$\Longrightarrow$	$O(\frac{M_0^2}{2})$	$\ll 1$
$\frac{M_0^2}{2}v_{r*}\frac{\partial p_*}{\partial r_*}$	$\Longrightarrow$	$O(\frac{M_0^2}{2})$	$\ll 1$
$\frac{\partial v_{x*}}{\partial x_*}$	$\Longrightarrow$	$O(1)$	1
$\frac{\partial v_{r*}}{\partial r_*}$	$\Longrightarrow$	$O(1)$	1

From this table one can see that the convective terms in the continuity equations are very small at low Mach numbers, thus, reducing Equation A.4 and Equation A.8 to:

$$\frac{1}{a^2}\frac{\partial p}{\partial t} + \rho\frac{\partial v_x}{\partial x} + \rho\frac{\partial v_r}{\partial r} + \frac{v_r}{r} = 0 \tag{A.9}$$

$$\frac{M_0^2}{2}\frac{\partial p_*}{\partial t_*} + \frac{\partial v_{x*}}{\partial x_*} + \frac{\partial v_{r*}}{\partial r_*} + \frac{1}{\rho_0}\frac{v_{r*}}{r_*} = 0 \tag{A.10}$$

This shows that the constraint $M_0^2 \ll 1$ is sufficient to neglect all convective terms in the continuity equations for one-dimensional and two-dimensional flow

A.2 Momentum

Applying the same non-dimensional variables to the momentum equations (Equation A.5 and Equation A.6):

$$\frac{V_0 V_0 \rho_0}{L_0}\frac{\partial v_{x*}}{\partial t_*} + \frac{V_0 \rho_0 V_0}{L_0} v_{x*}\frac{\partial v_{x*}}{\partial x_*} + \frac{V_0 \rho_0 V_0}{L_0} v_{r*}\frac{\partial v_{x*}}{\partial r_*} + \frac{\rho_0 V_0^2}{2L_0}\frac{\partial p_*}{\partial x_*}$$

$$= \frac{V_0 \rho_{f0} \nu_0}{L_0^2}\left(\frac{1}{r_*}\frac{\partial v_{x*}}{\partial r_*} + \frac{\partial^2 v_{x*}}{\partial r_*^2} + \frac{\partial^2 v_{x*}}{\partial x_*^2}\right)$$

$$\frac{V_0 V_0 \rho_0}{L_0}\frac{\partial v_{r*}}{\partial t_*} + \frac{V_0 \rho_0 V_0}{L_0} v_{x*}\frac{\partial v_{r*}}{\partial x_*} + \frac{V_0 \rho_0 V_0}{L_0} v_{r*}\frac{\partial v_{r*}}{\partial r_*} + \frac{\rho_0 V_0^2}{2L_0}\frac{\partial p_*}{\partial r_*}$$

$$= \frac{V_0 \rho_{f0} \nu_0}{L_0^2}\left(\frac{1}{r_*}\frac{\partial v_{r*}}{\partial r_*} + \frac{\partial^2 v_{r*}}{\partial r_*^2} + \frac{\partial^2 v_{r*}}{\partial x_*^2}\right)$$

Rearranging:

$$\frac{\partial v_{x*}}{\partial t_*} + v_{x*}\frac{\partial v_{x*}}{\partial x_*} + v_{r*}\frac{\partial v_{x*}}{\partial r_*} + \frac{1}{2}\frac{\partial p_*}{\partial x_*} = \frac{1}{Re_{L_0}}\left(\frac{1}{r_*}\frac{\partial v_{x*}}{\partial r_*} + \frac{\partial^2 v_{x*}}{\partial r_*^2} + \frac{\partial^2 v_{x*}}{\partial x_*^2}\right) \tag{A.11}$$

$$\frac{\partial v_{r*}}{\partial t_*} + v_{x*}\frac{\partial v_{r*}}{\partial x_*} + v_{r*}\frac{\partial v_{r*}}{\partial r_*} + \frac{1}{2}\frac{\partial p_*}{\partial r_*} = \frac{1}{Re_{L_0}}\left(\frac{1}{r_*}\frac{\partial v_{r*}}{\partial r_*} + \frac{\partial^2 v_{r*}}{\partial r_*^2} + \frac{\partial^2 v_{r*}}{\partial x_*^2}\right) \tag{A.12}$$

In Equation A.11 and Equation A.12 one clearly sees that the convective terms are of order one, $O(1)$, while the pressure terms are of order one half, $O(1/2)$. This means that the convective terms *can not in general be neglected* in the continuity equations for two-dimensional flow, even when Mach numbers are very small. By applying the relation from Equation A.10 into Equation A.11 and Equation A.12 one can show that $v_{x*}\frac{\partial v_{x*}}{\partial x_*}$ is small in Equation A.11 compared with $\frac{\partial v_{x*}}{\partial t_*}$, and similar for the radial velocity in Equation A.12 (see Equation A.15). However, the terms $v_{r*}\frac{\partial v_{x*}}{\partial r_*}$ and $v_{x*}\frac{\partial v_{r*}}{\partial x_*}$ can not be neglected unless this is a constraint of the flow (acoustics).

Flow in pipes is basically a one-dimensional phenomenon because the length to diameter ratio is large ($L_0/D_0 \gg 1$)[71]. Neglecting radial velocities and the variations in radial direction gives the following non-dimensional continuity and momentum equations:

$$\frac{M_0^2}{2}\frac{\partial p_*}{\partial t_*} + \frac{\partial v_{x*}}{\partial x_*} = 0 \tag{A.13}$$

$$\frac{\partial v_{x*}}{\partial t_*} + v_{x*}\frac{\partial v_{x*}}{\partial x_*} + \frac{1}{2}\frac{\partial p_*}{\partial x_*} = \frac{1}{Re_{L_0}}\frac{\partial^2 v_{x*}}{\partial x_*^2} \tag{A.14}$$

The $\frac{\partial v_{x*}}{\partial x_*}$ term in Equation A.14 is substituted with the relation in Equation A.13:

$$\frac{\partial v_{x*}}{\partial t_*} - \frac{M_0^2}{2} v_{x*}\frac{\partial p_*}{\partial t_*} + \frac{1}{2}\frac{\partial p_*}{\partial x_*} = \frac{1}{\mathrm{Re}_{L_0}}\frac{\partial^2 v_{x*}}{\partial x_*^2} \tag{A.15}$$

Considering $M_0^2 \ll 1$ the following relation can be seen:

Term		**Order**	**Smallness**
$\frac{M_0^2}{2} v_{x*} \frac{\partial p_*}{\partial t_*}$	$\Longrightarrow$	$O(\frac{M_0^2}{2})$	$\ll 1$
$\frac{\partial v_{x*}}{\partial t_*}$	$\Longrightarrow$	$O(1)$	1

Thus reducing Equation A.14 to:

$$\frac{\partial v_{x*}}{\partial t_*} + \frac{1}{2}\frac{\partial p_*}{\partial x_*} = \frac{1}{\mathrm{Re}_{L_0}} \frac{\partial^2 v_{x*}}{\partial x_*^2} \tag{A.16}$$

Showing that both the constraints, $M_0^2 \ll 1$ *and one-dimensional flow*, must be applied to be able to neglect convective terms in the momentum equations for a general flow field.

When neglecting the convective terms in the continuity equation because of the constraint: $M_0^2 \ll 1$, one obtain the equations describing so called *weakly compressible flow* [22] which are valid for a general flow field with large gradients governed by convective terms. In the one-dimensional case there is convection only in x-direction, and this term is very small compared to the term, $\frac{\partial v_{x*}}{\partial t_*}$, governed by the pressure gradient, thus leading to the same result as for acoustic approximation.

Appendix B

Neglecting radial inertia

When neglecting the radial inertia it is enough to look at Equation 3.6 and Equation 3.7 if considering frequencies below the first radial resonant-frequency:

$$\rho_f \frac{\partial v_x}{\partial t} + \frac{\partial p}{\partial x} = 0 \tag{B.1}$$

$$\rho_f \frac{\partial v_r}{\partial t} + \frac{\partial p}{\partial r} = 0 \tag{B.2}$$

and using the following non-dimensional variables:

$$\frac{\partial}{\partial t_*} = \frac{L_0}{a}\frac{\partial}{\partial t} \quad \frac{\partial}{\partial x_*} = L_0\frac{\partial}{\partial x} \quad \frac{\partial}{\partial r_*} = \frac{D_0}{2}\frac{\partial}{\partial r}$$

$$P_* = \frac{1}{a^2\rho_f}P \quad v_{x*} = \frac{1}{a}v_x \quad v_{r*} = \frac{1}{a}v_r$$

Equation B.1 and Equation B.2 becomes:

$$\frac{\rho_f aa}{L_0}\frac{\partial v_{x*}}{\partial t_*} + \frac{a^2\rho_f}{L_0}\frac{\partial p_*}{\partial x_*} = 0 \tag{B.3}$$

$$\frac{\rho_f aa}{L_0}\frac{\partial v_{r*}}{\partial t_*} + \frac{2a^2\rho_f}{D_0}\frac{\partial p_*}{\partial r_*} = 0 \tag{B.4}$$

Rearranging:

$$\frac{\partial v_{x*}}{\partial t_*} + \frac{\partial p_*}{\partial x_*} = 0 \tag{B.5}$$

$$\frac{D_0}{2L_0}\frac{\partial v_{r*}}{\partial t_*} + \frac{\partial p_*}{\partial r_*} = 0 \tag{B.6}$$

These two equations have the same characteristics only when:

$$\frac{D_0}{2L_0} = 1 \Rightarrow \frac{L_0}{D_0} = \frac{1}{2}$$

When introducing the constraint for general piping systems: $L_0/D_0 \gg 1 \Rightarrow D_0/L_0 \ll 1$, one can see that the term $\frac{D_0}{2L_0}\frac{\partial v_{r*}}{\partial t_*}$ becomes very small compared to the term $\frac{\partial v_{x*}}{\partial t_*}$, thus the radial inertia can be neglected.

One can also take the derivative of Equation B.5 with respect to r_* and the derivative of Equation B.6 with respect to x_*, combine these equations and obtain:

$$\frac{D_0}{2L_0}\frac{\partial v_{r*}}{\partial x_*} + \frac{\partial v_{x*}}{\partial r_*} = 0 \tag{B.7}$$

For $D_0/L_0 \ll 1$, the term $\frac{\partial v_{r*}}{\partial x_*}$ can be neglected, and Equation B.7 becomes:

$$\frac{\partial v_{x*}}{\partial r_*} = 0 \tag{B.8}$$

which is essentially the same as averaging the velocity in the cross section of the pipe (one-dimensional flow).

Appendix C

Viscoelastic equation

In this appendix it is proven that the linear "viscoelastic equations" and the waterhammer equations with added frequency-dependent friction are equivalent. The waterhammer equations (Equation 5.22 and Equation 5.23) with nonlinear steady state damping:

$$\frac{1}{K}\frac{\partial P}{\partial t} + \frac{\partial V}{\partial x} = 0 \tag{C.1}$$

$$\frac{\partial V}{\partial t} + \frac{1}{\rho_f}\frac{\partial P}{\partial x} = -f\frac{|V|\,V}{4R} + \frac{\lambda_f}{\rho_f}\frac{\partial^2 V}{\partial x^2} \tag{C.2}$$

Taking the derivative of Equation C.2 with respect to t:

$$\frac{\partial^2 V}{\partial t^2} + \frac{1}{\rho_f}\frac{\partial^2 P}{\partial x \partial t} = -\frac{\partial}{\partial t}\left[\frac{f\,|V|\,V}{4R}\right] + \frac{\lambda_f}{\rho_f}\frac{\partial^3 V}{\partial x^2 \partial t} \tag{C.3}$$

Then taking the derivatives of Equation C.1 with respect to x:

$$\frac{\partial^2 P}{\partial t \partial x} = -K\frac{\partial^2 V}{\partial x^2} \tag{C.4}$$

Using Equation C.4 in Equation C.3

$$\frac{\partial^2 V}{\partial t^2} - \frac{K}{\rho_f}\frac{\partial^2 V}{\partial x^2} = -\frac{\partial}{\partial t}\left[\frac{f\,|V|\,V}{4R}\right] + \frac{\lambda_f}{\rho_f}\frac{\partial^3 V}{\partial x^2 \partial t} \tag{C.5}$$

The linear "viscoelastic equations" as described on page 49:

$$\frac{1}{K}\frac{\partial P}{\partial t} + \frac{\partial V}{\partial x} + \frac{\lambda_f}{K}\frac{\partial^2 V}{\partial x \partial t} = 0 \tag{C.6}$$

$$\frac{\partial V}{\partial t} + \frac{1}{\rho_f}\frac{\partial P}{\partial x} = -f\frac{|V|\,V}{4R} \tag{C.7}$$

Taking the derivative of Equation C.7 with respect to t:

$$\frac{\partial^2 V}{\partial t^2} + \frac{1}{\rho_f}\frac{\partial^2 P}{\partial x \partial t} = -\frac{\partial}{\partial t}\left[\frac{f\,|V|\,V}{4R}\right] \tag{C.8}$$

Then taking the derivative of Equation C.6 with respect to x:

$$\frac{\partial^2 P}{\partial t \partial x} = -K\frac{\partial^2 V}{\partial x^2} - \lambda_f \frac{\partial^3 V}{\partial x^2 \partial t} \tag{C.9}$$

Using Equation C.9 in Equation C.8:

$$\frac{\partial^2 V}{\partial t^2} - \frac{K}{\rho_f}\frac{\partial^2 V}{\partial x^2} = -\frac{\partial}{\partial t}\left[\frac{f\,|V|\,V}{4R}\right] + \frac{\lambda_f}{\rho_f}\frac{\partial^3 V}{\partial x^2 \partial t} \tag{C.10}$$

Looking at Equation C.5 and Equation C.10 one can see that they are equal.

Appendix D

Bending element

There are several ways of making the Finite Element matrices [35, Rao] [33, Petyt]. Here they are made in a similar manner as for the longitudinal pipe equation. The equation describing the bending of the pipes (Equation 3.25):

$$EI_p \frac{\partial^4 w}{\partial x^4} + (\rho_p A_p + \rho_f A_f) \frac{\partial^2 w}{\partial t^2} = f(x,t) \tag{D.1}$$

Multiplying Equation D.1 with an arbitrary weight function δ, and integrating from node a to node b:

$$EI_p \int_a^b \delta \frac{\partial^4 w}{\partial x^4} + (\rho_p A_p + \rho_f A_f) \int_a^b \delta \frac{\partial^2 w}{\partial t^2} = \int_a^b \delta f(x,t) \tag{D.2}$$

Applying integration by parts *two* times on the $\delta \frac{\partial^4 w}{\partial x^4}$ term:

$$\begin{aligned} EI_p \int_a^b \frac{\partial^2 \delta}{\partial x^2} \frac{\partial^2 w}{\partial x^2} dx + (\rho_p A_p + \rho_f A_f) \int_a^b \delta \frac{\partial^2 w}{\partial t^2} dx = \\ - \left[\delta \frac{\partial^3 w}{\partial x^3} \right]_a^b + \left[\frac{\partial \delta}{\partial x} \frac{\partial^2 w}{\partial x^2} \right]_a^b + \int_a^b \delta f(x,t) dx \end{aligned} \tag{D.3}$$

The exact integrals on the right hand side of Equation D.3 are the boundary conditions at the nodes for the shear forces and bending moments respectively. Since the boundary conditions is properly taken care of with the external force term $f(x,t)$, they can be discarded. The weight functions are substituted with the shape function vector and the displacement is approximated with:

$$w(x,t) \approx \mathbf{N}^T \mathbf{w}$$

where

$$w_1(t) = w(0,t) \quad w_2(t) = \frac{\partial w}{\partial x}(0,t)$$

$$w_3(t) = w(L,t) \quad w_4(t) = \frac{\partial w}{\partial x}(L,t)$$

and L is the element length. Equation D.3 now becomes the Finite Element discretized equation:

$$EI_p \int_a^b \mathbf{N}_{xx}\mathbf{N}_{xx}^T dx\mathbf{w} + (\rho_p A_p + \rho_f A_f) \int_a^b \mathbf{N}\mathbf{N}^T dx\ddot{\mathbf{w}} = \int_a^b \mathbf{N} f(x,t) dx \tag{D.4}$$

The shape functions are third order Hermite polynomials:

$$n_1(x) = 1 - 3\left(\frac{x}{L}\right)^2 + 2\left(\frac{x}{L}\right)^3 \tag{D.5}$$

$$n_2(x) = x - 2L\left(\frac{x}{L}\right)^2 + L\left(\frac{x}{L}\right)^3 \tag{D.6}$$

$$n_3(x) = 3\left(\frac{x}{L}\right)^2 - 2\left(\frac{x}{L}\right)^3 \tag{D.7}$$

$$n_4(x) = -L\left(\frac{x}{L}\right)^2 + L\left(\frac{x}{L}\right)^3 \tag{D.8}$$

Bibliography

[1] F. Axisa and R. J. Gibert. Non-linear analysis of fluid-structure coupled transients in piping systems using finite elements. *Flow-Induced Vibrations of Circular Cylindrical Structures*, 63:151–165, 1982.

[2] H. Brekke. *A Stability Study on Hydro Power Plant Governing Including the Influence from a Quasi Nonlinear Damping of Oscillatory Flow and from the Turbine Characteristics.* PhD thesis, NTH, 1984.

[3] H. Brekke and B. Svingen. Self excited and hydromechanical vibrations in piping systems. In *Work Group on The Behavior of Hydraulic Machinery under Steady Oscillatory Conditions*, Lausanne, Switzerland, 1993. IAHR.

[4] Hermod Brekke, Li Xinxin, and Halvar Luraas. A review of modern turbine control systems for hydropower plants with high pressure tunnel. In *Hydropower'92*, pages 475–484, A.A. Balkema Publishers, P.O. Box 1675, Rotterdam, Netherlands, June 1992. A.A. Balkema.

[5] F. T. Brown. A quasi method of characteristics with application to fluid lines with frequency dependent wall shear and heat transfer. *Journal of Basic Engineering*, pages 217–227, June 1969.

[6] J. Charley and G. Caignaert. Vibroacoustical analysis of flow in pipes by transfer matrix with fluid-structure interaction. In *Work Group On The Behavior of Hydraulic Machinery under Steady Oscillatory Conditions*, Lausanne, Switzerland, 1993. IAHR.

[7] L. C. Davidson and J. E. Smith. Liquid-structure coupling in curved pipes. *The Shock and Vibration Bulletin*, (42):197–207, 1969. Part 4.

[8] Christ de Jong. *Analysis of Pulsations and Vibrations in Fluid-Filled Pipe Systems.* PhD thesis, TNO, Institute of Applyed Physics, 1994.

[9] Zeki Demirbilek, editor. *Tension Leg Platform: A State of the Art Review.* American Society of Civil Engineers, 345 East 47th Street, New York 10017-2398.

[10] W. W. Durgin and H. R. Graf. Flow excited acoustic resonance in a deep cavity: An analytical model. In *Fundamental Aspects of Fluid-Structure Interactions*, pages 81–91. ASME, 1992.

[11] P. Eichinger. *Untersuchung Des Reibungsverhaltens Bei Instationären Strömungsvorgängen in Rohrleitungen*. PhD thesis, Universität Stuttgart, 1992.

[12] G. C. Everstine. Dynamic analysis of fluid-filled piping systems using finite element techniques. *Advances in Fluid-Structure Interaction*, 78:125–139, 1984.

[13] A. Fiskvatn. *Elementmetoden*. Tapir Trykk, 7034 Trondheim, Norway, 1984. In Norwegian.

[14] A. Gajić, S. Pejović, Z. Stojanović, and K. Jozef. Fluid-structure interaction analysis in frequency domain. In *Work Group on The Behavior of Hydraulic Machinery under Steady Oscillatory Conditions*, Ljubljana, Slovenia, 1995. IAHR.

[15] R. J. Gibert, F. Axisa, and B. Villard. Flow induced vibrations of piping systems (vibration sources - mechanical response of the pipes). In *B.N.E.S Vibration in Nuclear Plant*, pages 617–631. B.N.E.S, 1978.

[16] H. R. Graf and S. Ziada. Flow induced acoustic resonance in closed side branches: An experimental determination of the excitation source. In *Fundamental Aspects of Fluid Structure Interaction*, pages 63–80. ASME, 1992.

[17] F. J. Hatfield, D. C. Wiggert, and R. S. Otwell. Fluid structure interaction in piping systems by component synthesis. *Journal of Fluids Engineering*, 104:318–325, September 1982.

[18] F. Haugen. *Automatiseringsteknikk*. NTH-Trykk, NTH, Trondheim, Norway, 1989.

[19] A. G. T. J. Heinsbroek and A. S. Tijsseling. The influence of support rigidity on waterhammer pressures and pipe stresses. In *Proceedings of the Second International Conference on Water Pipeline Systems*, pages 17–30. bHr Group, 1994.

[20] I. E. Idelchik. *Handbook of Hydraulic Resistance*. CRC Press, 2000 Corporate Blvd., N.W., Boca Raton, Florida 33431, 3 edition, 1994.

[21] F. Irgens. *Fasthetslære*. TAPIR, Trondheim, Norway, 1985.

[22] J. Jernsletten. *Analysis of Non-Stationary Flow in a Francis Reversible Pump Turbine Runner*. PhD thesis, The Norwegian Institute of Technology, 1995.

[23] M. T. Jonsson. *Geometrically Nonlinear Finite Element Formulation for Pipes and Bends*. PhD thesis, NTH, 1987.

[24] S. M. Karim and L. Rosenhead. The second coefficient of viscosity of liquids and gases. *Reviews of modern physics*, 24(2):108–116, April 1952.

[25] J. Köngeter. *Rohrreibungsverluste Einer Oszillierenden Turbulente Strömung in Einem Kreisrohr Konstanten Querschnitts*. PhD thesis, Technische Universität Berlin, 1980.

[26] P. Krus, K. Weddfelt, and J. O. Palmberg. Fast pipeline models for simulation of hydraulic systems. *Transactions of the ASME*, 116:132–136, March 1994.

[27] C. M. Larsen. Use of stochastic dynamic analysis in marine riser design. In *NSF Workshop on Riser Mechanics*, University of Michigan, September 1992.

[28] C. M. Larsen and E. Passano. Fatigue life analysis of production risers. In *19 Th Annual OTC in Houston*, pages 427–437, Texas, April 1987.

[29] C. S. W. Lavooij and A. S. Tijsseling. Fluid structure interaction in compliant piping systems. In *Pressure Surges-Proceedings of the 6th International Conference*, pages 85–100. BHRA, 1990.

[30] M. W. Lesmez, D. C. Wiggert, and F. J. Hatfield. Modal analysis of vibrations in liquid-filled piping systems. *Journal of Fluids Engineering*, 112:311–318, September 1990.

[31] W. E. Meador, G. A. Miner, and L. W. Townsend. Bulk viscosity as a relaxation parameter: Fact or fiction? *Phys. Fluids*, 8(1):158–261, January 1996.

[32] P. Obradovic. Fluid-structure interactions: An accident which has demonstrated the necessity for fsi analysis. In *Transactions of the 15th IAHR Symposium on Hydraulic Machinery and Cavitation*. IAHR, 1990.

[33] M. Petyt. *Introduction to Finite Element Vibration Analysis*. Cambridge University Press, Cambridge, 1990.

[34] B. R. Ramaprian and S. W. Tu. Fully developed periodic turbulent pipe flow. part 2. the detailed structure of the flow. *J. Fluid Mech.*, 137:59–81, 1983.

[35] S. S. Rao. *Mechanical Vibrations*. Addison-Wesley Publication Company, Reading, Massachusetts, second edition edition, 1990.

[36] G. Sandberg. *Finite Element Modelling of Fluid-Structure Interaction*. PhD thesis, Lund University, 1986.

[37] H. Schlichting. *Boundary-Layer Theory.* McGraw-Hill, New York, 1979.

[38] R. E. Schwirian. Methods for simulating fluid-structure interaction and cavitation with existing finite element formulations. In *Fluid Transients and FSI*, pages 261–285. ASME, 1982.

[39] R. E. Schwirian. On the use of finite element codes to perform fluid-dynamical and fluid-structure interactive analysis. In *Proceedings of the International Conference on Numerical Methods for Transient and Coupled Problems*, pages 186–197, 1984.

[40] R. E. Schwirian and M. E. Karabin. Use of spar elements to simulate fluid-solid interaction in the finite element analysis of piping system dynamics. In *Proceedings of the ASME Symposium on Fluid Transients and Structural Interactions in Piping Systems*, pages 1–11. ASME, 1981.

[41] R. Skalak. An extension to the theory of water hammer. *Transaction of the ASME*, pages 105–116, 1956.

[42] Society of Industrial and Applied Mathematics, SIAM, 3600 University City Science Center, Philadelphia, PA 19104-2688. *LAPACK User's Guide*, 1994. http://www.netlib.org.

[43] B. Stroustrup. *The C++ Programming Language.* Addison-Wesley Publishing Company, Reading, Massachusetts, 1991.

[44] B. Svingen. Undersøkelse av selveksiterende trykk-svingninger i rørsystemer tilkoblet en fjærende ventil. Master's thesis, NTH, 1991. In Norwegian.

[45] B. Svingen. A frequency domain solution of the coupled hydromechanical vibrations in piping systems by the finite element method. In *XVII IAHR Symposium*, pages 1259–1269. IAHR, 1994.

[46] B. Svingen. Dynamisk friksjonsdemping med elementmetoden. Technical Report STF12 A95039, SINTEF, 7034 Trondheim, Norway, 1995. In Norwegian.

[47] B. Svingen. Fluid struktur interaksjon i rørsystemer... Technical Report STF12 A95041, SINTEF, 7034 Trondheim, Norway, 1995. In Norwegian.

[48] B. Svingen. Frequency dependent friction and modal solutions of pipe flow by the finite element method. In *Work Group on The Behavior of Hydraulic Machinery under Steady Oscillatory Conditions*, Ljubljana, Slovenia, 1995. IAHR.

[49] B. Svingen. Fluid structure interaction in slender pipes. In *Pressure Surges and Fluid Transients in Pipelines and Open Channels*, pages 385–396, Bury st Edmunds and London, UK, 1996. bHr Group, Mechanical Engineering Publications Limited.

[50] B. Svingen and M. Kjeldsen. Fluid structure interaction in piping systems. In *Proceedings of the Ninth International Conference on Finite Elements in Fluids New Trends and Applications*, pages 955–963. IACM, 1995.

[51] A. R. D. Thorley. Pressure transients in hydraulic pipelines. *Journal of Basic Engineering*, 91:453–461, 1969.

[52] A. S. Tijsseling. *Fluid-Structure Interaction in Case of Waterhammer with Cavitation.* PhD thesis, Delft University of Technology, 1993.

[53] A. S. Tijsseling. Fluid-structure interaction in liquid-filled pipe systems: A review. *Journal of Fluids and Structures*, 10:109–146, 1996.

[54] A. S. Tijsseling, D. Fan, and A. Vardy. Transient fluid-structure interaction and cavitation in a single-elbow pipe system. In *Proceedings of the First International Conference on Flow Interaction*, pages 346–349, 1994.

[55] A. S. Tijsseling and C. S. W. Lavooij. Fluid structure interaction and column separation in a straight elastic pipe. In *Pressure Surges-Proceedings of the 6th International Conference*, pages 27–42. BHRA, 1990.

[56] A. S. Tijsseling and C. S. W. Lavooij. Waterhammer with fluid-structure interaction. *Applied Scientific Research*, 47:273–285, 1990.

[57] A. S. Tijsseling and A. E. Vardy. Axial modelling and testing of a pipe rack. In *Pressure Surges and Fluid Transients in Pipelines and Open Channels*, pages 363–383. bHr Group, 1996.

[58] A. K. Trikha. An efficient method for simulating frequency-dependent friction in transient liquid flow. *Journal of Fluids Engineering*, pages 97–105, March 1975.

[59] S. W. Tu and B. R. Ramaprian. Fully developed periodic turbulent pipe flow. part 1. main experimental results and comparison with predictions. *J. Fluid Mech.*, 137:31–58, 1983.

[60] A. Vardy and J. Brown. On turbulent, unsteady, smooth-pipe friction. In *Pressure Surges and Fluid Transients in Pipelines and Open Channels*, pages 289–313, Bury st Edmunds and London, UK, 1996. bHr Group, Mechanical Engineering Publications Limited.

[61] A. Vardy and D. Fan. Flexural waves in a close tube. In *Pressure Surges-Proceedings of the 6th International Conference*, pages 43–58. BHRA, 1990.

[62] R. Vennatrø. Unsteady frictions in pipelines. In *XVIII IAHR Symposium*, 1996. To be published.

[63] WATCOM, 415 Phillip Street, Waterloo, Ontario, Canada N2L 2X2. *Watcom Programmer's Guide*, 1994.

[64] F. M. White. *Fluid Mechanics*. McGraw-Hill Book Company, New York, second edition edition, 1986.

[65] F. M. White. *Viscous Fluid Flow*. McGraw-Hill Inc., New York, 1991.

[66] D. C. Wiggert. Coupled transient flow and structural motion in liquid-filled piping systems: A survey. In *ASME Pressure Vessels and Piping Conference*. ASME, 1986. Paper 86-PVP-4.

[67] D. C. Wiggert. Fluid transients in flexible piping systems. In *XVIII IAHR Symposium*, 1996. To be published.

[68] D. C. Wiggert and F. J. Hatfield. Time domain analysis of fluid-structure interaction in multi-degree-of-freedom piping systems. In *4th International Conference on Pressure Surges*, pages 175–187. BHRA, 1993.

[69] D. C. Wiggert, F. J. Hatfield, and S. Stuckenbruck. Analysis of liquid and structural transients in piping by the method of characteristics. *Journal of Fluids Engineering*, 109:161–165, June 1987.

[70] E. B. Wylie. Unsteady internal flows - dimensionless numbers & time constants. In *Pressure Surges and Fluid Transients in Pipelines and Open Channels*, pages 283–288, Bury st Edmunds and London, UK, 1996. bHr Group, Mechanical Engineering Publications Limited.

[71] E. B. Wylie and A. L. Streeter. *Fluid Transients in Systems*. Prentice-Hall, Inc., Englewood Cliffs, New Jersey 07632, 1993.

[72] Z. Xianglin, H. Shuhuai, and W. Yuangan. The FEM of fluid structure interaction in piping pressure transients. In *Proceedings of the First International Conference on Flow Interaction*, pages 532–535, 1994.

[73] L. Xinxin. Hydropower systems modeling by structure matrix method. NTH, Trondheim, Norway, 1988.

[74] L. Xinxin and T. Nielsen. A new method for pipe vibration analysis. Technical Report STF67 F 90033, SINTEF, 1990.

[75] K. Zaveri and M. Phil. *Modal Analysis of Large Structures-Multiple Exciter Systems*. Brüel & Kjær, Brüel and Kjær, DK-2850 NÆRUM DENMARK, 1984.

[76] W. Zielke. Frequency-dependent friction in transient pipe flow. *Journal of Basic Engineering*, pages 109–116, March 1968.

[77] O. C. Zienkiewicz and R. L. Taylor. *The Finite Element Method*, volume 1 and 2. McGraw-Hill Book Company, London, 4 edition, 1988.